HEAT AFFECTED ZONE STUDIES OF THERMALLY CUT STRUCTURAL STEELS

Murali T. Ramaswamy
M.E., Indian Institute of Science
Bangalore, India, 1987

A thesis submitted to the faculty
of the Oregon Graduate Center
in partial fulfillment of the
requirements for the degree
Master of Science
in
Materials Science and Engineering

July, 1989

TO

MY PARENTS WITH LOVE

The thesis "Heat Affected Zone Studies of Thermally Cut Structural Steels" by Murali Ramaswamy has been examined and approved by the following Examination Committee:

William E. Wood, Thesis Research Advisor
Professor

David G. Atteridge
Associate Professor

Jack H. Devletian
Professor

V.S. Rao Gudimetla
Assistant Research Professor

ACKNOWLEDGEMENTS

I am grateful to my thesis advisor and department chairman, Dr. William E. Wood, for his support and guidance throughout this work and I am extremely thankful to him. I am thankful to the other thesis committee members, Dr. David G. Atteridge, Dr. Jack H. Devletian, and Dr. V.S. Rao Gudimetla, for reviewing my thesis and for their valuable suggestions.

My sincere thanks are due to Mr. Robert Turpin and Mr. Andy Villeneuve for flame cutting the steel plates and making specimens for tension and Charpy impact tests. I also thank R. Parthasarathy, John Simmons, Rajesh Dighde, and Sin-Jang Chen for their help at various stages of this work. I am very thankful to Mrs. Jessie A. Atteridge for her recommendations and effort in the final typing of this thesis.

This work was supported by the U.S. Department of Transportation, Federal Highway Administration.

CONTENTS

LIST OF TABLES

LIST OF FIGURES

HEAT AFFECTED ZONE STUDIES OF THERMALLY CUT STRUCTURAL STEELS

ABSTRACT

Murali T. Ramaswamy
Oregon Graduate Center
1989

Supervising Professor: Dr. William E. Wood

There have been many studies on thermal cutting. However, few have considered the influence of the resulting heat affected zone (HAZ) on the tensile or impact properties. Hence, in the present work HAZ microstructure and mechanical properties for thermally cut A514, A572, and A588 structural steels were studied as a function of cutting speed. The effect of thermal cutting was analyzed microstructurally and by both tensile and impact tests at varying test temperatures and strain rates.

The HAZ of the three steels were found to have higher microhardness, higher strength, lower impact toughness, and lower ductility than the base metal. Also with increased flame cutting speed the HAZ hardness and strength increased while the ductility and impact toughness decreased. However, no brittle fracture initiation in the HAZ was observed. Scanning electron micrographs of the fractured tension and Charpy V-notch (CVN) impact specimens showed dimpled and quasi cleavage type fracture. The HAZ microstructure analysis was done and a correlation between microstructure and properties was made.

1. INTRODUCTION

1.1 THERMAL CUTTING

Thermal cutting[1] is a procedure that has been used in the manufacture and fabrication of steel for decades. Thermal cutting is particularly important in the production of plate steels, where it is commonly used for trimming the as rolled plate to the required rectangular dimensions.

Thermal cutting encompasses the entire range of electric arc and flame initiated cutting processes. Different types of thermal cutting process are discussed briefly[2] before going to oxy-fuel gas cutting (OFC).[2]

1.1.1 Metal Powder Cutting

Finely divided iron-rich powder suspended in a jet of moving air or dispensed by a vibratory device is directed in to the gas flame in metal powder cutting (POC). The iron powder passes through and is heated by the preheat flame so that it burns in the oxygen stream. Heat generated by the burning iron particles improves cutting action. Cuts can be made in stainless steel and cast iron at speeds only slightly lower than those for equal thickness of carbon steel. By adding a small amount of aluminum powder, cuts can be made through copper and brass. Typical POC applications include removal of risers; cutting of bars, plates, and slabs to size; and scrapping.

1.1.2 Chemical Flux Cutting

Chemical flux cutting processes are well suited to materials that form refractory oxides. Finely pulverized flux is injected into the cutting oxygen before it enters the cutting torch. The torch has separate ducts for the preheat oxygen, fuel gas, and cutting oxygen. When the flux strikes the material, the refractory oxides that are formed on the material surface when the cutting oxygen is turned on reacts with the flux to form a slag of lower melting temperature compounds than the material. This slag is driven out by the cutting oxygen, enabling oxidation of the metal to proceed. Chemical fluxing methods are used to cut stainless steel.

1.1.3 Oxy-Fuel Gas Gouging

The oxy-fuel gas gouging process makes grooves or surface cuts in material instead of cutting through the material in a single pass. This process uses special cutting torches and/or special tips. Tips for gouging vary to suit the size and shape of the desired groove or surface cut. Torches may include attachment for dispensing iron powder to increase the speed of cutting or to permit the scarring of stainless steel. Gas consumption, especially of oxygen, is much greater than in ordinary OFC.[2]

1.1.4 Plasma Arc Cutting

Plasma arc cutting (PAC) uses a high-velocity jet of high-temperature ionized gas to cut carbon steel, aluminum, copper, and other metals. At temperatures above about 5500°C (as in a welding arc), gases partially ionize and exist as a plasma, a mixture of free electrons, positively charged ions, and neutral atoms. The plasma jet melts and displaces the work piece material in its path. Because PAC does not depend on a chemical reaction between the gas and the work metal, because the process relies on heat generated from an arc between the torch electrode and the work piece, and because it generates very high temperatures (28,000°C compared to 3000°C for oxy-fuel), it can be used on almost any material that conducts electricity, including those that are resistant to OFC. The Process increase productivity of cutting machines over OFC without increasing space or machinery requirements.[2]

1.1.5 Air Carbon Arc Cutting and Gouging

Air carbon arc cutting (AAC) and gouging severs or removes metal by melting with the heat of an arc struck between a carbon-graphite electrode and the base metal. A stream of compressed air blows the molten metal from the kerf or groove. Its most common uses are (1) weld joint preparation; (2) removal of weld defects; (3) removal of welds and attachments when dismantling tanks and steels structures; and (4) removal of gates, risers, and defects from castings. The process

cuts almost any metal, because it does not depend on oxidation to keep the process going. The low heat input of air carbon arc gouging makes this process ideal for weld joint preparation, and for weld removal of high-strength steels.[2]

1.1.6 Oxygen Arc Cutting

Oxygen arc cutting uses a flux-covered tubular steel electrode. The covering insulates the electrode from arcing with the sides of the cut. The arc raises the work material to kindling temperature (minimum temperature needed for oxygen to react with the material); the oxygen stream oxidizes and removes the material away. Oxidation, or combustion, liberates additional heat to support continuing combustion of sidewall material as the cut progresses. The electric arc supplies the preheat necessary to obtain and maintain ignition at the point where the oxygen jet strikes the work surface. The process finds greatest use in underwater cutting. When cutting oxidation-resistant metals, melting action occurs. The covering on the electrode acts as a flux. The electrode covering functions in a manner similar to that of powdered flux or powdered metal injected in to the gas flames in the flux-injection method of OFC of stainless steel.[2]

1.1.7 Oxy-Fuel Gas Cutting

For oxidizable metal such as ferritic steel, OFC is the process of choice for manufacturers and fabricators. In comparison with other cutting methods OFC offers low initial equipment cost, high productivity and versatility, and little required operator training.[1]

Oxy-fuel gas cutting includes a group of cutting processes that use controlled chemical reactions to remove preheated metal by rapid oxidation in a stream of pure oxygen. A fuel gas/oxygen flame heats the work piece to ignition temperature, and a stream of pure oxygen feeds the cutting (oxidizing) action. The OFC process, which is also referred to as burning or flame cutting, can cut carbon and low alloy plate of virtually any thickness.

1.1.7.1 Tool and Work Piece Characteristics of Oxy-Fuel Gas Cutting

The classic conditions[3] that must be fulfilled to permit oxy-fuel flame cutting of steel materials are as follows:

1. The material must be oxidizable.
2. The ignition temperature of the material must be below its melting temperature.
3. The melting point of the oxides must be below the melting temperature of the work piece.

4. The combustion heat must be high.

5. The thermal conductivity must be low.

These requirements are met by plain carbon steels and low alloy steels. In addition, it is also possible to flame cut a number of higher alloyed steels without the need for special measures.

Since it is well known that titanium can be flame cut, the classic conditions need to be modified. The melting temperature of titanium is of the order of 1670°C; the melting temperature of the oxide (TiO_2), however, is around 300°C higher. Further the ignition temperature is not a chemical constant and therefore cannot be precisely determined.

1.1.7.2 Physical and Chemical Phenomena of the Process

In the OFC process the cutting oxygen is not in immediate contact with the parent metal, but is constantly enveloped by a shroud of liquid iron oxide (Fig. 1). Between this slag jacket and the solid parent metal there is a layer of partially molten iron. The iron atoms diffuse through the slag, and are largely combusted by the cutting oxygen to form FeO. Therefore, the cutting oxygen jet fulfills a dual function: on one hand, its purpose is to further a chemical reaction by forming a compound with the iron atoms. On the other hand, it has the task of ejecting the slag, which is formed continuously during the cutting process, out of the cutting kerf.

The combustion of iron to form FeO is a highly exothermic reaction which, in conjunction with the heating flame, provides the heat necessary to maintain the process of progressively melting the parent metal during a continuous cut. Recent research has shown that the parent material is not completely combusted as the oxides are interspersed with uncombusted iron. This indicates that the oxide layer in the cutting kerf is diluted with molten iron on account of turbulence.

The amount of liquid iron oxide removed increases towards the bottom edge of the cut, in other words, the layer of iron oxide becomes progressively thicker (Fig. 2). This reduces the diffusion rate of the iron atoms released from the molten layer. However, the diffusion rate is a determining factor with regard to cutting speed. Therefore, the thicker the plate, the lower the cutting speed.

Figure 2 also shows that the heating flame can only be effective near the surface of the plate. This is because the heat which it introduces cannot, in the case of thicker materials, make its way immediately to the bottom edge of the plate. The parent metal at the bottom of the plate is heated and melted by the hot slag.

1.2 BACKGROUND LITERATURE

The properties of thermal cut steels had been reported by earlier workers and few of them are discussed in this section. Most of them studied the flame cut steel's properties and very few discuss the HAZ properties. It is important to study the HAZ produced by thermal cutting to understand the variations in the edge

related properties induced by thermal cutting. As the flame cut HAZ is a few mm wide it is necessary to use sub-size specimens for CVN tests to study the HAZ's CVN impact properties exclusively. Some of the earlier works on sub-size CVN tests are also discussed here.

1.2.1 Thermal Cutting

There are many works[3-8] that describe the standard methods of thermal cutting steel plates. Parameters like oxygen purity and fuel gas selection in OFC are discussed[8] along with other related cutting processes. Also the procedure for cutting high alloyed steels and thicker plates are outlined.

It is well known that the flame-cut surfaces are not as smooth as machine-cut surfaces.[6,9-11] The recommendation[11] for constructional steel components that are subjected to fatigue loading is that the roughness of the cut surface should not exceed 150 μm. This is valid only for steels that are weldable without preheat, have a yield strength below 420 N/mm^2, and thickness below 40 mm. The effect of cutting variables including oxygen pressure, cutting speed, nozzle type, and preheat flame on the quality of the cut surface are discussed by other workers.[8,12]

For steels the cutting operation requires sufficient heating to bring a small portion of the piece to be cut to a high (kindling) temperature, around 1350°C.[13] During cooling, the cut edges undergo metallurgical transformations which may result in hardening near the cut edge. Generally the HAZ consists of one of the

two series of structures[14] shown in Fig. 3 depending on whether the cutting operation was performed with or without preheating. In fatigue strength studies of flame-cut AE355, steel Piraprez[15] observed the following characteristics of oxygen-cut edges:

(a) The carbon concentration is increased along the cut edge in a very thin layer about 0.1 mm deep. As hardness is a direct function of carbon content, the thin region along the cut edge is very hard. According to Piraprez, this increased carbon content does not come from the cutting flame nor from the diffusion of carbon towards the cut edges, but from the material which was melted during the cutting. It is only at depths of 1.5 mm (and not 0.1 mm) that the hardness begins to decrease to reach the value for the base material about 3 mm from the surface.

(b) The heat distribution due to the oxygen-cutting produces a field of residual stresses in the cut pieces. The distribution of these stresses along the edge has not yet been defined neither in sign nor in value. Studies to date are not conclusive as some authors speak of compression stresses[14,16] while others speak of fraction stresses.[16-18]

(c) The cut surfaces develop grooves oriented in the direction of the cutting flame. In most cases these grooves are perpendicular to the service induced stress fields, which is very unfavorable for fatigue resistance. Moreover the fatigue resistance may be further reduced by additional imperfections.

Additionally grooves may also affect the resistance to brittle fracture which depends mostly on the depth and the sharpness of the grooves.[15] When cutting with preheat the hardness of the thin high-carbon martensite layer is reduced. If the material and the cut surface is of good quality the fatigue strength is then reduced by 10%. The same reduction is obtained if the cut surface receives a heat-treatment after cutting to reduce hardness. These are valid only for constructional steels with a yield strength below 420 N/mm^2 and thickness below 40 mm.[11]

Nibbering, Thomas, and Bos[19] studied the properties of plasma cut structural steel Fe510, thickness 25 mm. They found a maximum hardness of 450HV located at a depth of 0.1 to 0.3 mm under the surface of the cut. The hardness of plasma-cut edge was much lower than the hardness of oxy-acetylene cut edges (non pre-heated), cut with the same cutting speed. The surface contained a layer of low-carbon martensite with a thickness of about 50 μm. This layer was followed by a transition zone consisting of bainite and very fine ferrite-pearlite. The white (non-etching) high-carbon martensite such as was found at the surface of an oxy-acetylene cut was not present. Other investigators have reported[20-22] similar trends in their results regarding the HAZ hardness and microstructure produced by oxy-fuel cutting and PAC.

The effect of thermal cutting on mechanical properties has been studied by relatively few investigators. Ho, Lawrence, and Altstetter[21] evaluated the effect of

oxygen cutting on the fatigue resistance of A572 and quenched and tempered A514 steels. For the A572 steel, the differences in the fatigue resistance resulting from different cutting methods (flame cut and plasma arc cut) were very small. For the A514 steel with a fatigue life greater than 1.5×10^4 cycles, machined surface has greater fatigue resistance than flame-cut and quenched, and, tempered (after cutting) surfaces. Heat treatment of the flame-cut surface did not improve fatigue resistance much. All flame-cut surface failures initiated at the roots of serrations (valleys of the surface). It seems that geometry of flame-cut surface defects is more important than microstructure in determining the fatigue crack initiation site. For the plasma arc cut A572 specimens, the fatigue crack initiation point was mainly at the upper edge of the flame-cut surface, as Goldberg reported.[23] Surface residual stresses alter the mean stress which, in turn, greatly influences the fatigue crack initiation life. Compressive residual stresses reduce the mean stress level so that the fatigue life is longer, and the fatigue strength is higher. Tensile residual stresses shorten the fatigue life. The Netherlands group[14] showed this effect for flame-cut surfaces of A572 steel.

The fatigue properties of oxygen-cut surfaces may be altered as a result of changes in chemical composition, microstructure, residual stresses, and geometrical features such as roughness, gouges (pits due to lateral torch instability), drag lines (curved lines brought by insufficient oxygen flow), and melted edges. The differences in the fatigue resistance between flame-cut and small gouged surfaces is

negligibly small for both A572 and A514 steels. Deep surface gouges have a negative influence on the fatigues resistance. Neither grinding nor repairing gouges by welding increases the fatigue resistance compared with the gouged surface for both steels. At lives greater than 2 x 10^5 cycles A572 flame-cut surfaces have greater fatigue resistance than A514, but at lives less than 10^5 cycles the fatigue resistance of A514 flame-cut surface is greater than that of A572.[21]

Honda, Kitamura, and Yamada[20] conducted fatigue tests for HT80 steel racks. They found during fatigue testing that cracks were first initiated on the surface of a compressive fillet, but ultimately stopped growing. Cracks were then initiated on the surface of a tensile fillet resulting in rack failure. Defects resulting from torch-cutting were observed on the surfaces and the surface roughness for the torch-cut specimens were remarkably higher than that for the machined specimens. The fatigue strength of the torch-cut racks were of lower value compared to the machined racks.

Several investigators[14,19,23-26] have shown that the fatigue resistance and other properties of flame-cut surfaces are quite variable due to the use of different materials and cutting conditions.

Recently A588, A572, and A36 steels have been studied[1] for their performance in bend tests. Based on the results, bend rating of these thermally cut

steels were formulated. It is found that the average thermal cut edge hardness is the primary variable in predicting bend rating, followed generally by carbon content, plate temperature, cutting speed, and CVN toughness.

1.2.2 Sub-Size Charpy Specimen Impact Tests

Many workers have studied[27-35] the effect of specimen thickness on the CVN toughness values of ferritic steels. Some of them tested 10 mm thick laminated specimens made up of sub-size specimens bonded together. It is usual to extract a specimen of reduced thickness for small section thickness or inconveniently shaped components,[36] if standard Charpy specimen of cross sectional dimensions 10 x 10 mm and length 55 mm cannot be extracted. The most commonly specified "sub-size" specimen thicknesses are 7.5, 5, and 2.5 mm, but specimens of two-thirds and one-third the normal 10 mm thickness (i.e. 6.7 and 3.3 mm) have been also tested. There is no simple relationship between results obtained using sub-size specimens and results from full size, 10 mm thickness specimens. The loss of through thickness constraint is sub-size specimens causes a shift in the ductile to brittle transition temperature in ferritic steels. It can also influence upper shelf, or fully ductile, specimen behavior. The influence of reduced CVN specimen thickness on ferritic steels which display a transition from ductile to brittle behavior with temperature, is a reduced transition temperature, unless splitting occurs. A reduction in transition temperature of $0.7(10\text{-}t)^{2}$°C, where t = the specimen thickness in mm,

appear to fit the data reasonably well for ferritic steels of room temperature being defined at a constant absorbed energy per unit ligament area.[36]

For ferritic steels:[37] (a) when a sub-size specimen is used because the section is too thin, the reduced thickness of the test specimen must be used to model the benefits of a reduced section thickness with regard to the risk of brittle fracture rather than attempting to correlate back to the result which would have been obtained in a full size specimen; and, (b) where a sub-size specimen is used because a component has an inconvenient configuration, an empirically derived correlation may be required to deduce the result which would have been obtained in a full size specimen or at least a larger specimen. Hence, it is recommended for ferritic steels that the test temperature for the sub-size specimen should be reduced which would otherwise have been required for the full size specimen, to model the effect of thickness on the transition temperature.[37] The decreasing transition temperature with decreasing CVN specimen thickness has also been observed by other[38,39] workers.

1.3 PRESENT WORK OBJECTIVE

The aim of the present work is to characterize the HAZ in thermally cut A514, A572, and A588 steels and to study its fracture behavior under tension and impact test conditions.

1.4 PRESENT WORK APPROACH

In the present work the HAZs of thermally cut A514, A572, and A588 steels were studied. The effect of cutting speed on HAZ appearance and microstructure was studied by thermally cutting these steels with oxy-acetylene flame at two different cutting speeds, namely, 12.7 and 38.1 cm/min. The effect of the cutting speed on HAZ mechanical properties was evaluated by microhardness tests across HAZ, by tension tests and by impact tests. Both the effects of temperature and strain rate on tensile properties were studied. Also, limited tests on tensile specimens of different thickness were done to find the effect of specimen size when tested at a low temperature and at a high strain rate. Sub-size Charpy specimens with different notch orientations with respect to flame-cut surface and HAZ were used for impact tests. Both flame-cut surfaces and fractured tension and impact test surfaces were subjected to scanning electron microscopy analysis.

2. EXPERIMENTAL PROCEDURE

2.1 MATERIALS

The steels chosen for this work were 25 mm thick ASTM A514, A572, and A588 plate steel. Their chemical composition and physical properties are given in Table 1. All steels are low carbon, low alloy steels with 1% Mn content. Both A572 and A588 steels were in the hot rolled condition whereas the A514 was in quenched and tempered condition. Hence, the yield strength (YS) and ultimate tensile strength (UTS) values of A514 steel were higher than A572 and A588 steels. The top of the plates and rolling direction were marked for identification purposes in thermal cutting experiments.

2.2 THERMAL CUTTING

The thermal cutting process employed throughout this work was OFC process. The fuel gas used was acetylene and the various cutting parameters used are listed in Table 2.

2.2.1 Tip Size and Tolerance Between Plate and Tip

There are listed available from torch tip manufacturers for the tip sizes to be used for the range of metal thickness values for fuel gas. The tip dimensions

increase with the thickness of the steel to be cut. These lists can be referred to if the plate to be cut is not painted or rusty and the flame to be used is a neutral flame. The tip size used for the present work was #2 and, as the thickness was more than 12.7 mm, the torch tip was held straight up and down perpendicular to the face of the horizontal surface. The distance between tip and plate was kept in the range 3.2 to 4.8 mm in order to hold the part of the preheat flame with the highest amount of heat close to the surface of the plate. If the tip is too far off, then it won't preheat fast enough and the cutting speed will slow down. If it is too close, then the cutting tip will overheat, start to melt the plate and the tip will start backfiring. (Backfiring is the momentary recession of the flame into the torch tip followed by immediate reappearance or complete extinguishment of the flame.) This leads to delay in the cutting process as the torch needs to be relighted to start the cutting process again.

2.2.2 O_2/C_2H_2 Pressure and Flow Rate

The acetylene pressure is adjusted until sufficient acetylene emerges to form a gap of about 3.2 mm between the tip and the flame. Then the oxygen pressure is adjusted until the flame burns with the desired balance or neutral characteristic. The neutral flame is produced with a mixing ratio of approximately 1 volume of oxygen to 1 volume of acetylene. When the flame is on the carburizing side, whitish streamers of unburned acetylene are seen leaving the blue inner cone and

entering the sheath flame. As the acetylene supply is decreased, these streamers decrease in length until there remains only the sharply defined blue inner cone and the sheath flame. At that instant, the neutral oxy-acetylene flame has been formed. The acetylene pressure was 5 x 10^3Pa and oxygen pressure was 42 x 10^3Pa in this work. Correspondingly the flow rates of oxygen and acetylene were 46.2 and 6.6 m^3/hr, respectively.

2.2.3 Cutting Speed

It is important that the forward cutting speed of the torch be correct. It must be just fast enough so that the cutting oxygen jet passes completely through the plate thickness to make a clean cut on the top and the bottom of the steel. At the correct travel speed the slag will be thrown out at the bottom of the plate in the same direction of the movement of the torch. For 2.54 cm plate thickness 38.1 cm/min is the correct flame cutting speed. In this work both 38.1 and 12.7 cm/min cutting speeds were used to cut the steel plates. Other cutting parameters were constant.

2.3 MICROHARDNESS TESTS

As the HAZ width is uniform only in the middle region along the thickness of the plate, as revealed by the macro profile obtained by etching with Nital solution, the microhardness tests were carried out in the mid-thickness of the plate. The

hardness traverse was thus taken across the mid-thickness as shown schematically in Fig. 4. This surface (A in Fig. 4b) is perpendicular to both the flame-cut surface and the top (rolling) surface. Hardness values were measured using a LECO (M-400) microhardness tester. This procedure was repeated for each steel and each cutting speed. Knoop hardness versus distance from flame-cut edge plots were made for all the cases. Before each set of tests the tester was calibrated using standard test blocks. The load used in these tests we 300 gms, same as the one used for tester calibration.

2.4 METALLOGRAPHY

2.4.1 Location Studied on HAZ

Metallographic examination of the HAZ was done across the mid-thickness of side A marked in Fig. 4. This was the region where HAZ width was uniform. Microstructure pictures were taken starting from the flame-cut edge, travelling through HAZ into the base metal.

2.4.2 Procedure

To retain the flame-cut edge during polishing, the specimen was nickel plated using Watts solution. First the specimen was washed thoroughly with acetone and then it was kept immersed in hot NaOH solution. Then it was rinsed with water

and then it was electroplated with nickel in the Watts solution. The specimen was mounted in bakelite and polished starting from coarse grinding papers (80 mesh) ending with 0.05 micron fine emery paper. It was then washed with water, etched with 2% Nital solution and washed with water, ethanol, and dried. The same procedure was repeated for each steel and for each cutting speed. The pictures were taken at 1000X magnification using oil immersion lens in Nikon Ephiphot microscope.

2.5 TENSION TESTS

2.5.1 Specimen Geometry

Two specimen types were used for the tension tests. Both were derived from ASTM standard A370 sheet type specimen geometries, with some modifications. In the Type 1, the width of the specimen was reduced at the middle region (38.1 mm length) of the gage length to 10.2 mm to facilitate necking and to insure fracture would occur within this region. The actual elongation was measured by marking a 2.54 cm gage length within this region. This specimen geometry is given in Fig. 5 (a). In the Type 2 specimen, along with reduction at the middle region of the gage length, the thickness was increased to 6.4 mm to study the effect of thickness on tensile properties. It is shown in Fig. 5 (b).

2.5.2 Specimen Location in HAZ

The tensile specimens were taken from the HAZ through the plate mid-thickness as shown in Fig. 6. The Type 1 specimen was entirely in the HAZ. Since the HAZ width was uniform in the mid-thickness of the plate representative properties should be measured. Base metal specimens were taken from the same region with respect to rolling directions.

2.5.3 Tensile Test Variables

Temperature and strain rate were the two test variables studied. Specimens were tested at room temperature and one steel-specific low temperature. The ASHTO temperature for which the impact test results are reported for these steels was chosen as the low temperature. This is -34.4°C for A514 steel and -12.2°C for A572 and A588 steels. A low (quasi-static) strain rate and an intermediate strain rate were used to study strain rate effects. Low strain rate required 30 seconds for failure and the intermediate strain rate required 1 second for failure.

2.5.4 Procedure

Tension tests were carried out in an Instron-1035 machine. Low temperature tests were done by keeping the specimen and grips immersed in methanol cooled by a low temperature bath (Endocal) recirculating coils assembly. The desired low temperature was controlled by the recirculating bath. Actual bath temperature was

monitored by an immersion thermometer. Load versus elongation was recorded during the test using an X-Y plotter. Elongation was measured from the change in length of the gage length markings. For each steel three conditions, namely base metal, flame cut at 12.7 cm/min, and flame cut at 38.1 cm/min, were studied. For each test condition three specimens were tested and the mean values of YS, UTS, and percentage elongation were taken. All three steels were tested using the same procedure.

Tension tests with Type 2 specimens (6.4 mm thick) were done for A514 and A572 for both base metal and flame cut at 12.7 cm/min conditions at low temperature and intermediate strain rate. The results were obtained in the same manner as in the case of Type 1 specimens.

2.6 CHARPY V-NOTCH IMPACT TESTS

2.6.1 Specimen Geometry, Location, and Notch Orientation

For Charpy impact toughness studies specimens of three different geometries were used (Fig. 7). The notch angles for these specimens are shown in Fig. 8. The overall dimensions of the normal and sub-size specimens conform to ASTM-E23 specifications. Based on the length along the notch direction with respect to the normal 10 x 10 x 55 mm specimens, the specimens are termed as full size

(normal size) and quarter (thickness) size and half size (sub-size) specimens. It was decided to test for two conditions in relation to the HAZ.

(1) To test the impact toughness of the HAZ alone, the Charpy specimen should lie entirely in HAZ. Since the HAZ width was small in thermal cutting, the quarter size specimen geometry was suitable for carrying out this test. As the thermal cutting direction was along the rolling direction, the specimen was also extracted from the thermally cut plate such that its length was lying along the rolling direction and the notch lying across the HAZ as shown in Fig. 7. The flame-cut surface of the specimen was left unmachined so that the specimen was completely in HAZ.

(2) To test the impact toughness with the crack initiation in HAZ and propagation in base metal, the notch needs to be in HAZ with the rest of the specimens in base metal. As the HAZ width was uniform at the mid-thickness of the plate the specimen needed to be taken from this region. Half size specimens with 0.75 mm notch depth and 2° notch angle (Fig. 8) were suitable for this test with the specimen length lying along rolling direction and the notch length lying along the HAZ.

Full size specimens were made of base metal for all three steels with the same specimen and notch location and orientation as that of quarter size specimens. Quarter and half size specimens were made for the three steels for base metal, flame cut at slower speed, and flame cut at faster speed conditions.

2.6.2 Impact Testing Procedure

A Tinius Olsen Model-774 universal impact testing machine was used for testing the CVN specimens and an Endocal cooling tower unit was used for low temperature tests in the range 0 to -70°C using methanol as the liquid bath. Two walled cylindrical containers were used, with methanol or n-butane inside and pouring liquid nitrogen outside, to get temperatures less than -70°C.

Impact tests were conducted for each steel for different geometries and metal conditions discussed earlier and dial energies were recorded manually.

The impact energies were normalized by dividing them with the area below the notch (ligament area). As there was always time lag between the specimen removal from low temperature bath and impact, the specimen temperature was higher at impact than that of the low temperature bath. Hence, temperature corrections were given to get actual test temperatures based on the heating rate experiment results[40] and time between specimen removal and impact.

2.7 FRACTOGRAPHY

JEOL JSM-35 Scanning Electron Microscope (SEM) with a secondary electron voltage of 25 kV was used for studying the flame-cut surfaces and fractured surfaces. The general procedure followed for analyzing the surface was as follows.

The specimen surface was cleaned ultrasonically in acetone. Then it was mounted in the SEM and the surface was scanned at suitable magnification to study the features of interest. Representative pictures were taken after scanning the whole surface. Flame-cut surfaces of each steel cut at two different speeds, tensile specimen fractured surfaces and CVN impact test fractured surfaces were studied in SEM.

3. RESULTS AND DISCUSSION

3.1 EFFECT OF CUTTING SPEED ON HAZ APPEARANCE, HARDNESS, AND MICROSTRUCTURE

The effect of cutting speed on the HAZ appearance is shown in Fig. 9 for A514. At the slow cutting speed the heat input to the material was high and it resulted in wider HAZ as shown in Fig. 9 (a) whereas at a faster cutting speed the heat input was lower and a correspondingly narrower HAZ was obtained, which is shown in Fig. 9 (b). Since the cutting torch flame is in contact with the top surface, the HAZ is wider at top surface and narrows to a constant width away from the top, at both speeds. Similar effects of cutting speed on HAZ appearance were observed in both A572 and A588 steels.

Microhardness plots for the two cutting speeds for A514 steel are given in Figs. 10 and 11. At both cutting speeds the hardness was maximum near the flame-cut edge and decreased sharply moving towards the base metal. The HAZ hardness was higher for the faster cutting speed, Fig. 11, which can be explained by the respective HAZ microstructures. Figure 12 (a and b) illustrate schematically HAZ microstructures for A514 at the two cutting speeds. The A514 steel HAZ microstructures at three distances from the flame-cut edge for the two cutting speeds are given in Figs. 13 and 14. At the slow cutting speed, the structure observed,

within 0.15 mm from the edge, Fig. 13 (a), was identified as bainite from its appearance and hardness.[41] As the distance from the cut edge was increased, tempered martensite, Fig. 13 (b and c), which was same as the base metal structure, was observed. This explains the lower edge hardness for the slower cutting speed than for the faster cutting speed, where plate and lath martensite formed at distances less than 0.1 mm from the cut edge, Fig. 14 (a) and the martensite was not auto tempered to the extent of the base metal until reaching a distance of 0.8 mm from the edge.

Hardness profiles of A572 for the two cutting speeds are given in Figs. 15 and 16 and HAZ microstructures are shown in Figs. 17 and 18. Hardness profiles of A572 steel, Figs. 15 and 16, and A588 steel, Figs. 19 and 20, revealed that the material cut at higher cutting speed had a higher hardness at distances less than 0.05 mm from the flame-cut edge. This was due to the wider martensitic zone at the higher cutting speed and, conversely, increased auto tempering of the martensite at the slow cutting speed, as illustrated in Fig. 12 (c and f). For A588 cut at the slow speed, the structure changed from tempered martensite to bainite, Fig. 21, up to 4 mm from the flame-cut edge. The base metal structure of ferrite and pearlite was changed to auto tempered (referred as tempered here after) martensite phase near the flame-cut edge for A588 at the faster cutting speed and for A572 at both cutting speeds (Figs. 17, 18, and 22). The cutting speed had little influence on

microhardness values beyond a distance of 0.50 mm from the flame-cut edge for all steels. Within 0.50 mm distance from the flame-cut edge, the hardness decreased from the edge into the HAZ except A588 steel flame cut at the slower speed where it remained nearly constant as the tempered martensite near the edge and the bainite had nearly the same hardness.

3.2 TENSION TEST RESULTS

The YS, UTS, and percentage elongation of 1 mm thick (Type 1) specimens are listed in Tables 3-5, respectively. The UTS & YS comparison for 1 mm thick (Type 1) and 6.4 mm thick (Type 2) specimens along with their percentage elongation values are given in Table 6.

3.2.1 Effect of Cutting Speed

All the three steels, under all test conditions, had higher YS in the flame-cut HAZ than in the base metal except for A514 tested at the high strain rate. Generally the HAZ yield strength was higher for steels flame cut at the faster speed than for those flame cut at the slower speed for all the three steels. The UTS also showed a similar trend.

The increased HAZ yield and ultimate strengths as well as the increased strength with increased cutting speed can be understood from the HAZ microstructures. Since the Type 1 tensile specimens were 1 mm in thickness, the entire flame cut tensile specimen was removed from inside the HAZ (Fig. 6). The tensile specimen properties thus depended on the microstructures contained in the 1 mm distance from the HAZ flame-cut edge. From the schematic representation of the HAZ microstructures for the three steels, Fig. 12 (a-f), it can be seen that for A514 the HAZ within 1 mm from the flame-cut edge consisted of bainite and tempered martensite for slower cutting speed, Fig. 12 (a), and tempered martensite for the faster cutting speed case, Fig. 12 (b). Microhardness analysis showed that the HAZ martensite was less auto tempered than the martensite in base metal. Hence, the high speed flame-cut HAZ had higher strength than the base metal. The flame-cut HAZ resulting from the slower cutting speed received more heat input than the faster cutting speed and, hence, more time for auto tempering the resulting martensite. The less auto tempered martensite had higher strength than bainite formed at slower cutting speed. Hence, the YS and UTS increased with increasing cutting speed. Due to the same reasons a similar trend was observed for A514 tested at low temperature.

For both A572 and A588 steels the presence of tempered martensite in the flame-cut HAZ increased the strength compared to the base metal. As the martensite was auto tempered less when cutting at a higher speed, it had higher strength.

The percentage elongation was less in the flame-cut HAZ than in the base metal for all steels (Table 5). Also the percentage elongation decreased with increased cutting speed. The A514 steel HAZ martensite was less tempered than the base metal. So its ductility was less than the base metal. As the martensite was less auto tempered with increased cutting speed the ductility decreased with increasing cutting speed. As the base metal structure was ferrite and pearlite while flame-cut HAZ had tempered martensite the ductility of base metal was higher than flame-cut HAZ for A572 and A588 steels. The amount of martensite was nearly the same at both cutting speeds for these steels, Fig. 12 (c-f). As the martensite was less auto tempered with increased cutting speed, the ductility decreased with increased cutting speed.

3.2.2 Effect of Strain Rate and Temperature

Generally base metal yield strength and ultimate tensile strength increased with increasing strain rate and decreasing test temperature (Tables 3 and 4) for all three steels. The flow stress[42] is related to strain rate ($\dot{\varepsilon}$) and test temperature (T) as given in the following equation,

$$\sigma = f[\dot{\varepsilon}\exp(\Delta H/Rt)] \quad (1)$$

where ΔH is the activation energy and R is the gas constant. Since the flow stress σ, is related to nominal stress S by the relation,

$$\sigma = S(1+e) \quad (2)$$

where e is the elongation, both the YS and UTS increased with increased strain rate and decreased temperature. Equation (1) has been applied only to metals with homogeneous microstructure throughout the test specimen.[42] As the flow properties depend on a material's dislocation structure, such a simple equation of state as Equation (1) cannot be applied to a flame-cut HAZ due to its non-uniform microstructure. The overall effect of strain rate and temperature on the flame cut induced HAZ tensile properties was less than the effect of cutting speed.

3.2.3 Effect of Specimen Thickness

Increasing the base metal tensile specimen thickness slightly increased both the UTS and YS values (Table 6) for A514 base metal and flame-cut HAZ and A572 base metal but did not increase the YS of A572 base metal. The increase in strength with increase in specimen thickness was due to increased specimen thickness constraint with increasing thickness. But in the case of A572 the YS and UTS values for flame cut condition decreased with increased specimen thickness. As the HAZ was very narrow compared to the gage thickness in the thicker

specimen, HAZ contribution to tensile properties was less and so there was little difference in YS and UTS values between base metal and flame-cut metal. Since the specimen sizes had different cross sectional areas, their elongations cannot be directly compared since elongation is directly proportional to the square root of the tensile specimen cross sectional area.[43] Area normalization of the thicker specimen elongation data was done relative to the thinner specimen, Table 6. The normalized percentage elongation for the specimen flame cut at the slower speed increased with increasing thickness for both steels, due to the increased amount of more ductile base metal in the thicker specimen. The percentage elongation for base metal increased slightly with increasing specimen thickness for A514 steel but for A572 steel there was a decrease in normalized percentage elongation. Since elongation depends on the microstructure of the material, base metal elongation was nearly same with increasing thickness. Additional specimens would need to be tested to confirm the anomalous decrease of elongation for base metal of A572 steel with increasing tensile specimen thickness.

3.3 CHARPY V-NOTCH IMPACT TEST RESULTS

3.3.1 Effect of Specimen Size

Area normalized CVN energy versus test temperature plots were made for each steel (base metal) for the three different specimen sizes to study the effect of

specimen size on the impact properties. Results for the three steels are presented in Figs. 23-25. The lower shelf energy values were the same but the upper shelf energy values varied for the three sizes in all the steels. This is because normalizing the energy values based on the specimen cross sectional area (A), is applicable only when the fracture mode is fully cleavage, which was the case only at the lower shelf. Better correlation of upper shelf energy data was obtained for the three sizes by applying volume ($A^{3/2}$) normalization.[38] The volume normalized plots are shown in Figs. 26-28. Lower upper shelf energies were obtained for full size specimens than for sub-size specimens,[44] due to the increased constraint present in the thicker specimen.

The transition temperature for quarter size specimens was less than for the full size specimen since the plastic constraint at the notch was reduced with the reduced width, Figs. 23-25. However, the half size specimen had a higher transition temperature than both the other sizes, since the plastic constraint at the notch was much higher due to a higher flank angle of the notch in this case, Fig. 8. Plastic constraint factor at notch produces triaxial state of stress, and from the relation

$$K_\sigma = (1 + \frac{\pi}{2} - \frac{\omega}{2}),$$

where K_σ is the maximum plastic stress concentration and ω is the included flank angle of the notch, K_σ values for full, quarter, and half size specimens were obtained as 1.79, 1.79, and 2.54, respectively. The increased plastic stress

concentration of half size specimen explains the higher transition temperature of these specimens compared to the full size and quarter size specimens.

3.3.2 Effect of the Notch Location in HAZ

The effect of the notch location in HAZ was studied by plotting area normalized energy values versus temperature for each specimen size for three test conditions, Figs. 29-34.

The trend of these plots can be understood by schematic diagrams, Figs. 35-37, of notch orientation in relation to the microstructure of the HAZ. In quarter size specimens, most of the notch root structure was tempered martensite for A514 steel, Fig. 35 (a and c), and tempered martensite and fine pearlite for A572 and A588 steels, Figs. 36-37, except for A588 flame cut at the slower cutting speed where most of the notch root microstructure was tempered martensite and bainite, Fig. 37 (a). But in the case of half size specimens, due to the orientation and since the notch depth was 0.75 mm, the notch was entirely in tempered martensite for A514 steel, Fig. 35 (b and d), and was entirely in fine pearlite for A572 and A588 steels, Figs. 36 and 37, except A588 flame cut at slower speed where the notch root was entirely in bainite, Fig. 37 (c).

3.3.3 Effect of Cutting Speed

The A514 steel impact toughness values in both quarter size, Fig. 29, and half size specimens, Fig. 32, were nearly identical, because A514 steel is quenched and tempered and flame cutting did not change the microstructure very much. The flame-cut HAZ microstructures were tempered martensite and bainite for the slower cutting speed and tempered martensite for the faster cutting speed. In quarter size A514 specimens the metal had slightly more impact toughness than A514 flame cut at the faster speed. This small difference was due to the presence of bainite in samples cut at the slower cutting speed and due to more auto tempering of the martensite at slower speed. For flame-cut half size specimens the impact energy values were close to one another as the notch was entirely in tempered martensite. In half size specimens, the specimens taken from the top of mid-thickness had higher impact toughness than those taken from the bottom of the mid-thickness. As the top of the plate was in contact with the cutting torch, there was more auto tempering of the HAZ microstructure at the top of the mid-thickness than at the bottom. This explains the higher toughness of the specimens taken form the top of the mid-thickness than those taken from the bottom.

Both A572 and A588 steels showed decreased impact toughness and increased transition temperature with increasing cutting speed. This was due to the tempered martensite present in flame-cut HAZ while the base metal consisted of ferrite and pearlite, and more auto tempering of martensite in the case of specimens cut at

slower cutting speed. Again in the case of half size specimens, for each flame cut steel, the impact toughness values were similar since the notch was entirely in the ferrite and pearlite region.

3.4 FRACTOGRAPHY

The appearance of flame-cut surfaces for A514, A572, and A588 steels at the two cutting speeds are given in Figs. 38 through 41. The scanning electron micrographs of fractured surfaces of tension tests and impact tests are given in Figs. 42 through 54. A514 steel had very few cracks, Fig. 38 (a and b), on the flame-cut surface while A572, Fig. 39 (a and b) and A588, Fig. 40 (a and b) had cracks all over the surface with A572 having more cracks than A588 steel.

The fracture surfaces in tension tests for A572 steel base metal at room temperature are shown in Fig. 42. The dimples at both the low strain rate, Fig. 42 (a), and the intermediate strain rate, Fig. 42 (b), show ductile mode of failure. The flame-cut steel at faster cutting speed also shows ductile dimple failure, Fig. 43 (a and b), on the fractured surfaces at both strain rates. The large pits might have been caused by inclusions being pulled out during fracture. Even though the fractured surfaces were flat in low temperature tests, the fracture appearance, Fig. 44 (a and b), always exhibited a ductile failure mode. Thus the flame-cut surface cracks did not induce brittle failure.

A similar trend was seen in both A514 and A588 steels. Fig. 45 shows fracture surfaces for A514 steel for two extreme cases, one for base metal tested at room temperature and low strain rate, Fig. 45 (a), and the other for faster cutting speed flame cut condition at low temperature and intermediate strain rate, Fig. 45 (b). Both show ductile mode of failure. Increasing the specimen thickness to 6.4 mm did not produce brittle failure, Figs 46 and 48.

The fractured surfaces for A572 steel in CVN impact tests, for full, quarter, and half size specimens, are revealed for the lower shelf energy value (a), for the transition temperature region (b), and for the upper shelf energy value (c), in Figs. 48 through 54.

Room temperature tests (upper shelf), for A572 base metal (full size), produced dimple fractured surfaces, as seen in Fig. 48 (c) showing ductile fracture. At the transition temperature region, Fig. 48 (b), and at low temperature, Fig. 48 (a), fracture occurred by quasi cleavage mode. For quarter size A572 steel base metal, both at room temperature and transition temperature region, Fig. 49 (b and c) respectively, ductile fracture mode was observed and at low temperature quasi cleavage fracture, Fig. 49 (a), was observed. For the flame-cut steel, at slower cutting speed, (quarter size specimen) the fracture was ductile at room temperature and quasi cleavage type at transition temperature region and lower shelf temperature (Fig. 50) and for the flame-cut steel at faster cutting speed the fracture was ductile at room temperature and transition temperature but quasi cleavage at lower shelf

temperature as shown in Fig. 51. Similar fracture appearance trends were seen in half size CVN specimens for both base metal and flame-cut conditions, the fracture mode varying between ductile and quasi cleavage at the transition temperature, ductile at high temperature and quasi cleavage type at low temperature. These are shown in Figs 52 to 54.

Similar fracture appearances were seen for both A514 and A588 steels in impact tests. From the presence of flame-cut surface cracks, brittle cleavage failure was expected to occur in Charpy impact tests at low temperature. Though the test conditions, like low temperature and high strain rate of impact tests, were favorable for brittle fracture, fully cleavage facets, as would be seen in failure entirely by brittle mode, did not occur in any of these steels. These results show that even in impact tests the flame-cut surface cracks did not produce brittle failure in the temperature range studied. These results also show that none of the constituents of the HAZ, like martensite, result in brittle fracture.

3.5 SUMMARY OF RESULTS

1. The HAZ of each alloy was wider at the top of the plate, decreasing to a narrower, essentially constant width away from the top. The width decreased with increase in cutting speed.

2. The microhardness values were maximum at/near the flame-cut edge and decreased towards the base metal in all the steels. The maximum hardness increased with increase in cutting speed.
3. The HAZ consists of mostly tempered martensite in the case of all the steels with the presence of bainite in the case of A514 steel flame cut at slower cutting speed and fine ferrite and pearlite in the case of A572 and A588 steels.
4. The YS and UTS values increased and percentage elongation decreased from base metal to flame cut metal and with increase in cutting speed in all three steels. A change in strain rate, temperature, and specimen size had little if any effect on the tensile properties.
5. Generally, impact toughness decreased and transition temperature increased with increase in cutting speed in the three steels. Decrease in specimen size decreased the transition temperature.
6. Flame-cut surface cracks did not induce brittle fracture in either tension and CVN impact test, at all test conditions, in all three steels.

4. CONCLUSIONS AND SUGGESTIONS FOR FURTHER WORK

4.1 CONCLUSIONS

1. The flame cut HAZs of the three steels had higher strength, lower ductility and lower impact toughness values than the base metal.
2. Brittle cleavage fracture was not produced in the temperature and strain rate regime tested by flame-cut HAZ in all three steels in tensile and CVN impact tests.

4.2 SUGGESTIONS FOR FURTHER WORK

1. It is recommended that the various HAZ structure's properties of these steels can be studied individually by knowing the heating and cooling cycles during flame cutting and simulating the same on individual test specimens.
2. Conduct surface chemical analysis to explain the change in hardness near the flame-cut surface.
3. Conduct fatigue tests of the flame-cut steels to test the resistance of the HAZ structure to the flame-cut surface crack propagation.

REFERENCES

1. Alexander D. Wilson, Ed., "Thermal Cutting of HSLA Bridge Steels," Final Report, American Iron and Steel Institute Sponsored Project, Aug 1987, p 2 and Appendix A.
2. Rosalie Brosilow, "Thermal Cutting," Metals Hand Book, vol 6, pp 896-925.
3. Manfred Nicolai, Griesheim Gmblt. Darmstadt, A Graham, "Flame Cutting in Modern Industrial Production," Welding Review, Nov 1983, pp 297-300.
4. Brayton, W.C., J.A. Hogen, "Shipyard Welding & Cutting, Plasma Processes of Cutting and Welding," Final Report Sponsor United Carbide Corp., Forensa, S.C., Maritime Administration, Washington, D.C.; Bethlehem Steel Corp., Sparrows Pt., MD, Rep No. MA-RD-77039, Feb 1976, p 85.
5. Geary, D., The Welder's Bible, A Hands-on Guide to All Kinds of Oxy-Acetylene Welding and Cutting, TAB Books Inc., Blue Ridge Summit, PA, 1980, p 416.
6. Kearns, W.H., Ed, Welding Processes-Arc and Gas Welding and Cutting Brazing and Soldering, Welding Hand Book, vol 2, 7th ed, American Welding Society, Miami, FL, 1978.

7. Smith, D., "Flame Cutting Shapes, Edges and Holes," Chapter 5, Welding Skills and Technology, Mercer, W.H., R.E. Barnett, Eds, M°Grawhill, NY, 1984,

pp 99-137.

8. The Oxy-Acetylene Hand Book, Union Carbide Corporation, Linde Division, New York, NY, April 1972.

9. Nishiguchi, K., K. Matsuyama, "Kerf Formation and Slag Adhesion in Plasma Jet Cutting with Arc Transfer," Soudage Tech Connexes, 34, (Y2), Jan-Feb 1980, pp 49-54.

10. Shukhmaister, V.L., V.T. Kotik, "Improving the Quality of Edges in Air Plasma Cutting," Svar. Proiz, No. 3, 1981, p 28.

11. Thomas, H. and F. Goldberg, "Recommendations Concerning the Quality of Thermal Cut Surfaces in Steel Structures Subjected to Fatigue Loading," Welding in The World, vol 17, No. 7/8, International Institute of Welding, 1979, pp 192-195.

12. Kugler, A.N., Oxyacetylene Welding and Oxygen Cutting Instruction Course, Air Reduction Company, Inc., New York, NY, June 1966.

13. Baus, R. and W. Chapean, "Application du Soundage aux Constructions," Sciences et Letters, Liĕge.

14. Netherlands Institute of Welding-Working Group 1913, "The Properties of Flame Cut Edges," Final Report, May 1973.

15. Piraprez, E., "Fatigue Strength of Flame Cut Plates," Fatigue of Steel and Concrete Structures, Proceedings IABSE Colloquium Lausanne, March 1982, IABSE Reports, vol 37, Publ. International Association for Bridge and Structural Engineering, Zurich, Switzerland, 1982, pp 23-26.

16. Von Kurlagunda N. Rao, Jurgen Ruge und Heinz Schimmoller, "Determination des Contraintes Rēsiduelles dues ā l'Oxy Coupage des Tôles," For Schunng n°, 36, 1970.

17. Young, B.W. and J.B. Dwight, Residual Stresses due to Longitudinal Welds and Flame Cutting, University of Cambridge, Department of Engineering.

18. Jurgen Ruge und Alfred Krahl, "Etude dela Capacitē au formage ā Froid des Zones Thermiquement Influencēes des Tôles Oxycoupēes," Schweissen und Schneider, n°, 19, 1967.

19. Nibbeing, J.J.W., H. Thomas, and T.J. Bos, "The Properties of Plasma Cut Edges," Welding in the World, vol 18, Nos. 9&10, 1980, pp 182-195.

20. Honda, H., S. Kitamure, and T. Yamada, "On the Strength of Racks for Jack-up Units," No. 1, Report: Fatigue Behaviour of Large Scale, Torch Cut and Machined High Tensile Strength Steel Racks,: Bulletin of the JSME, vol 27, No. 234, Dec 1984, pp 2879-2888.

21. Ho, N-J, F.V. Lawrence, C.J. Alstetter, "The Fatigue Resistance of Plasma and Oxygen Cut Steel," Welding Research Supplement," Nov 1981, pp 231-236.

22. Kharitonov, E.P., et al, "The Surface Plasma-Arc Cutting of Low-Alloy Steels 10Kh SND and 10Kh N1M," Svar. Proiz, No. 11, 1980, pp 33-34.

23. Goldberg, F., "Influence of Thermal Cutting and Its Quality on the Fatigue Strength of Steel," Welding Journal, 52 (9), 1973, pp 392s-404s.

24. Koenigsberger, F. and Z. Farcia-Margin, "Fatigue Strength of Flame-Cut Specimens of Bright Mild Steel," British Welding Journal, Jan 1965, pp 37-41.

25. Koenigsberger, F. and H.W. Green, "Fatigue Strength of Flame-Cut Specimens in Block Mild Steel," British Welding Journal, July 1955, pp 313-321.

26. Plecki, R., R. Yeske, C. Alstetter, and F.V. Lawrence, Jr., "Fatigue Resistance of Oxygen-Cut Steel," Welding Journal, 56 (8), 1977, pp 225s-230s.

27. Gross, J.H., "Transition Temperature Data for Five Structural Steels," Weld Research Council Bulletin, No. 147, Jan 1970.

28. M^{c}Nicol, R.C., "Correlation of Charpy Test Results for Standard and Nonstandard Size Specimens," Welding Journal, 44 (9), 1965, pp 3855-3935.

29. Hogen, B., and B. Cottrell, "Behaviour of Sub-Standard Charpy V-Notch Impact Specimens for Mild Steel," British Welding Journal, 15 (12), 1968, pp 584-589.

30. Zeno, R.S., "Effect of Specimen Width on the Notch Bar Impact Properties of Quenched and Tempered and Normalized Steels," ASTM Special Technical Publication, 176, 1955, pp 59-69.

31. Cracknell, A., "Comments Submitted by the United Kingdom on the Subject of Subsidiary Standard Test Pieces," Submitted to ISO/TC 17/WG15, document (United Kingdom-1), N30, Jan 1978, pp 1-7.

32. Embury, J.D., N.J. Petch, A.E. Wraith, and E.S. Wright, "The Fracture of Mild Steel Laminates," Trans Metallurgical Soc. of AIME, 239 (1), 1967, pp 114-118.

33. Fergusen, B.L., "The Relationship Between Splitting Phenomena and Sample Thickness in Charpy V-Notch Impact Testing," Proceedings Symposium, What Does the Charpy Test Really Tell Us?, Publ. American Soc. for Metals, 1978, pp 99-107.

34. Hussmann, W., and Krisch, "Effect of Test Bar Width and Structure on the Notched Bar Impact Strength of Structural Steels for General Use," Archir für das Eisenhüttenwesen, 43 (9), 1972, pp 675-679, (in Germany), Welding Institute Trans. 586, Jan 1982, (in English).

35. Kuvera, J., I. Talpa, and V. Smid, "On the Fracture of Laminated Charpy Specimens," Proceedings of Conference, Analytical and Experimental Fracture Mechanics, Publ. Sijthoff and Noordhoff, 1981, pp 515-525.

36. Towers, O.L., "Testing Sub-Size Charpy Specimens; Part 1- The Influence of Thickness on the Ductile/Brittle Transition," Metal Construction, March 1986, pp 171R-176R.

37. Towers, O.L., "Testing Sub-Size Charpy Specimens; Part 3- The Adequacy of Current Code Requirements," Metal Construction, May 1986, pp 319B-325B.

38. Corwin, W.R., and A. M. Hougland, "Effect of Specimen Size and Material Condition on the Charpy Impact Properties of 9 Cr-1Mo-V-Nb Steel," The Use of Small-Scale Specimen for Testing Irradiated Material, ASTM STP 888, W.R. Corwin and G.E. Lucas, Eds., American Society for Testing and Materials, Philadelphia, PA 1986, pp 325-338.

39. Lucas, G.E., G.R. Odette, J.W. Sheckherd, P. M°Connell, and J. Perrin, "Sub-Size Bend and Charpy V-Notch Specimens for Irradiated Testing," The Use of Small Scale Specimen for Testing Irradiated Material, ASTM STP 888, W.R. Corwin and G.E. Lucas, Eds., American Society for Testing and Materials, Philadelphia, PA, 1986, pp 305-324.

40. Department of Materials Science and Engineering, "Heating Rate Experiments on CVN Impact Specimens," Oregon Graduate Center, Beaverton, OR, (Unpublished).

41. Hehemann, R.F., "Ferrous and Non-Ferrous Bainitic Structures," Metals Hand Book, vol 8., pp 194-196.

42. Zener, C., J.H. Hollomon, "Effect of Strain Rate Upon Plastic Flow of Steel," Journal of Applied Physics, vol 18, 1944, pp 22-23.

43. Barba, M.J., Mem. Soc. Ing. Civils, pt. 1, 1980, p 682.

44. Towers, O.L., "Testing Sub-Size Charpy Specimens, Part 2- The Influence of Specimen Thickness on Upper Shelf Behaviour," Metal Construction, Apr 1986, pp 254R-258R.

Table-1 : Steels studied

1. A514 Rolled and austenized at 898.9°C for 1hr, water quenched and tempered at 648.9°C for 1hr and aircooled.
2. A572 Rolled and aircooled.
3. A588 Rooled and aircooled.

Physical properties

Steel	Yield strength MPa	UTS MPa	Percentage elongation(5.1cm)	CVN Joules (J)
A514	834.3	889.5	27	42 at -34.4°C
A572	427.5	561.9	22	104.4 at-12.2°C
A588	355.1	520.6	17	195.3 at-12.2°C

Chemical composition

Steel	Percent by weight												
	C	Mn	P	S	Si	Cu	Ni	V	Al	Cr	Mo	Ti	B
A514	.19	.92	.009	.009	.26	.23	.1	.04	.059	.46	.18	.034	.0019
A572	.15	1.3	.009	.009	.29	-	-	.02	.037	-	-	-	-
A588	.14	.95	.007	.007	.39	.27	.06	.02	.04	.45	.03	-	-

Table-2 : Flame cutting parameters

Torch tip	Clearance between tip & plate (mm)	Pressure x 10^5 Pa		Cutting speed cm/min.	
		O_2	C_2H_2	Slower cutting speed	Faster cutting speed
#2	3.2 to 4.8	42.0	5.0	12.7	38.1

Table-3 : Tension test results : Yield strength

Yield Strength (MPa)							
Room temperature (R.T.) 80.6F (27°C) Low temperature (L.T) 10F (-12.2°C) for A572 and A588 steels -30F (-34.4°C) for A514 steel.							
Metal condition	Temperature	A588		A572		A514	
		Low strain rate	Intermediate strain rate	Low strain rate	Intermediate strain rate	Low strain rate	Intermediate strain rate
Base metal	R.T.	335.8	376.5	401.3	408.9	837.1	897.1
	L.T.	328.9	363.4	415.8	495.1	934.9	915.7
Flame cut at slower cutting speed	R.T.	634.3	617.8	619.9	602.6	882.6	834.3
	L.T.	651.6	585.4	617.1	605.4	934.9	779.1
Flame cut at faster cutting speed	R.T.	686.7	544.1	666.1	585.4	1039.8	969.4
	L.T.	597.8	561.9	601.9	452.3	1029.4	1043.9

Table-4 : Tension test results : Ultimate tensile strength

Ultimate tensile strength (MPa)							
Room temperature (R.T.) 80.6F (27°C) Low temperature (L.T) 10F (-12.2°C) for A572 and A588 steels -30F (-34.4°C) for A514 steel.							
Metal condition	Temperature	A588		A572		A514	
		Low strain rate	Intermediate strain rate	Low strain rate	Intermediate strain rate	Low strain rate	Intermediate strain rate
Base metal	R.T.	519.2	545.4	566.8	581.9	897.1	928.1
	L.T.	506.1	537.8	601.2	641.9	1001.8	1005.9
Flame cut at slower cutting speed	R.T.	813.6	823.3	763.9	776.4	1043.4	1001.2
	L.T.	865.3	795.7	804.7	781.2	1074.2	957.1
Flame cut at faster cutting speed	R.T.	856.4	774.9	899.8	841.2	1227.3	1170.8
	L.T.	770.9	735.7	815.7	712.3	1232.8	1305.2

Table-5 : Tension test results : Percentage elongation

Percentage elongation (2.54 cm gage length)							
Room temperature (R.T.) 80.6F (27°C) Low temperature (L.T) 10F (-12.2°C) for A572 and A588 steels -30F (-34.4°C) for A514 steel.							
Metal condition	Temperature	A588		A572		A514	
		Low strain rate	Intermediate strain rate	Low strain rate	Intermediate strain rate	Low strain rate	Intermediate strain rate
Base metal	R.T.	20.3	17.9	20.9	17.7	8.5	7.8
	L.T.	19.6	11.3	19.0	19.1	6.5	6.1
Flame cut at slower cutting speed	R.T.	9.2	8.3	7.2	6.9	4.7	4.7
	L.T.	7.2	6.4	7.5	5.9	3.8	4.1
Flame cut at faster cutting speed	R.T.	7.9	6.9	5.5	2.2	3.1	3.0
	L.T.	5.4	5.2	4.6	4.1	2.8	2.6

Table-6 :

Tension test results : Effect of specimen thickness

Tested at low temperature and intermediate strain rate for base metal and flame cut metal at slower speed. L.T. : 10F (-12.2°C) for A572 and -30F (-34.4°C) for A514.						
Steel	Thickness (mm)	Metal	UTS MPa	YS MPa	Percentage elongation (2.54 cm)	Normalized percentage elongation
A514	1.0	Base metal	1006	916	6	6
		Flame cut metal	957	779	4	4
	6.4	Base metal	1056	985	20	8
		Flame cut metal	1052	896	19	7
A572	1.0	Base metal	642	495	19	19
		Flame cut metal	781	605	6	6
	6.4	Base metal	656	461	27	11
		Flame cut metal	725	504	24	10

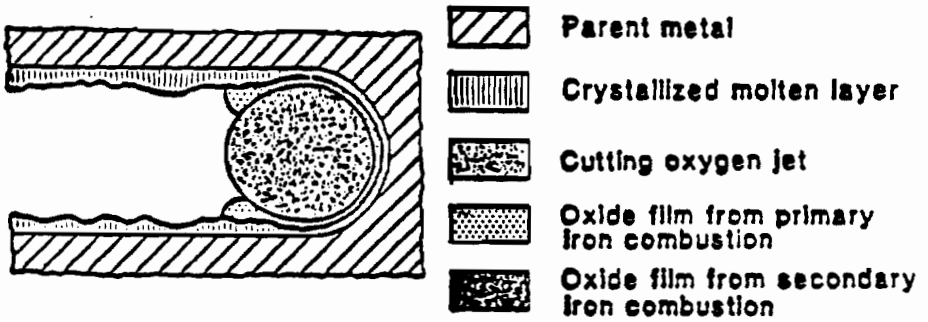

Figure-1 : Flame cutting process in the direction of the cut. (Manfred Nicolai, 1983)

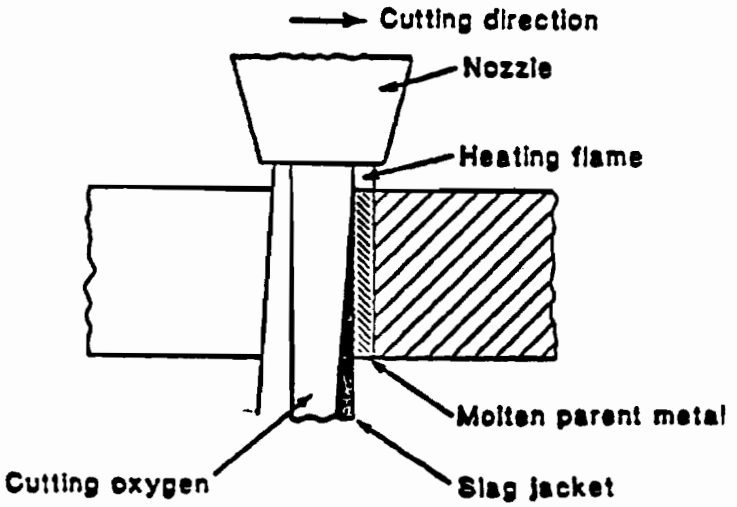

Figure-2 : Schematic view of the cutting process. (Manfred Nicolai, 1983)

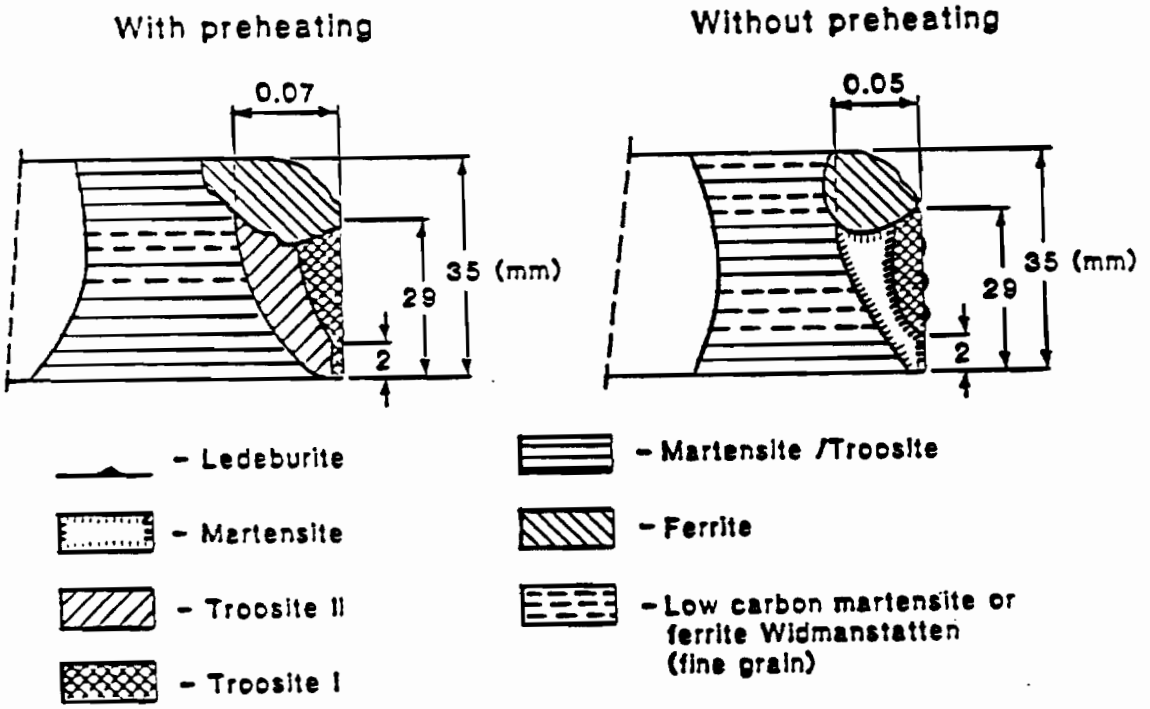

Figure-3 : Structure of the heat affected zone (HAZ) after oxygen cutting. (Piraprez, 1982)

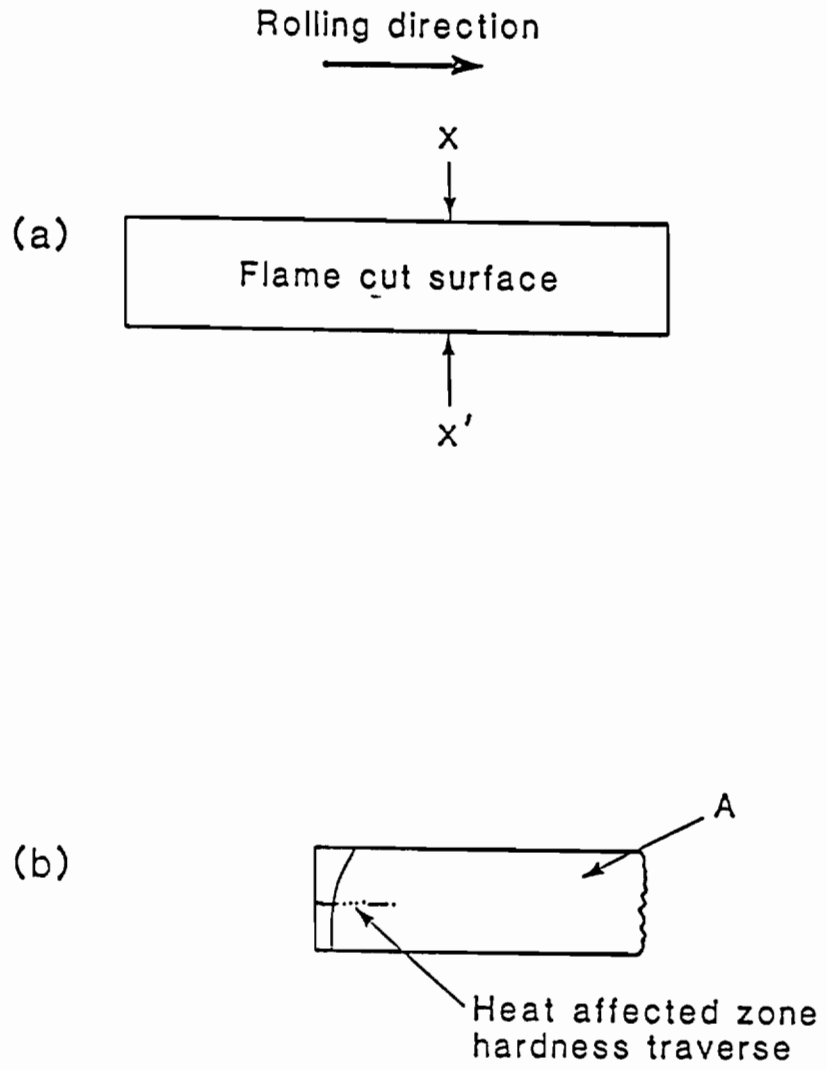

Figure-4 : Hardness tests and metallographic examinations' location on HAZ.

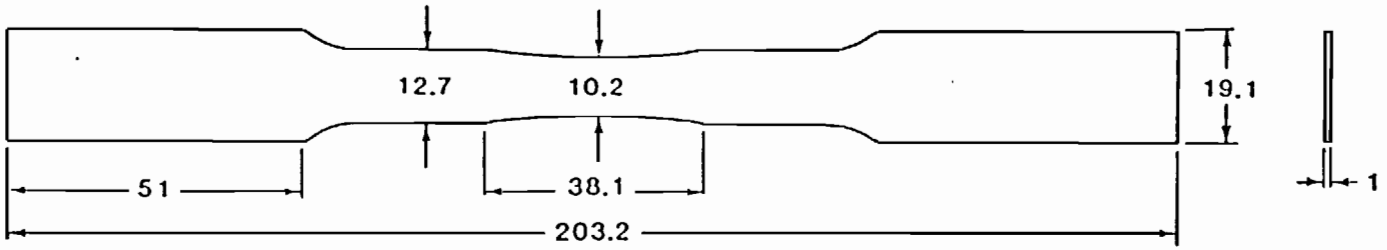

(a) Type-1

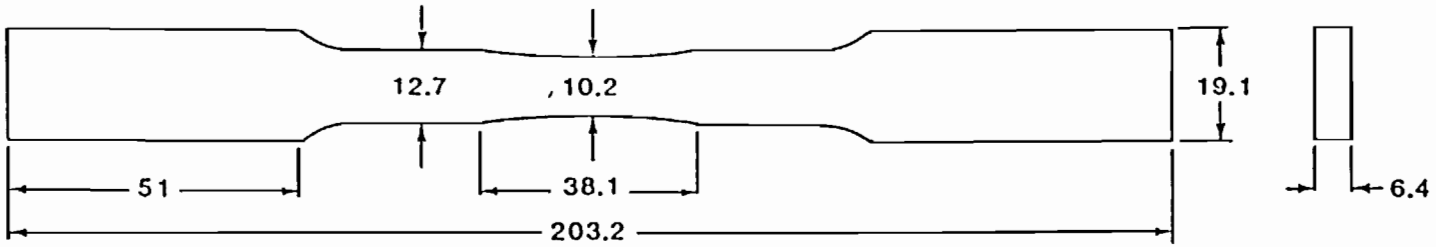

(b) Type-2

Dimensions in mm

Figure-5 : Tensile specimens' geometry.

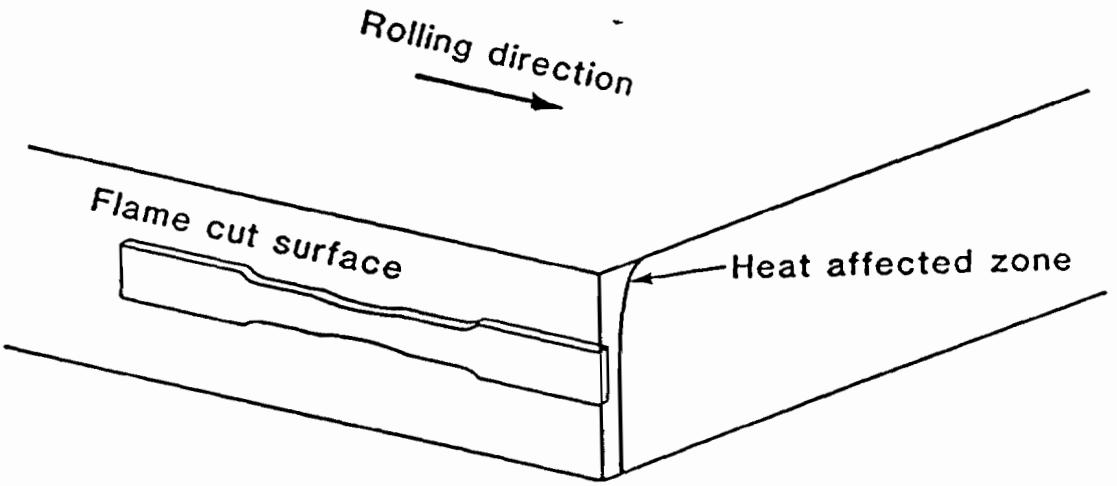

Figure-6 : Tensile specimens location in HAZ.

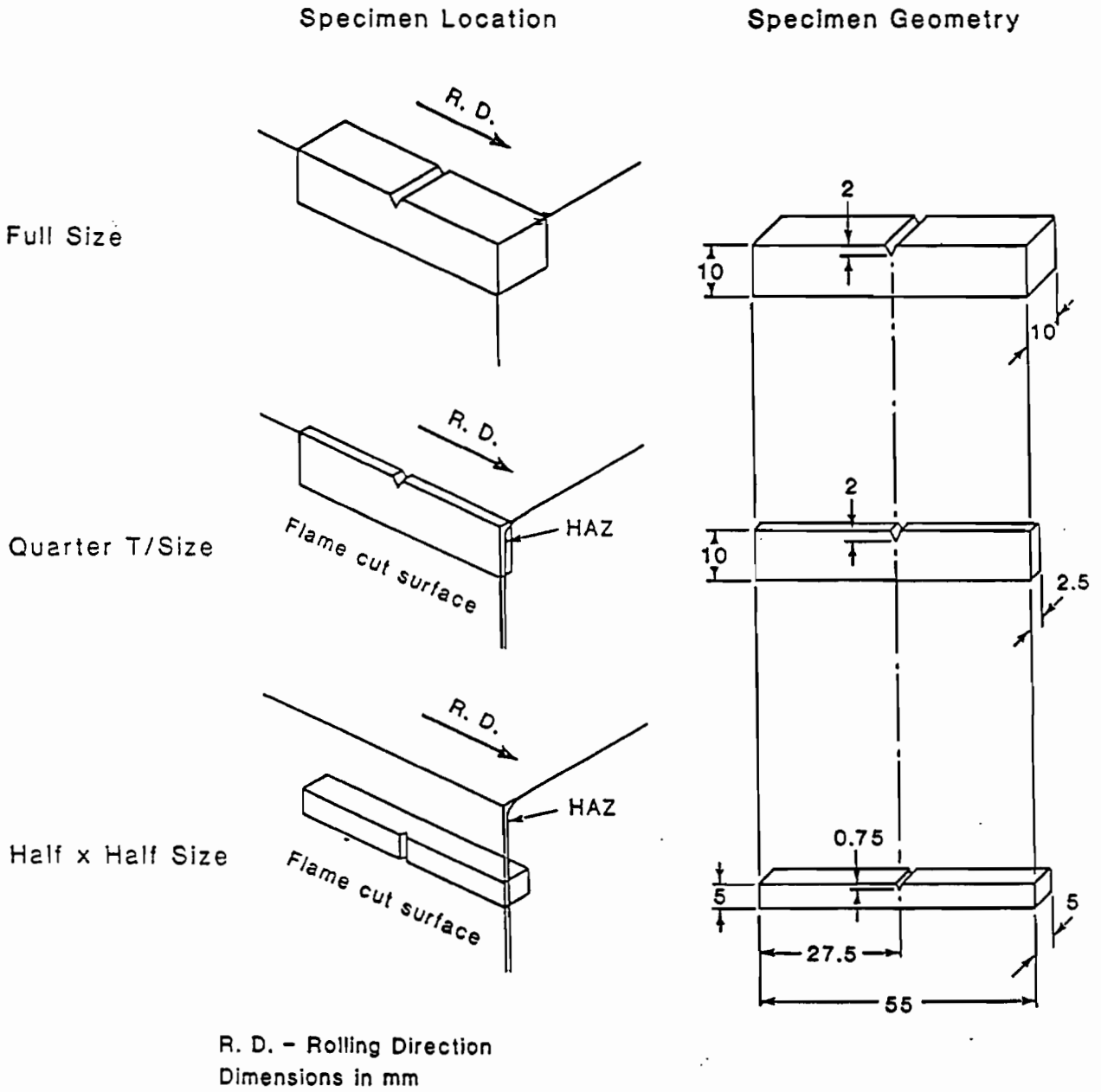

R. D. – Rolling Direction
Dimensions in mm

Figure-7 : Charpy V-notch (CVN) specimens' geometry and notch orientation.

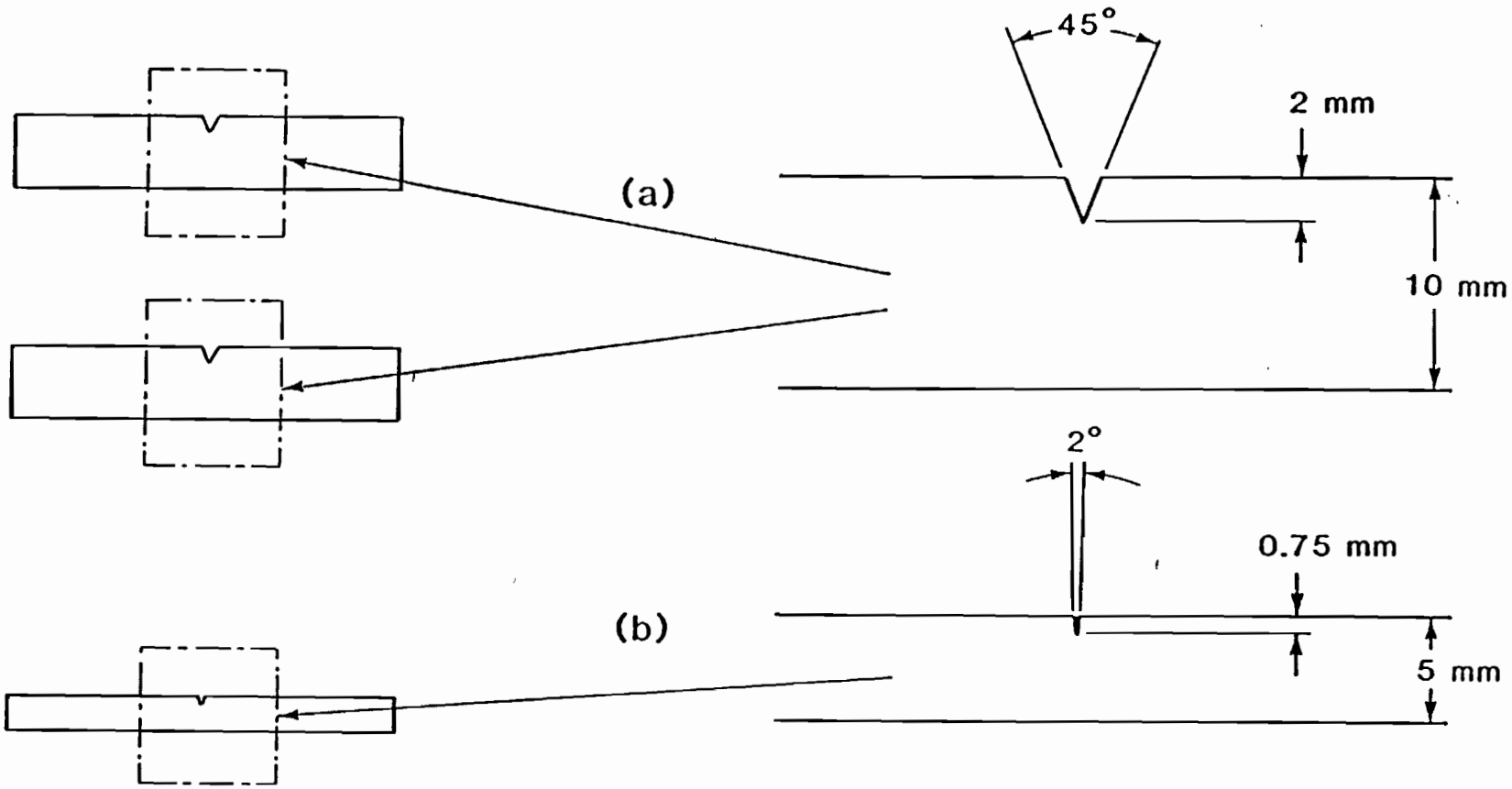

Figure-8 : Notch angles for full size and quarter size (a), and half size (b) CVN specimens.

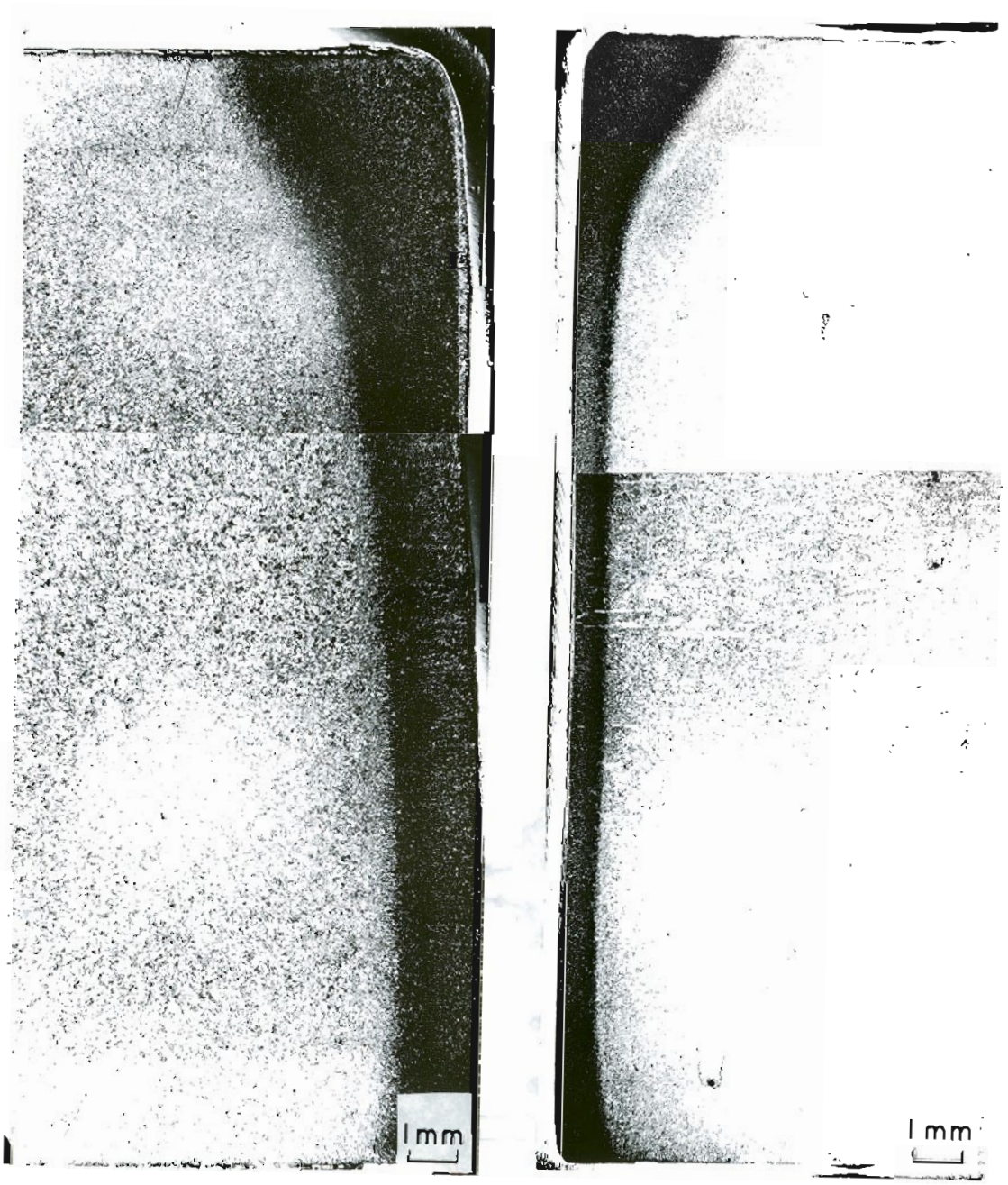

(a) Flame cut at slower cutting speed

(b) Flame cut at faster cutting speed

Figure-9 : Optical micrographs for A514 steel HAZ.

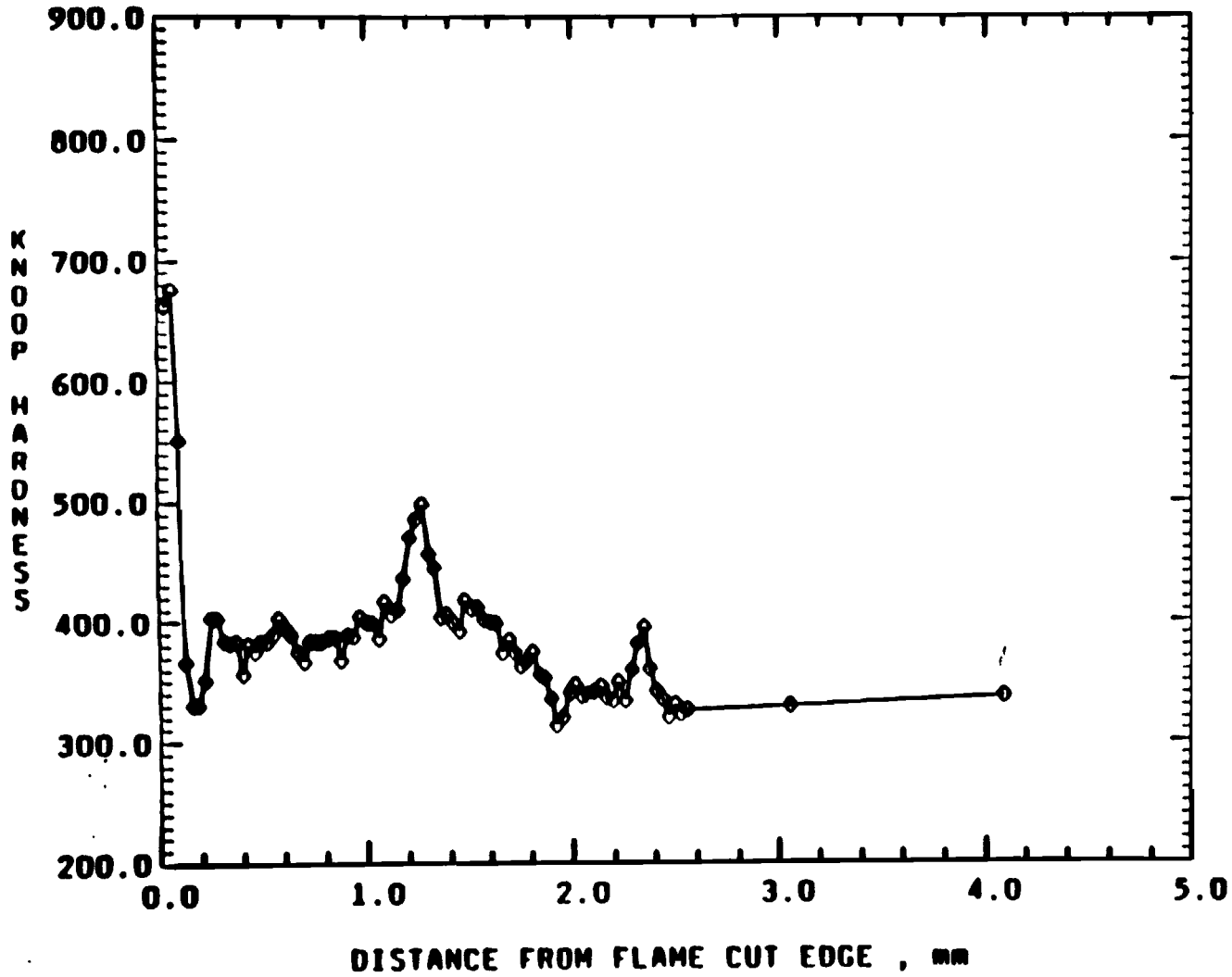

Figure-10 : Microhardness plot across HAZ for A514 steel flame cut at slower cutting speed.

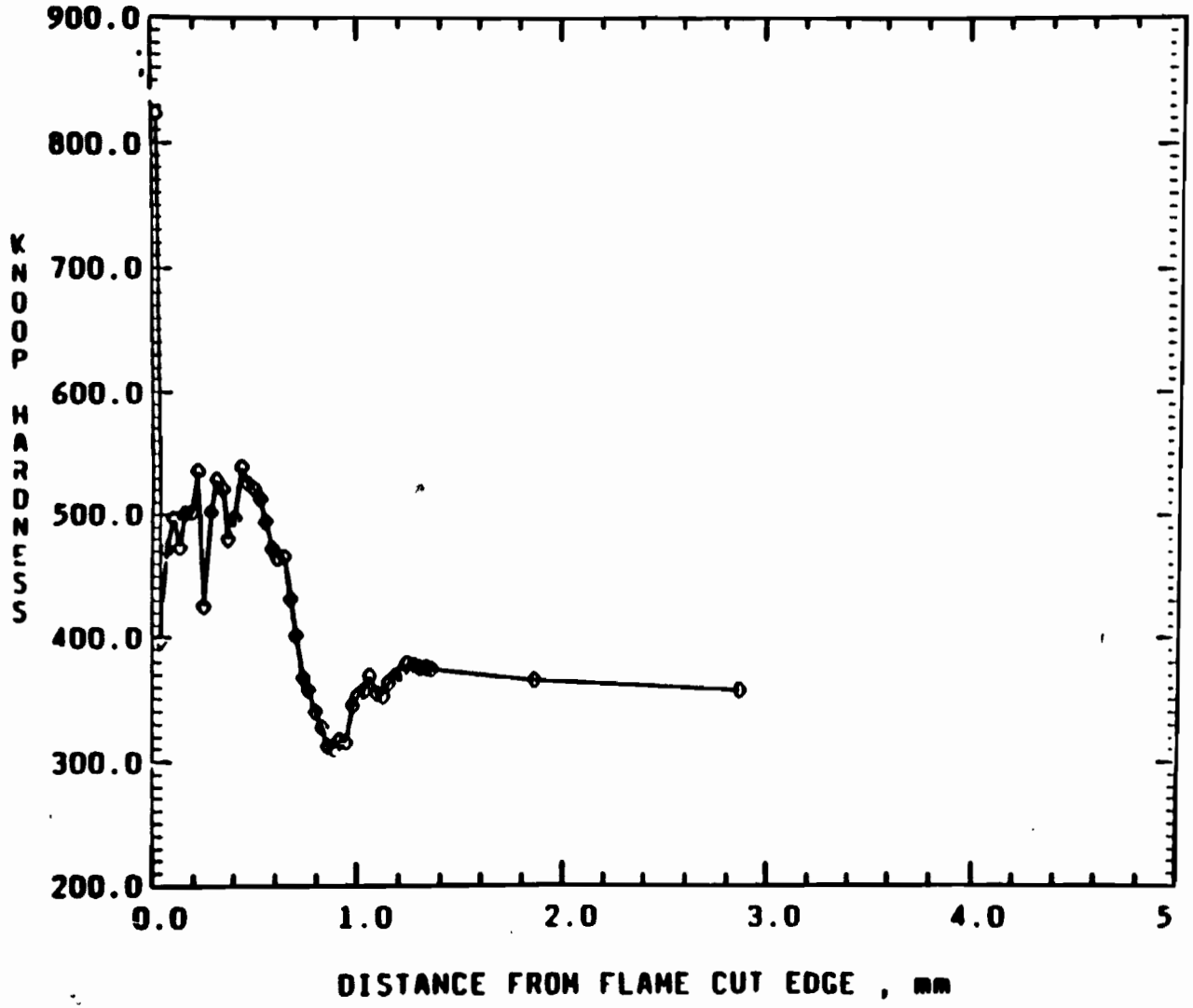

Figure-11 : Microhardness plot across HAZ for A514 steel flame cut at faster cutting speed.

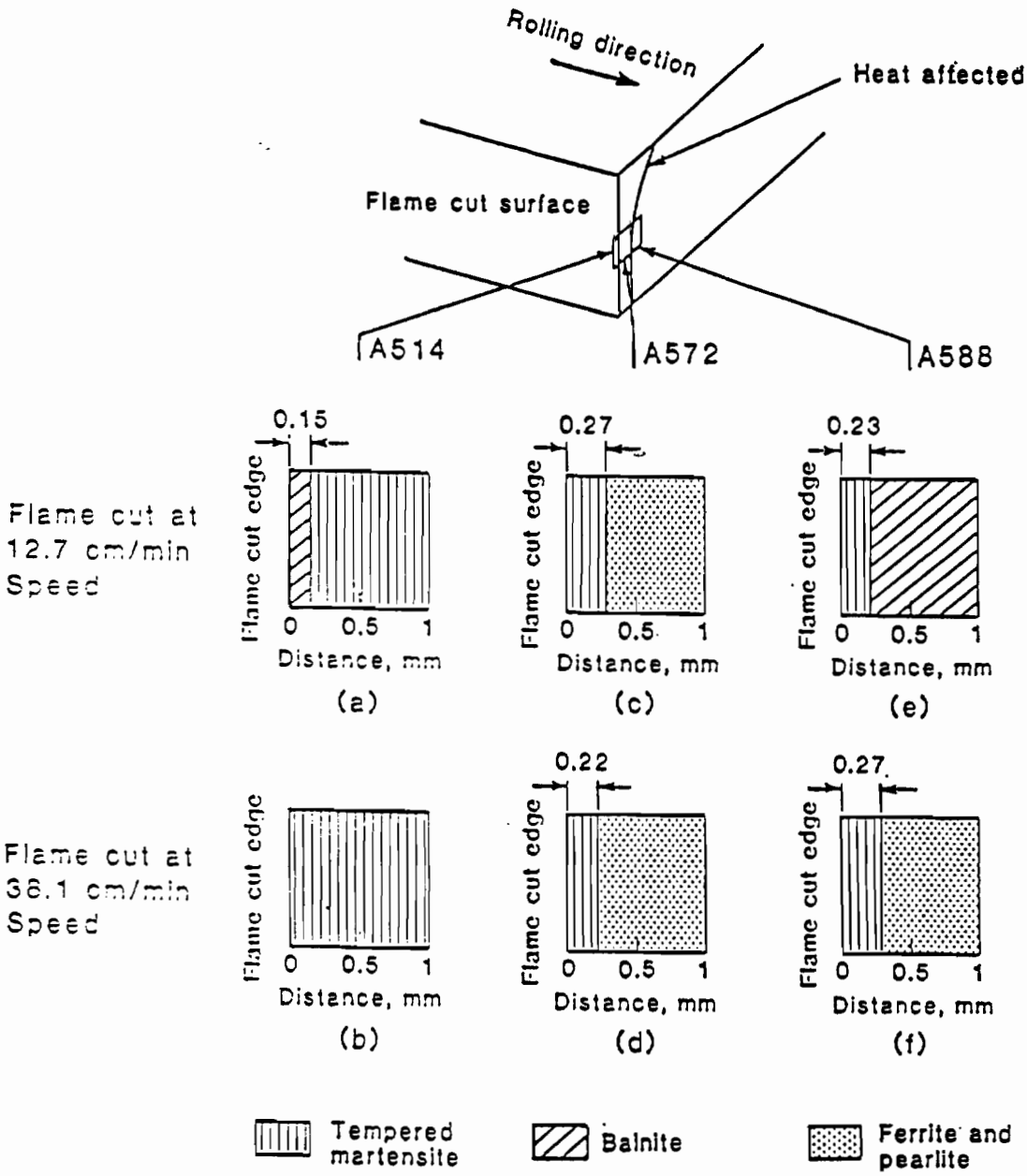

Figure-12 : Schematic representation of flame cut HAZ microstructures.

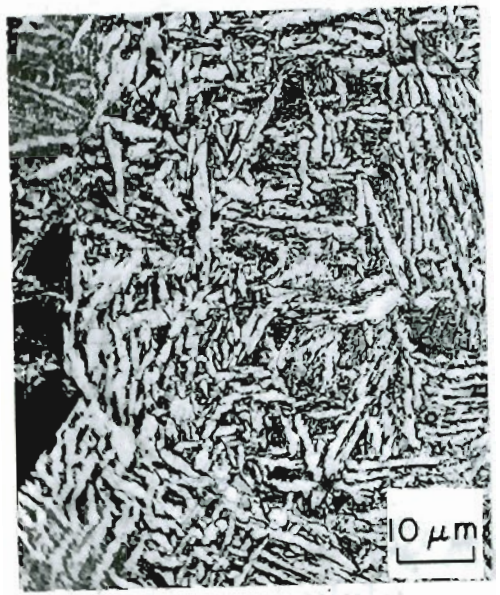

(a) Bainite at 0.1mm distance

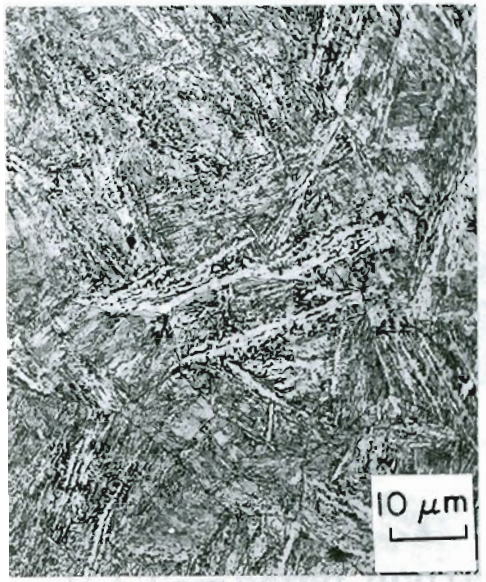

(b) Tempered martensite at 0.6mm distance

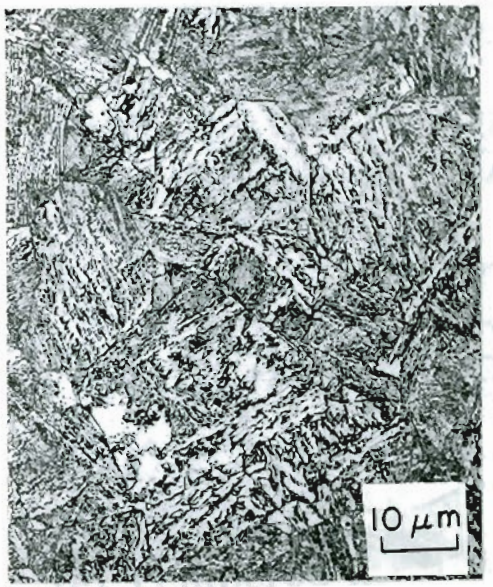

(c) Tempered martensite at 0.8mm distance

Figure-13 : HAZ microstructure for A514 steel flame cut at slower cutting speed.

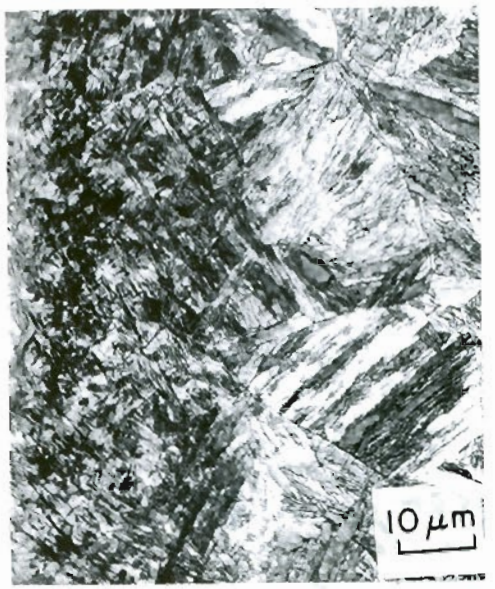

(a) Lath and plate martensite at 0.1mm distance

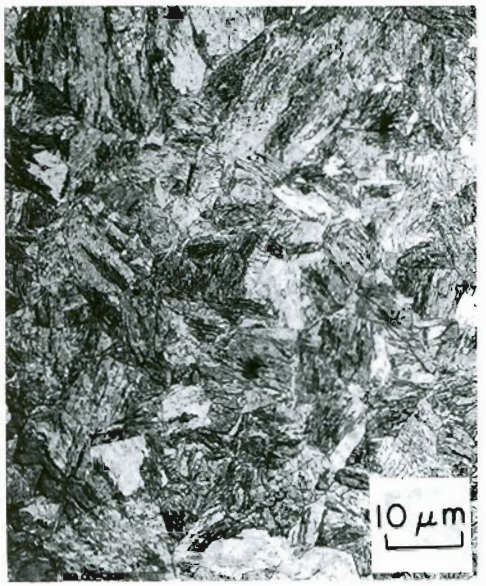

(b) Tempered martensite at 0.5mm distance

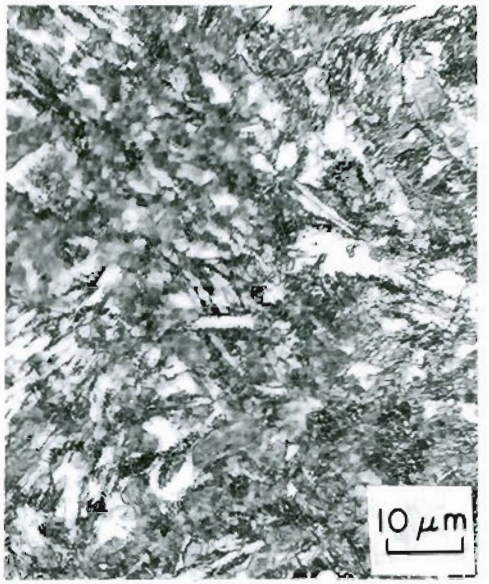

(c) Tempered martensite at 0.8mm distance

Figure-14 : HAZ microstructures for A514 steel flame cut at faster cutting speed.

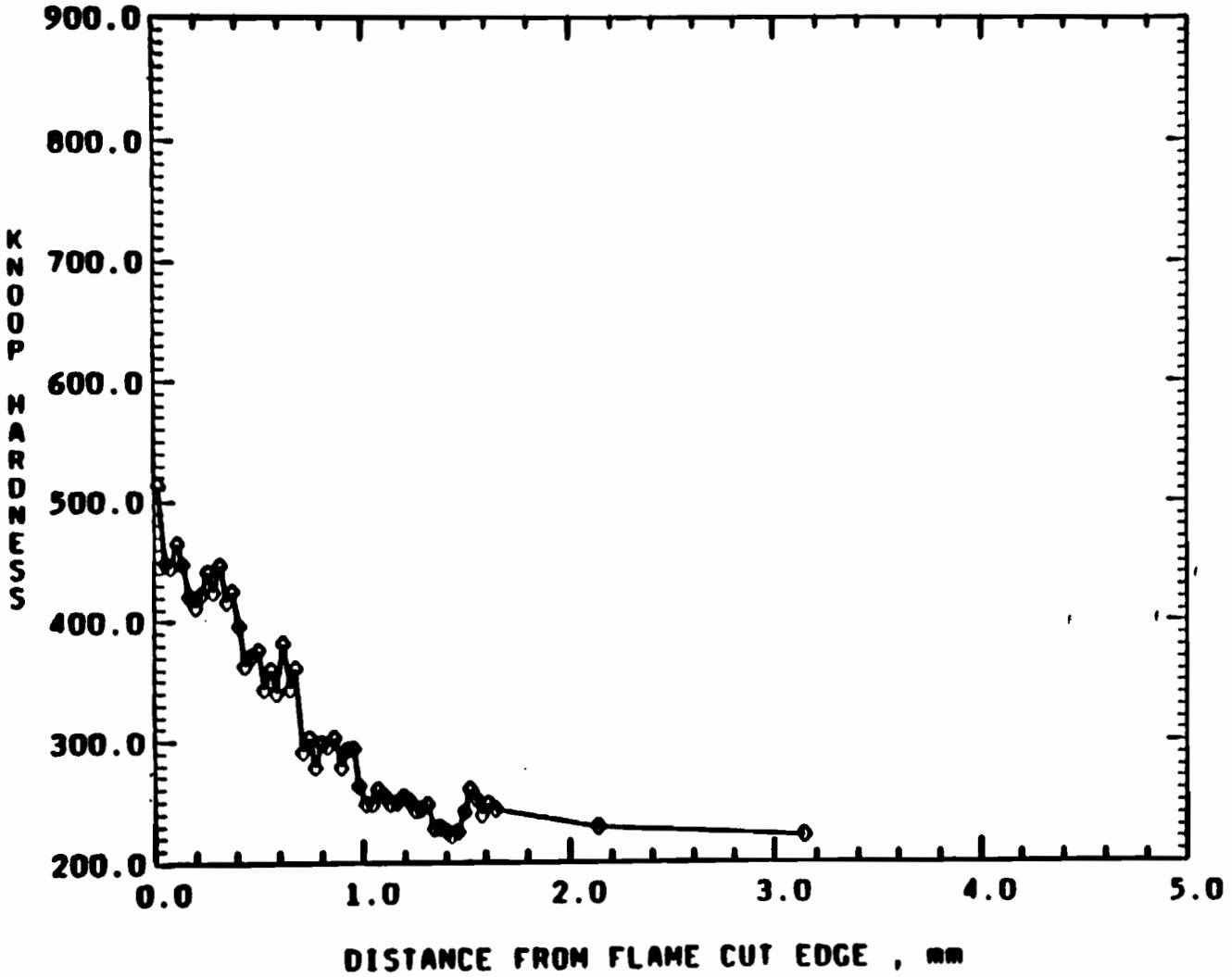

Figure-15 : Microhardness plot across HAZ for A572 steel flame cut at slower cutting speed.

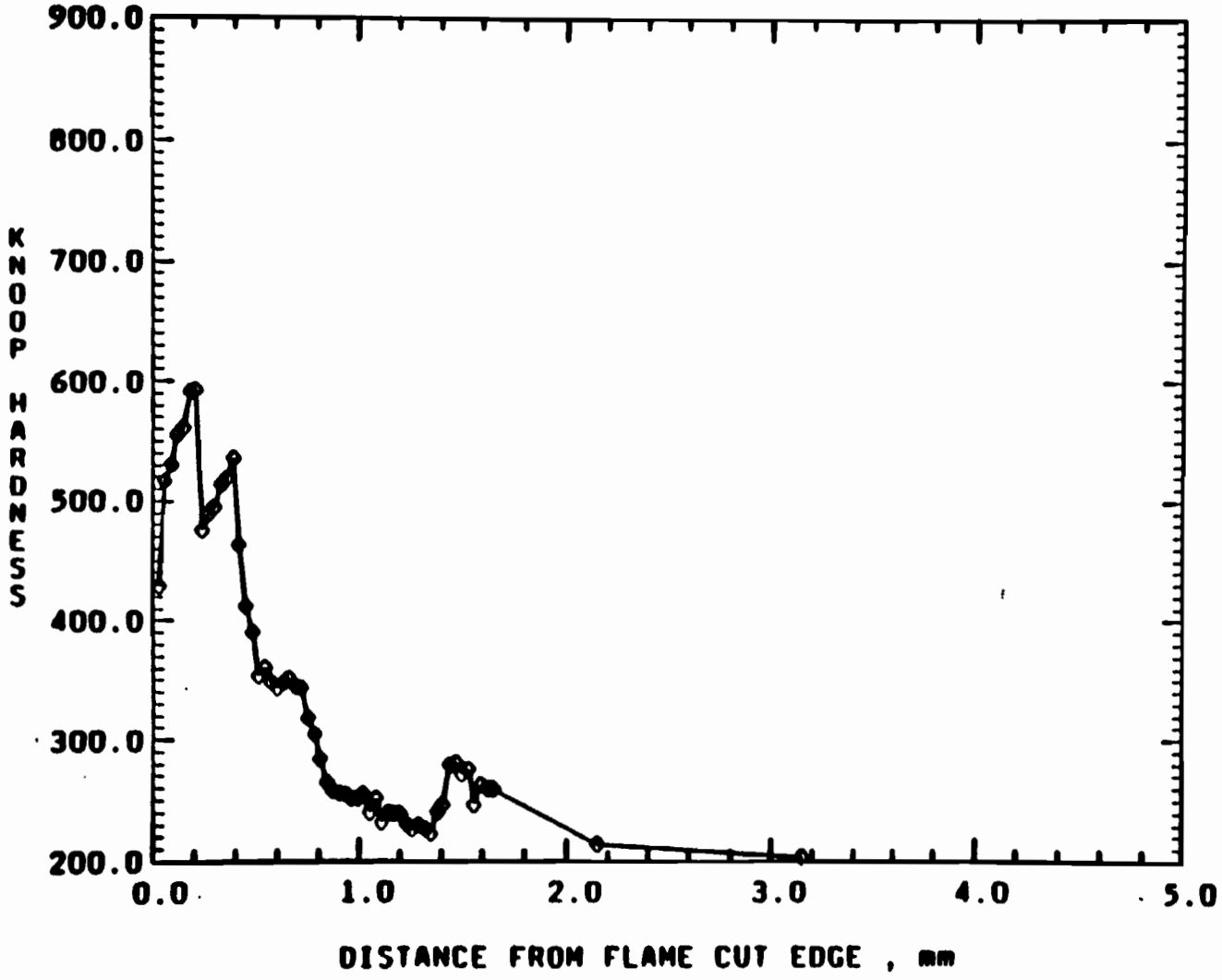

Figure-16 : Microhardness plot across HAZ for A572 steel flame cut at faster cutting speed.

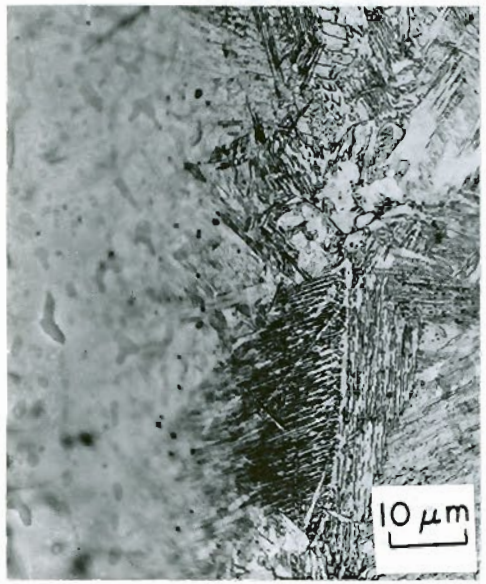

(a) Lath martensite at 0.05mm distance

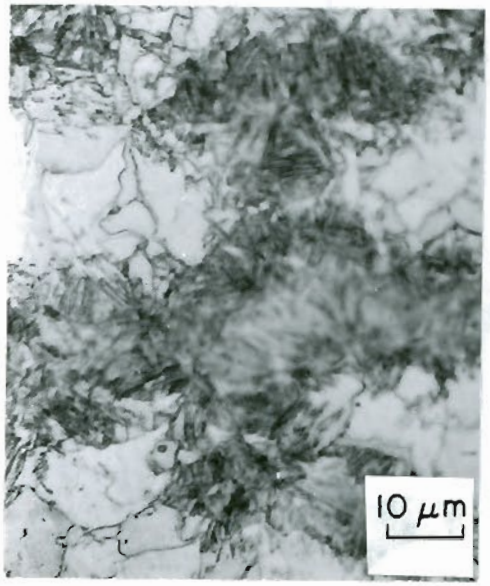

(b) Ferrite and Pearlite at 0.6mm distance

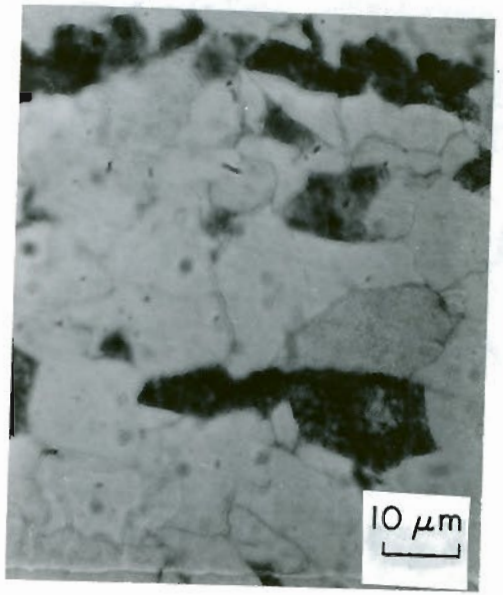

(c) Ferrite and Pearlite at 3mm distance

Figure-17 : HAZ microstructures for A572 steel flame cut at slower cutting speed.

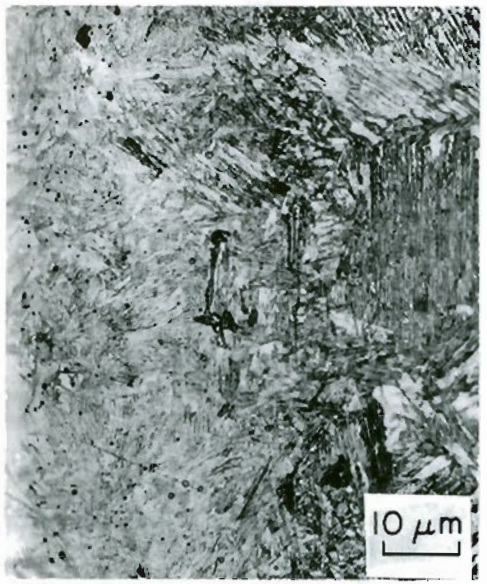

(a) Lath martensite
at 0.05mm distance

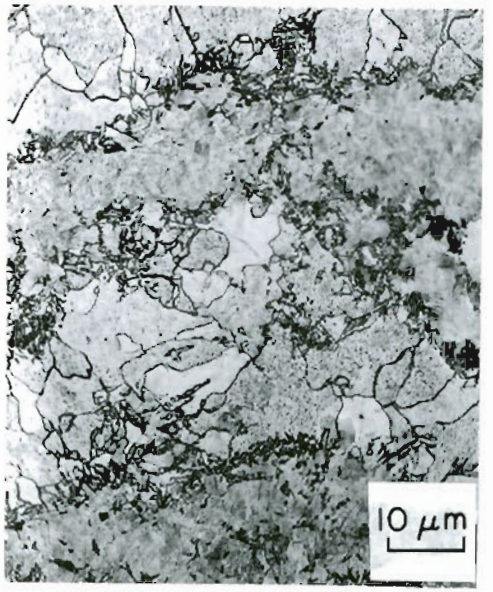

(b) Ferrite and Pearlite
at 0.6mm distance

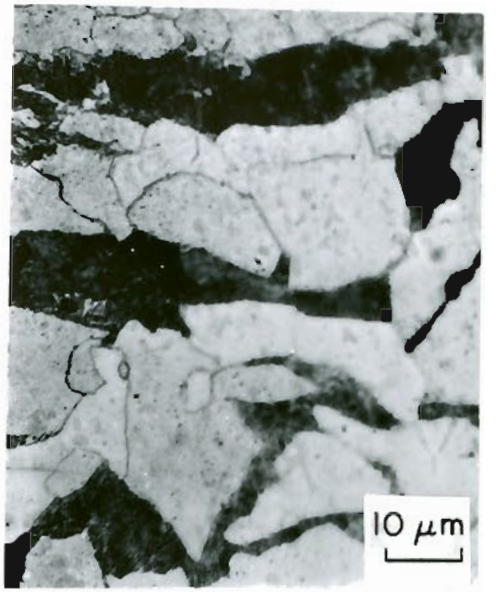

(c) Ferrite and Pearlite
at 1.2mm distance

Figure-18 : HAZ microstructures for A572 steel flame cut at faster cutting speed.

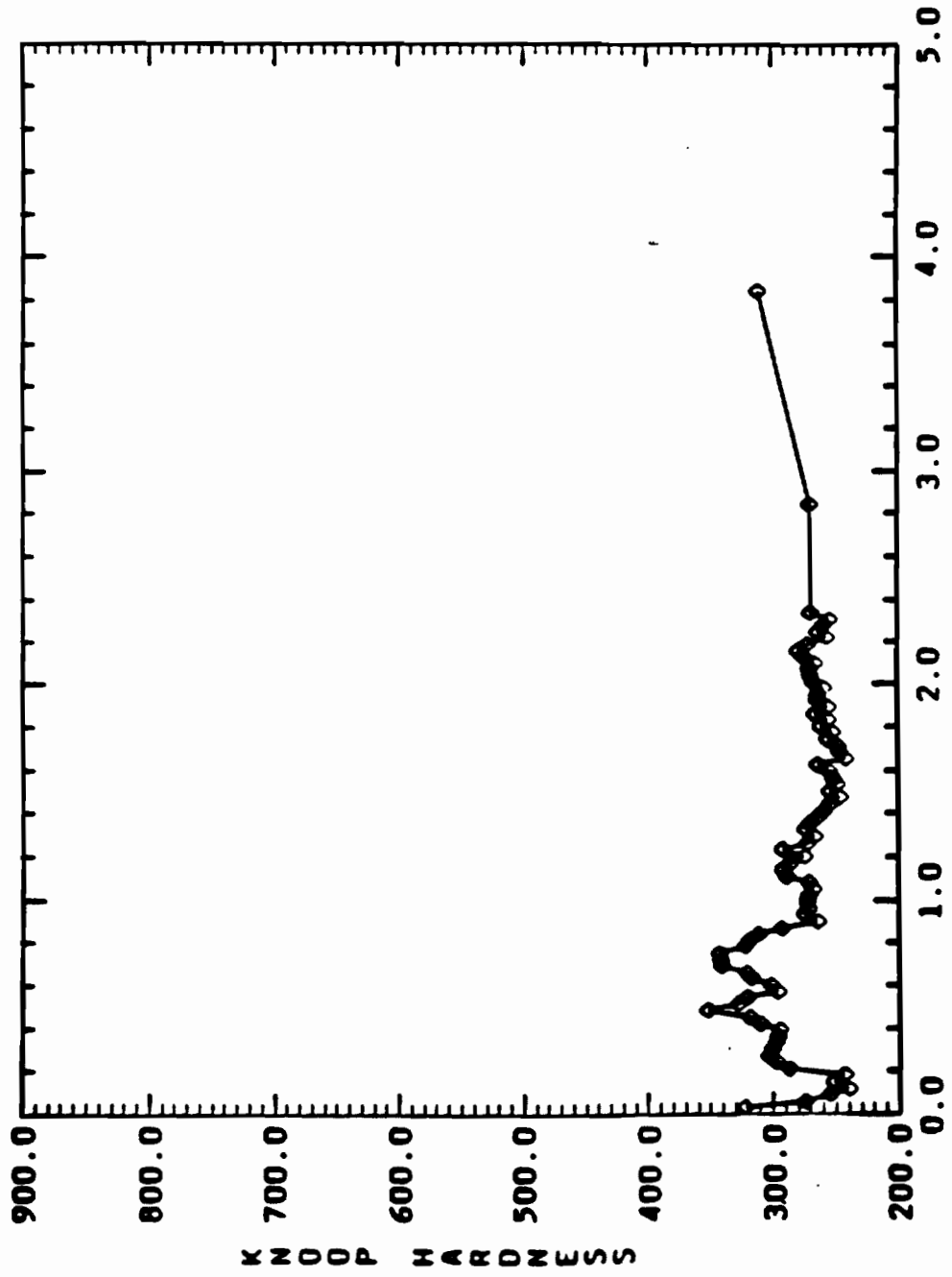

Figure-19 : Microhardness plot across HAZ for A588 steel flame cut at slower cutting speed.

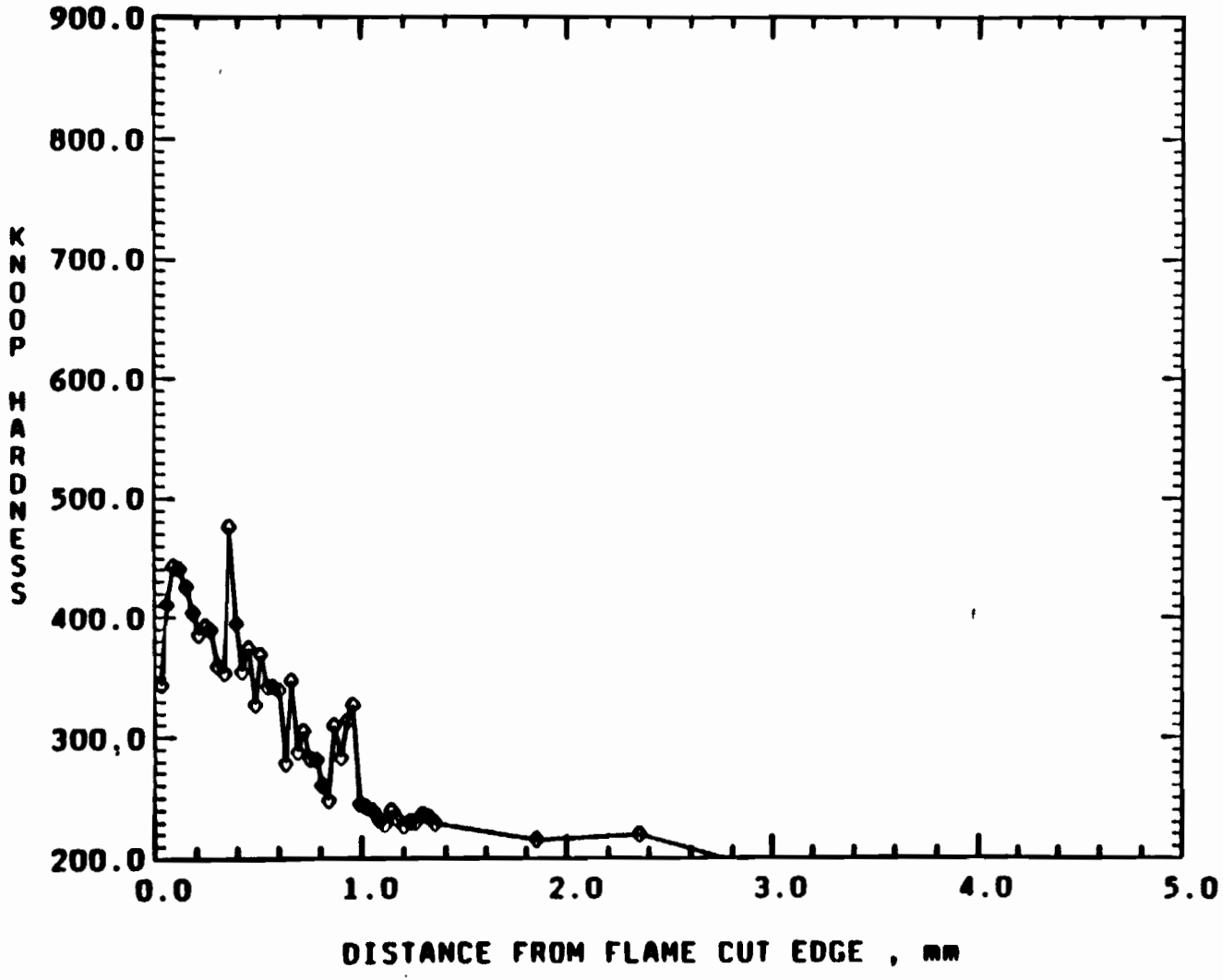

Figure-20 : Microhardness plot across HAZ for A588 steel flame cut at faster cutting speed.

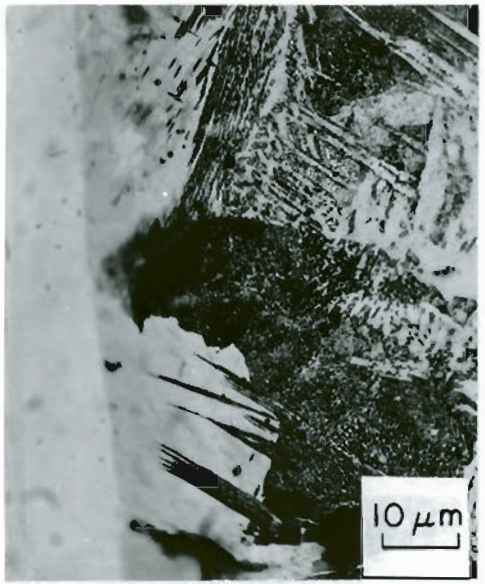

(a) Lath martensite at 0.05mm distance

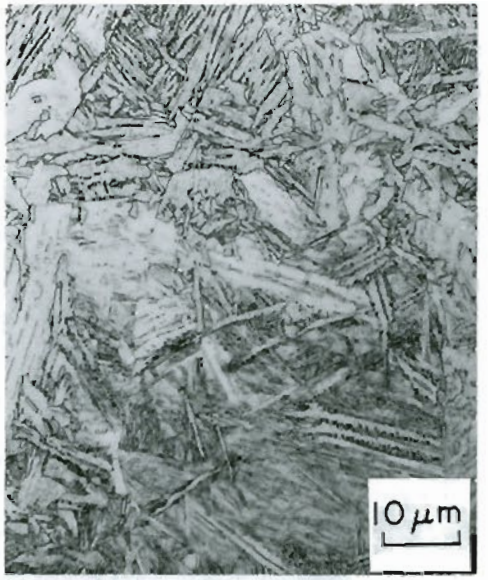

(b) Bainite at 0.5mm distance

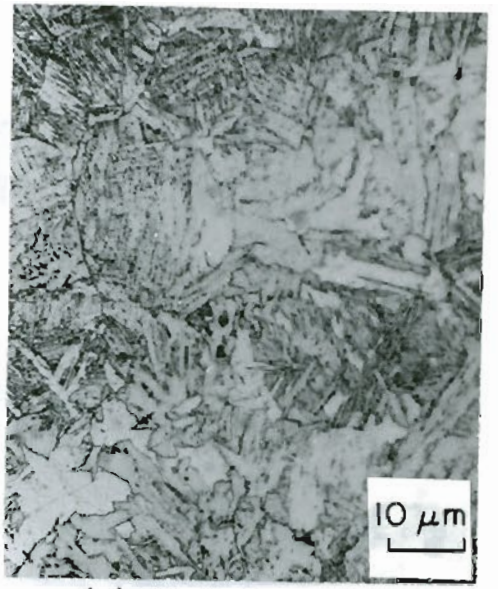

(c) Bainite at 4mm distance

Figure-21 : HAZ microstructures for A588 steel flame cut at slower cutting speed.

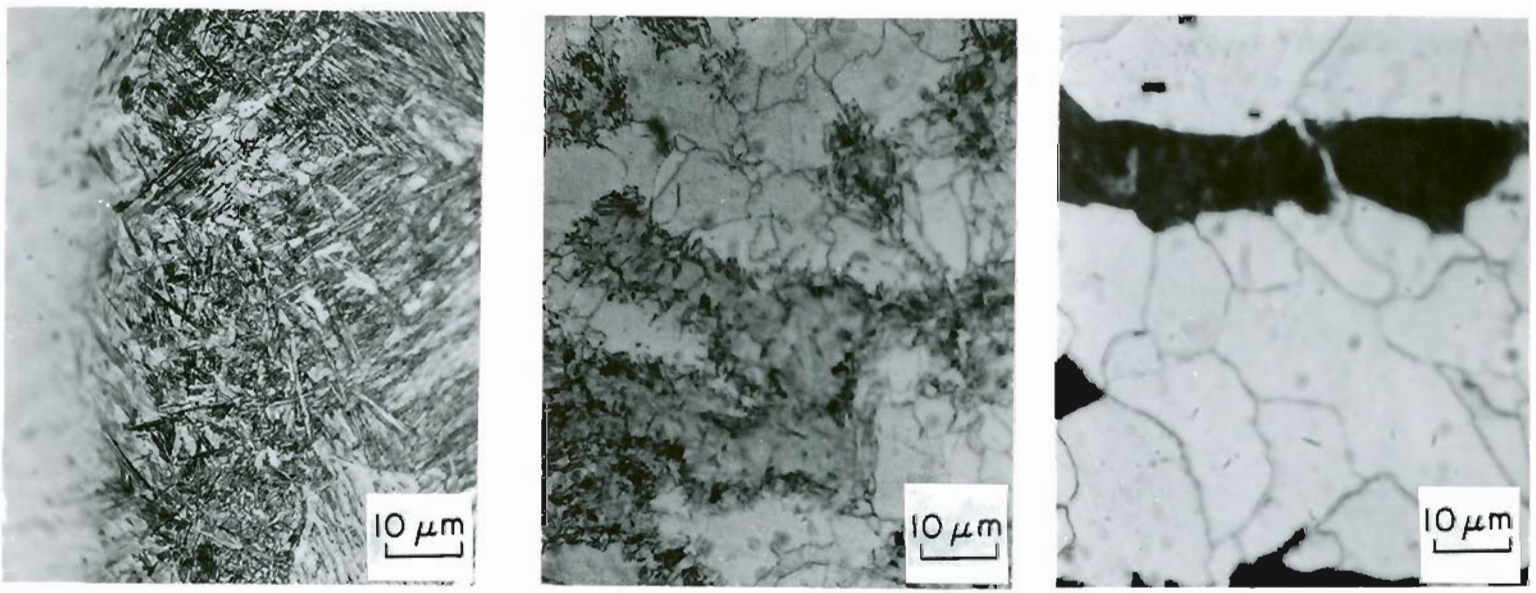

(a) Lath martensite at 0.05mm distance

(b) Ferrite and Pearlite at 0.6mm distance

(c) Ferrite and Pearlite at 2.5mm distance

Figure-22 : HAZ microstructures for A588 steel flame cut at faster cutting speed.

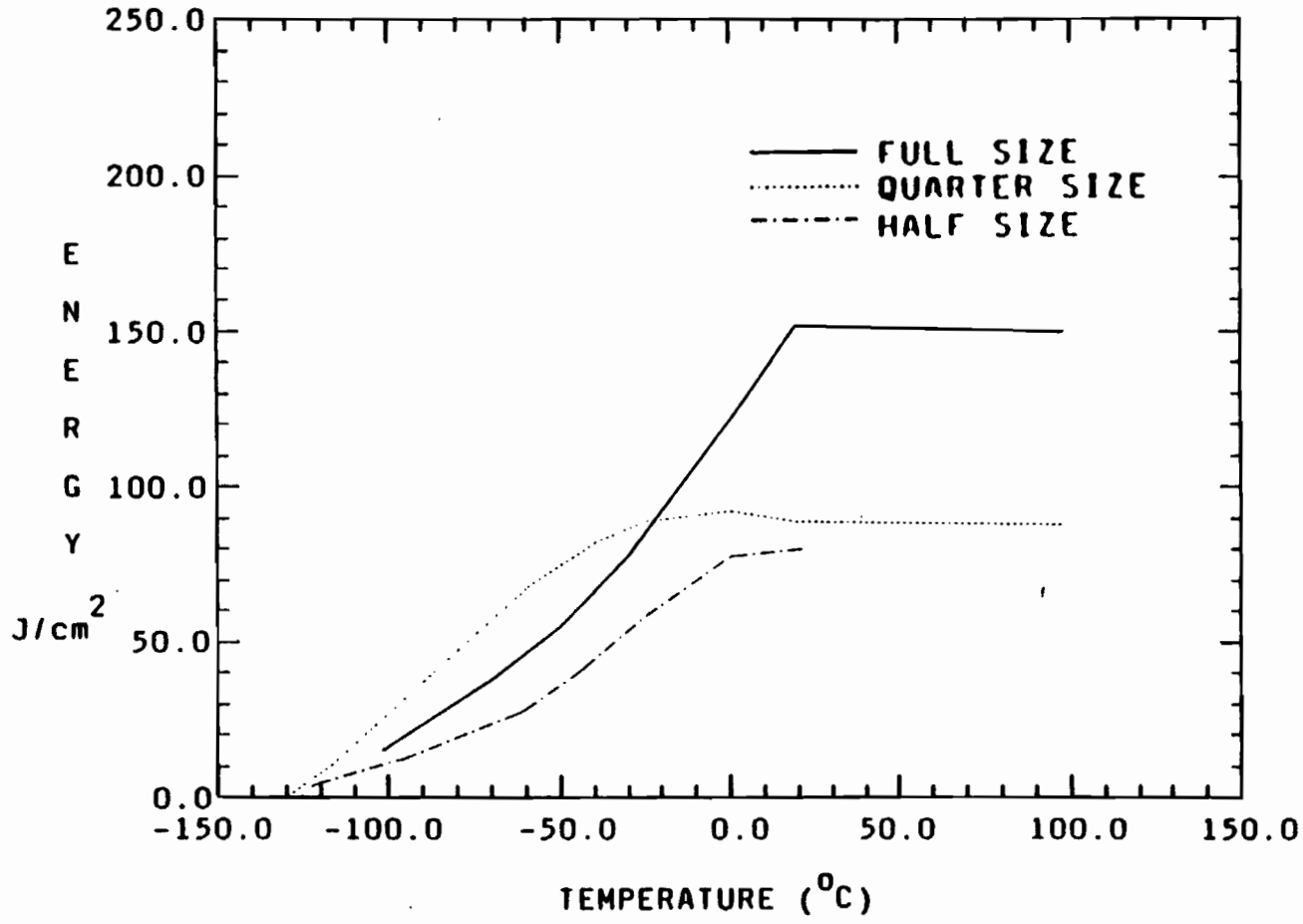

Figure-23 : Area normalized energy versus test temperature plots for CVN specimens of A514 steel, base metal.

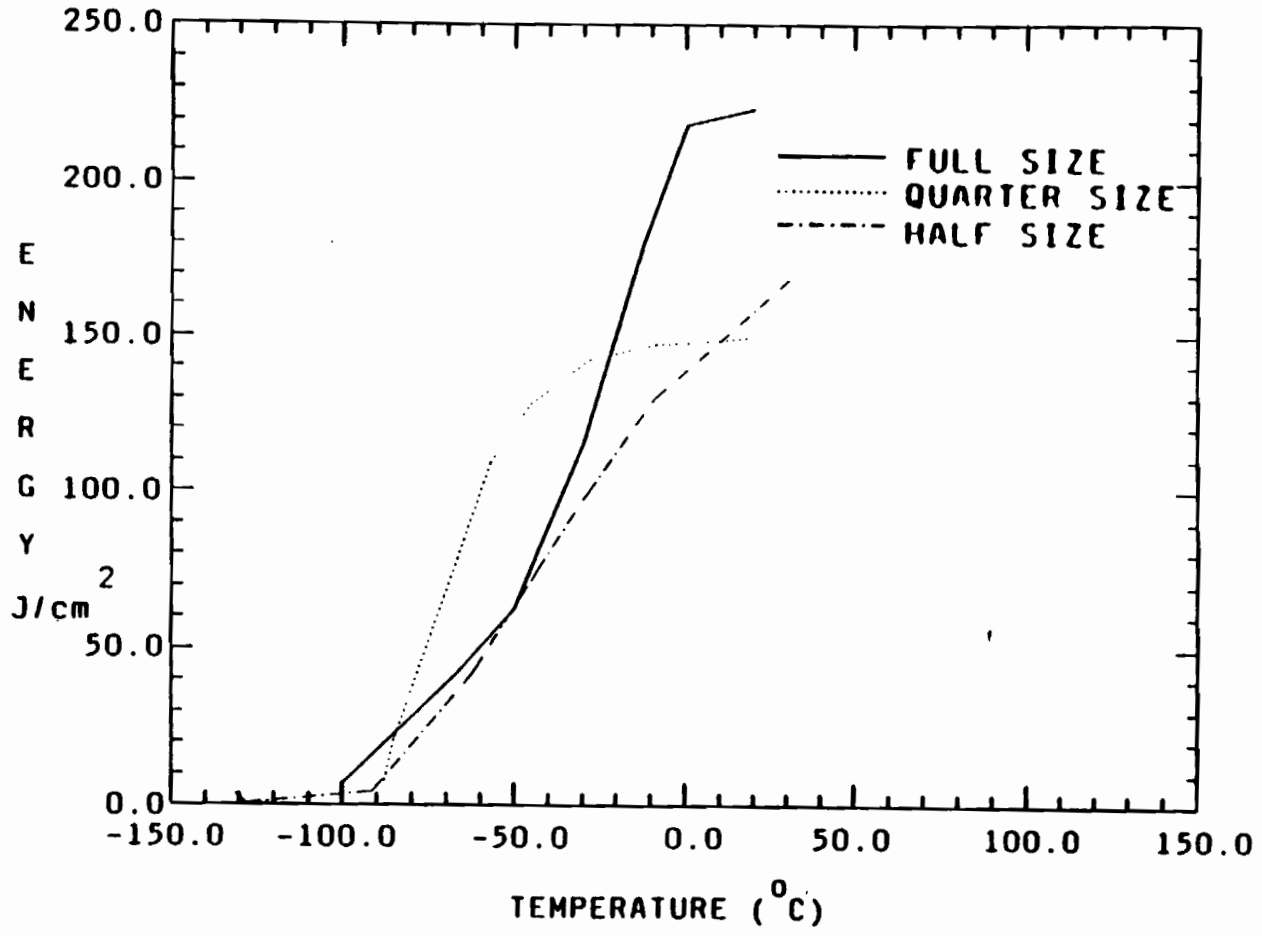

Figure-24 : Area normailzed energy versus test temperature plots for CVN specimens of A572 steel, base metal.

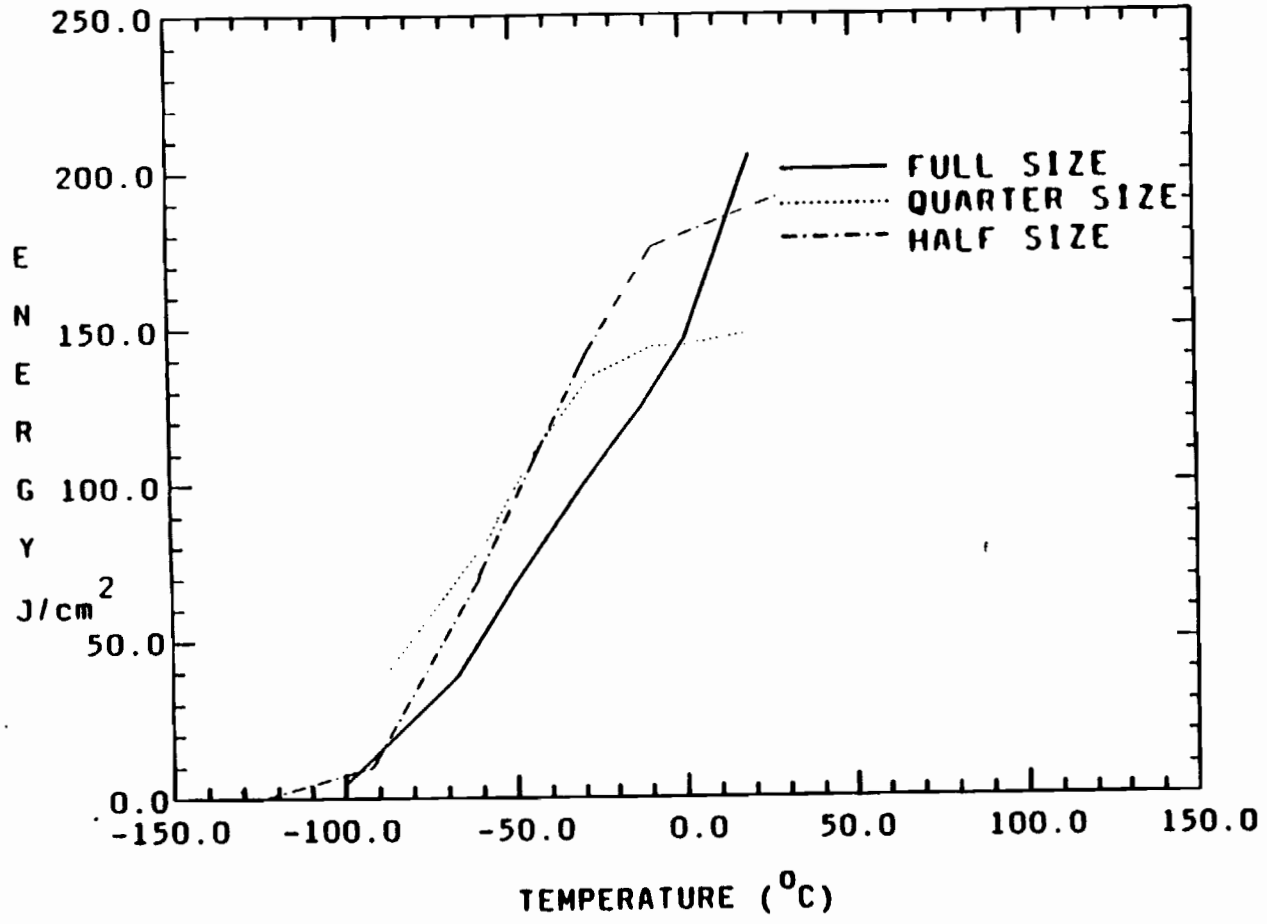

Figure-25 : Area normalized energy versus test temperature plots for CVN specimens of A588 steel, base metal.

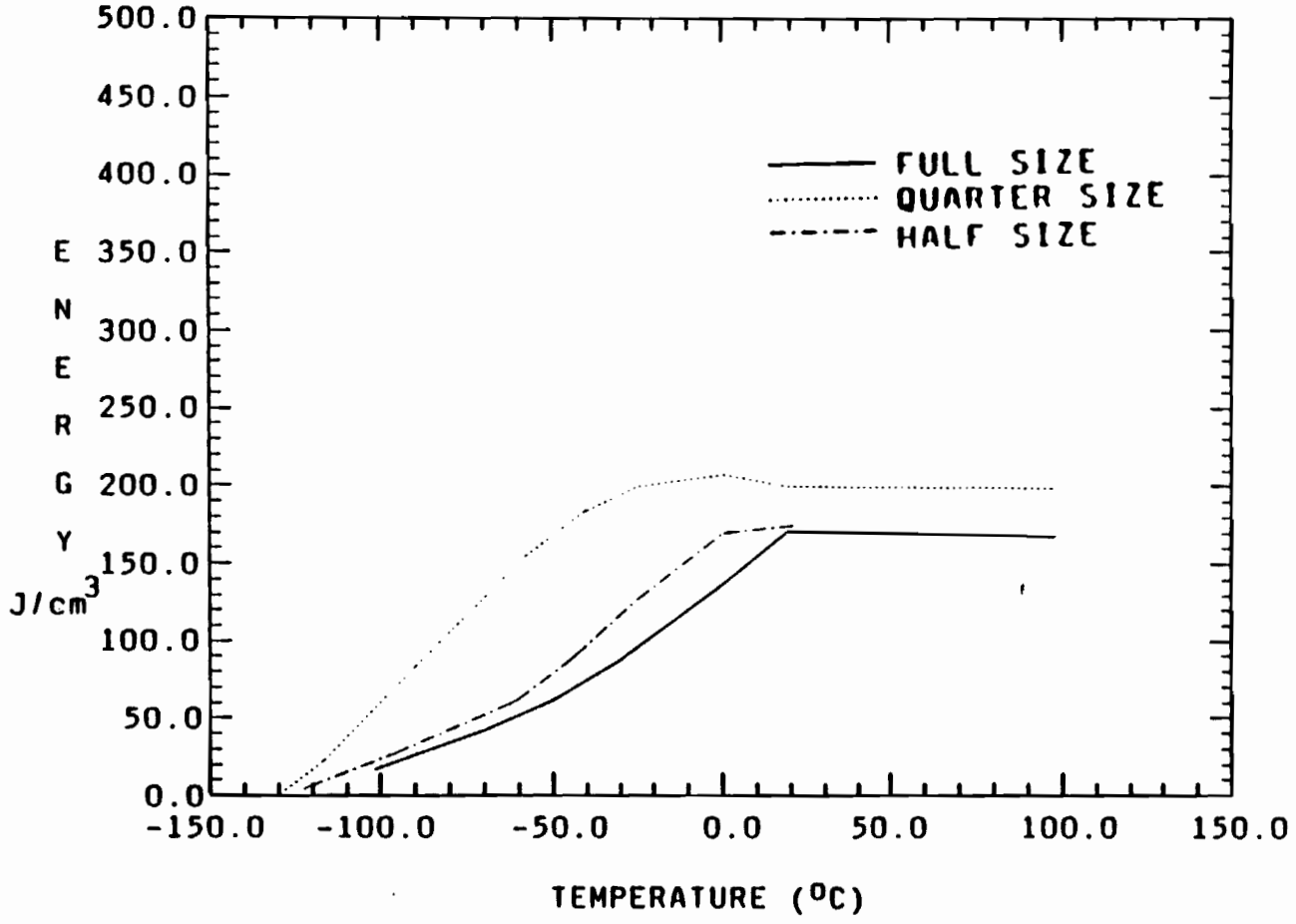

Figure-26 : Volume normalized energy versus test temperature plots for CVN specimens of A514 steel, base metal.

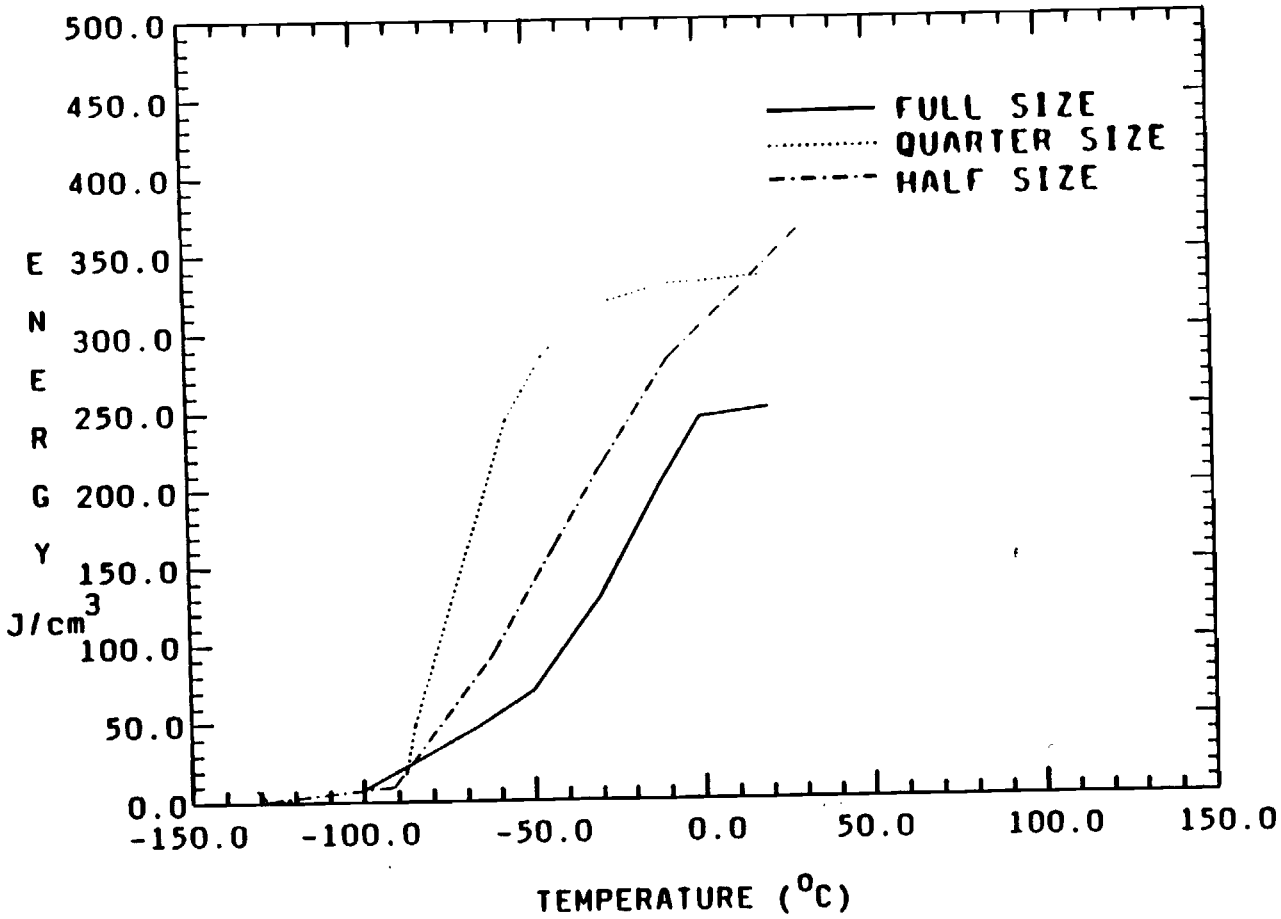

Figure-27 : Volume normalized energy versus test temperature plots for CVN specimens of A572 steel, base metal.

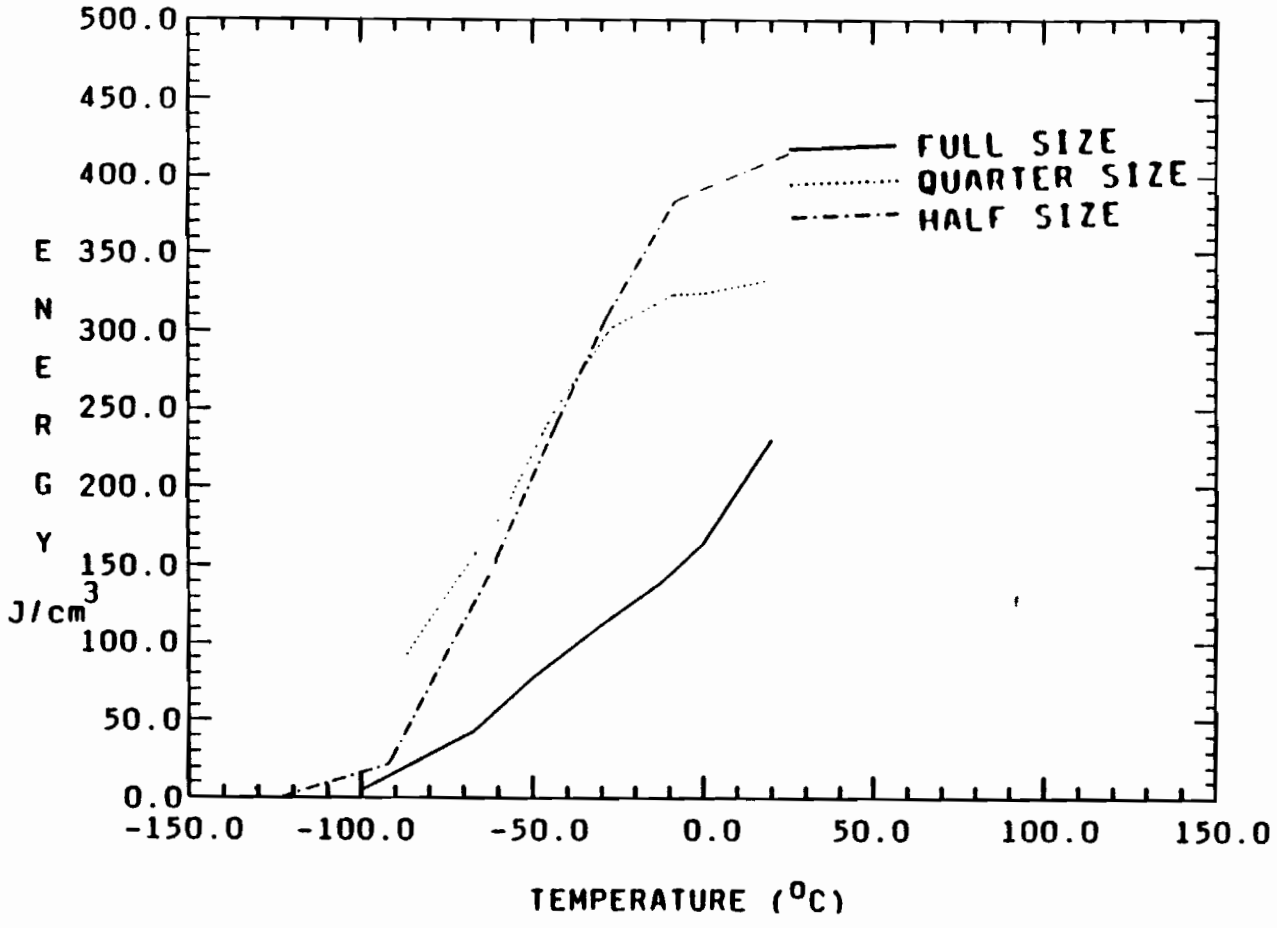

Figure-28 : Volume normalized energy versus test temperature plots for CVN specimens of A588 steel, base metal.

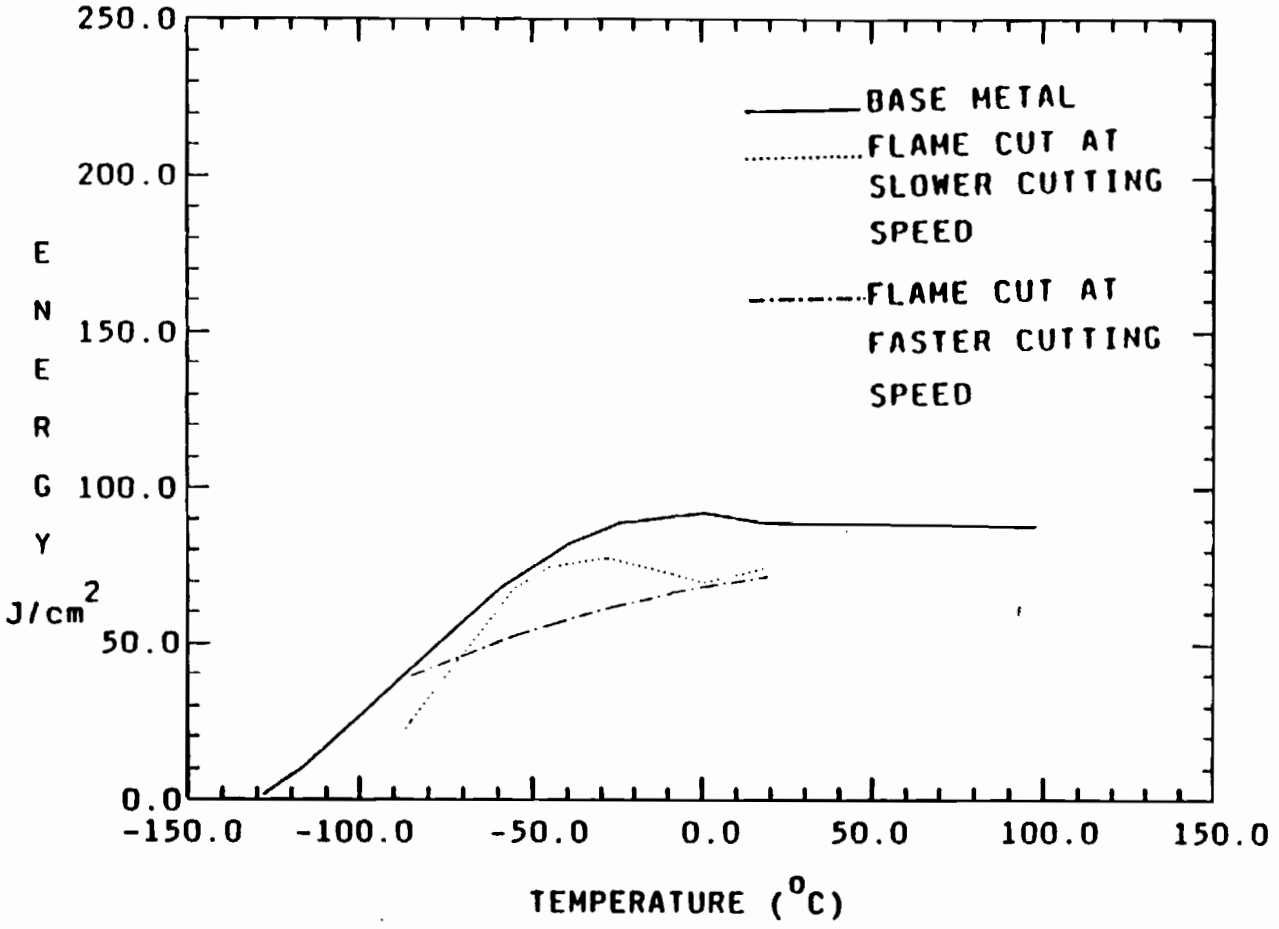

Figure-29 : Area normalized energy versus test temperature plots for quarter size CVN specimens of A514 steel.

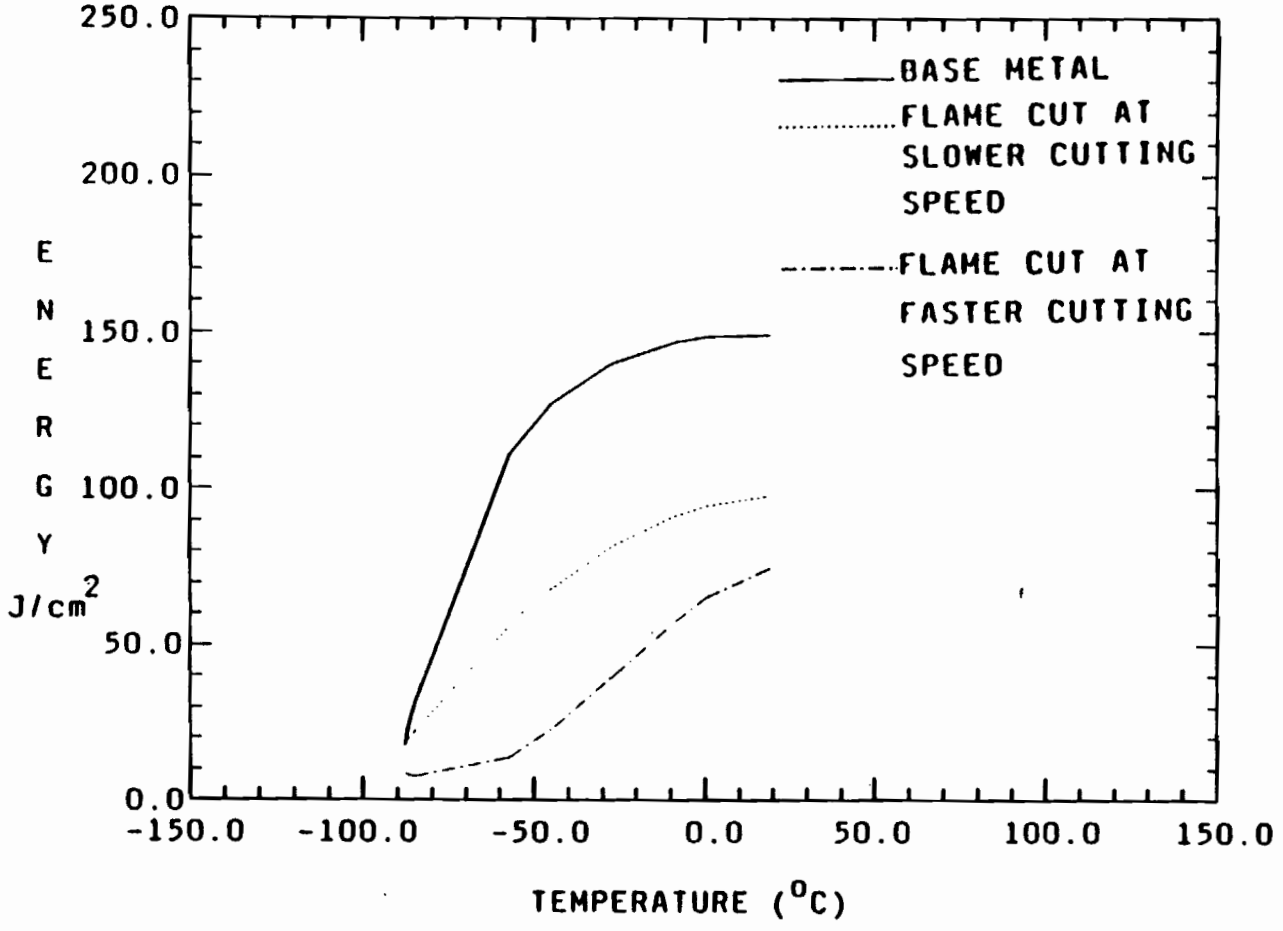

Figure-30 : Area normalized energy versus test temperature plots for quarter size CVN specimens of A572 steel.

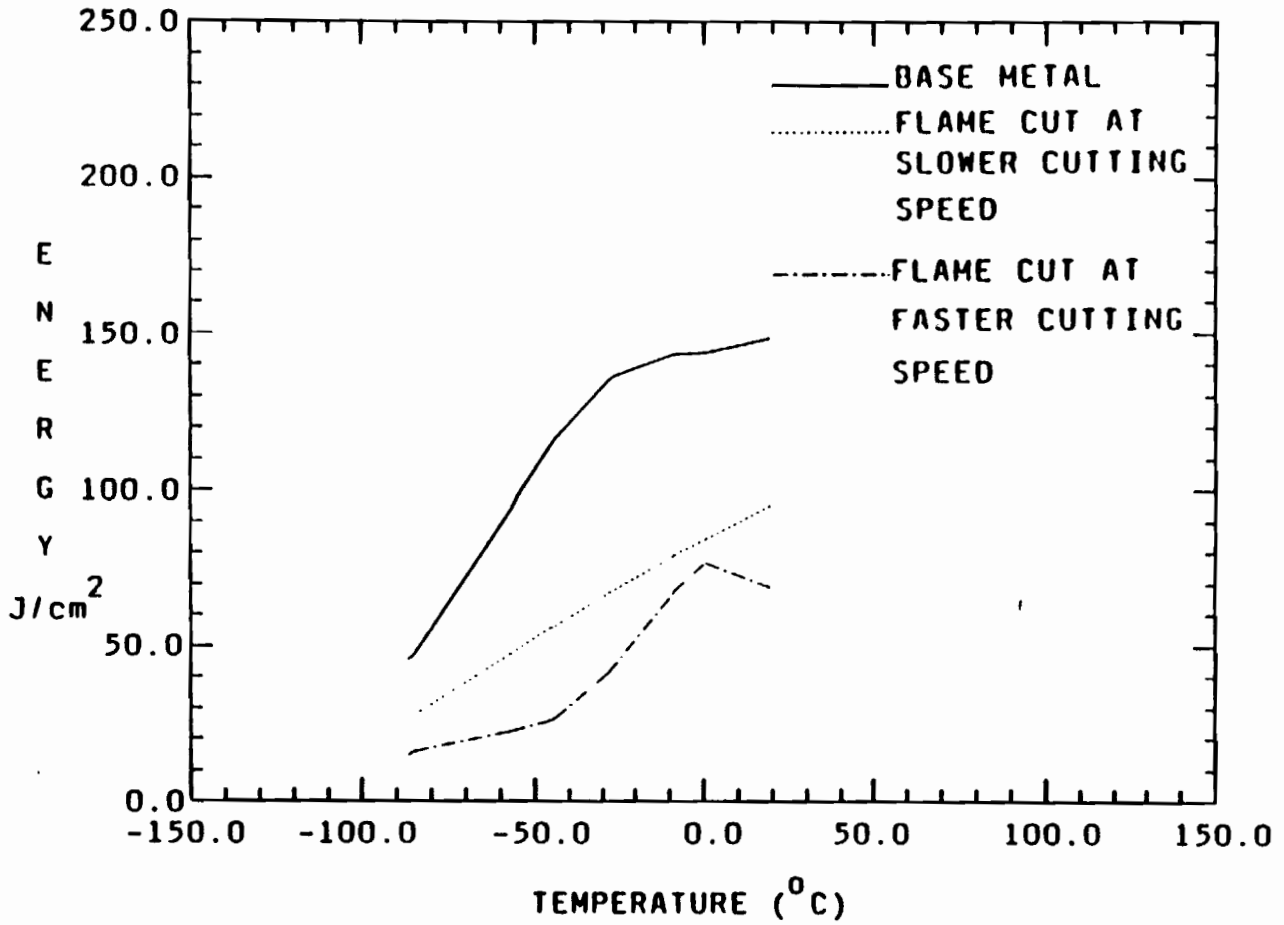

Figure-31 : Area normalized energy versus test temperature plots for quarter size CVN specimens of A588 steel.

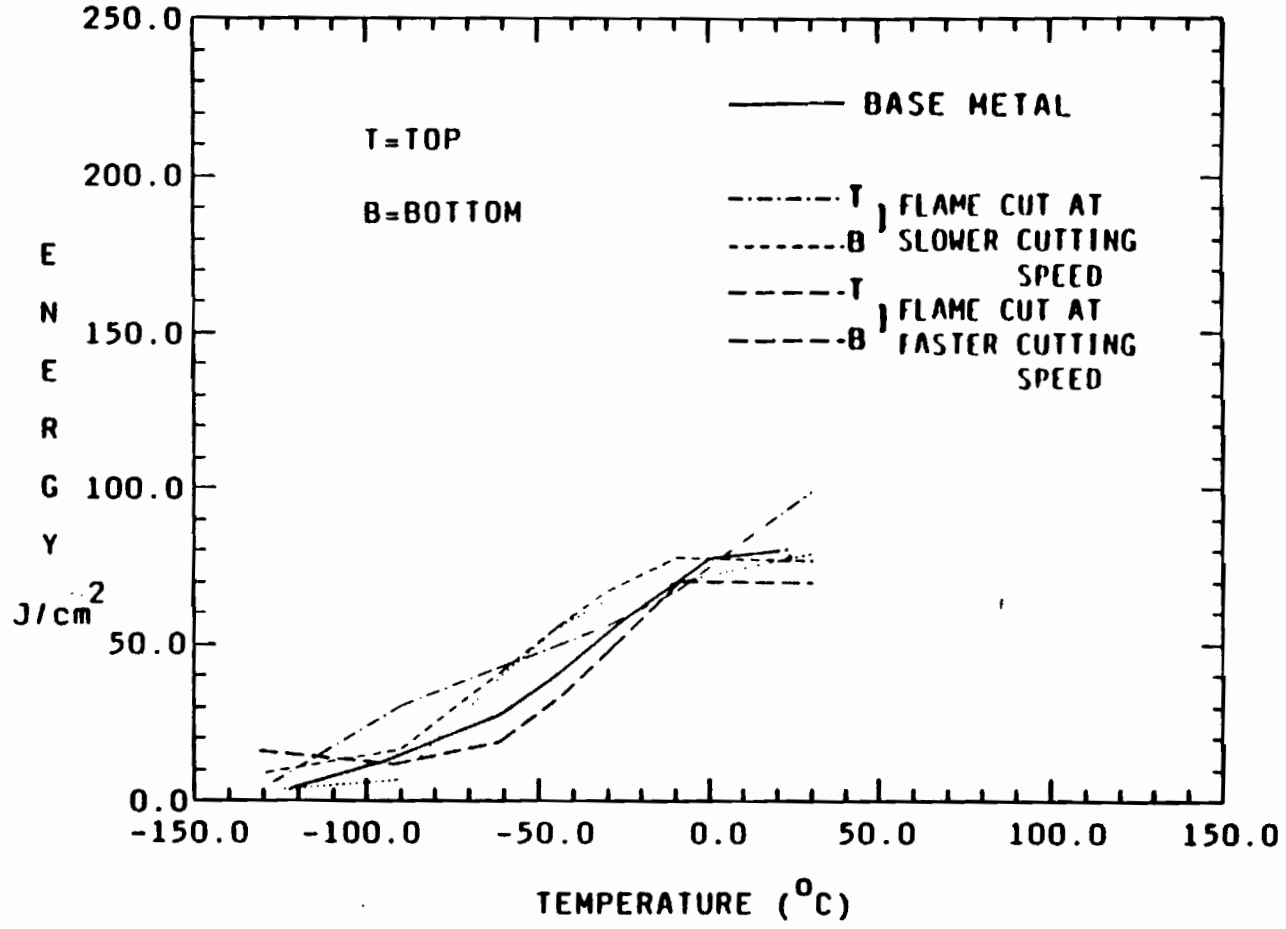

Figure-32 : Area normalized energy versus test temperature plots for half size CVN specimens of A514 steel.

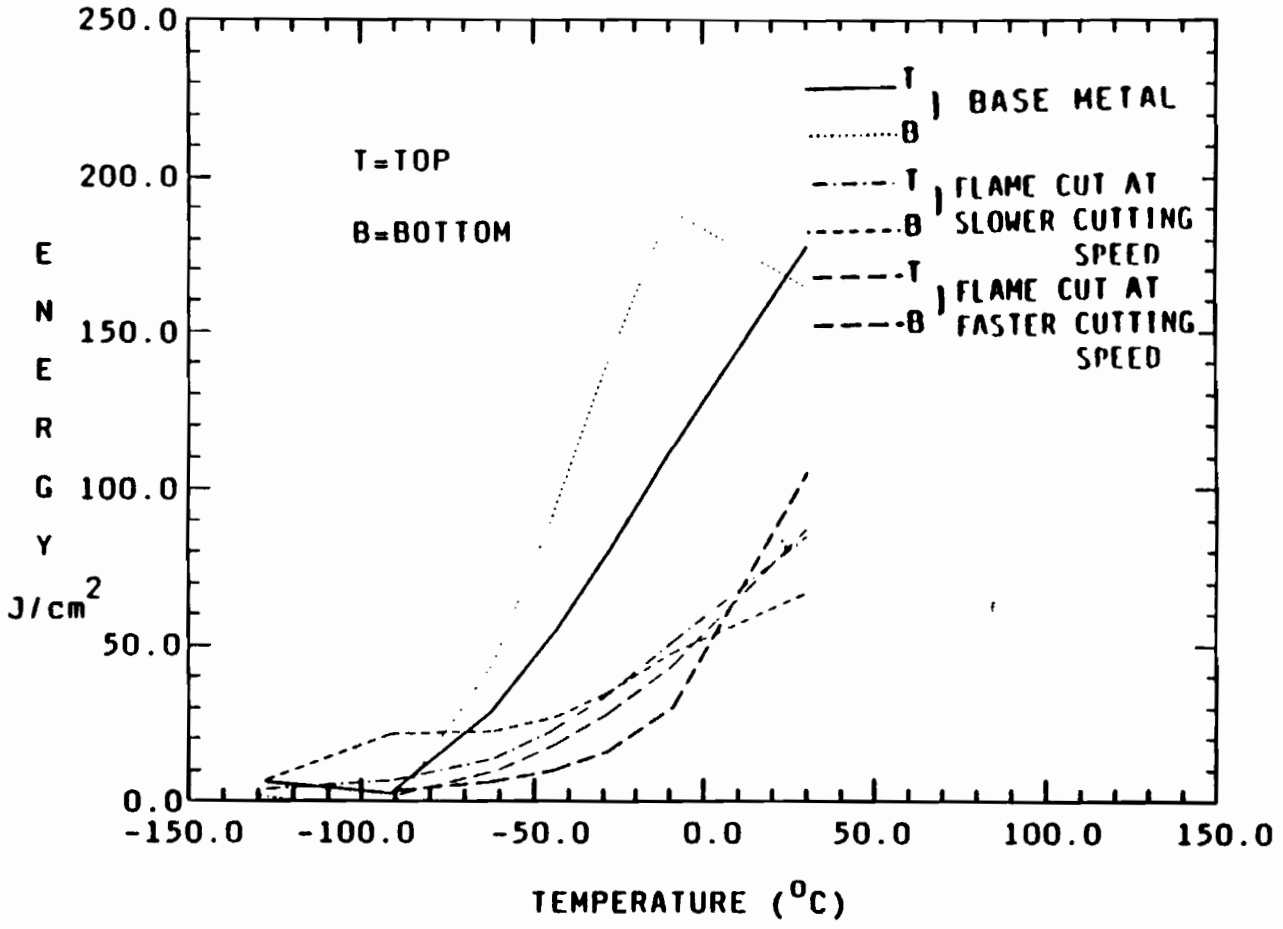

Figure-33 : Area normalized energy versus test temperature plots for half size CVN specimens of A572 steel.

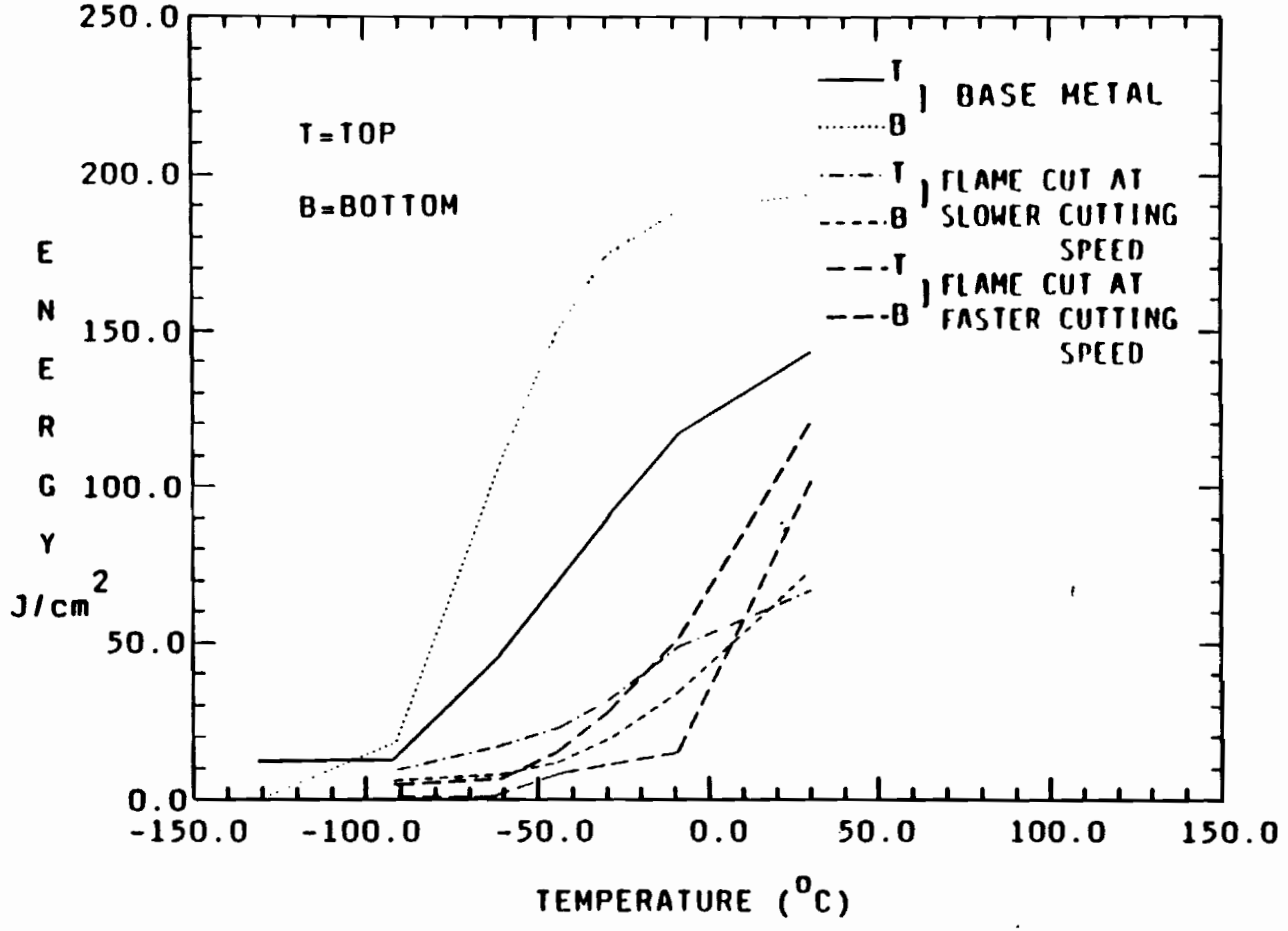

Figure-34 : Area normalized energy versus test temperature plots for half size CVN specimens of A588 steel.

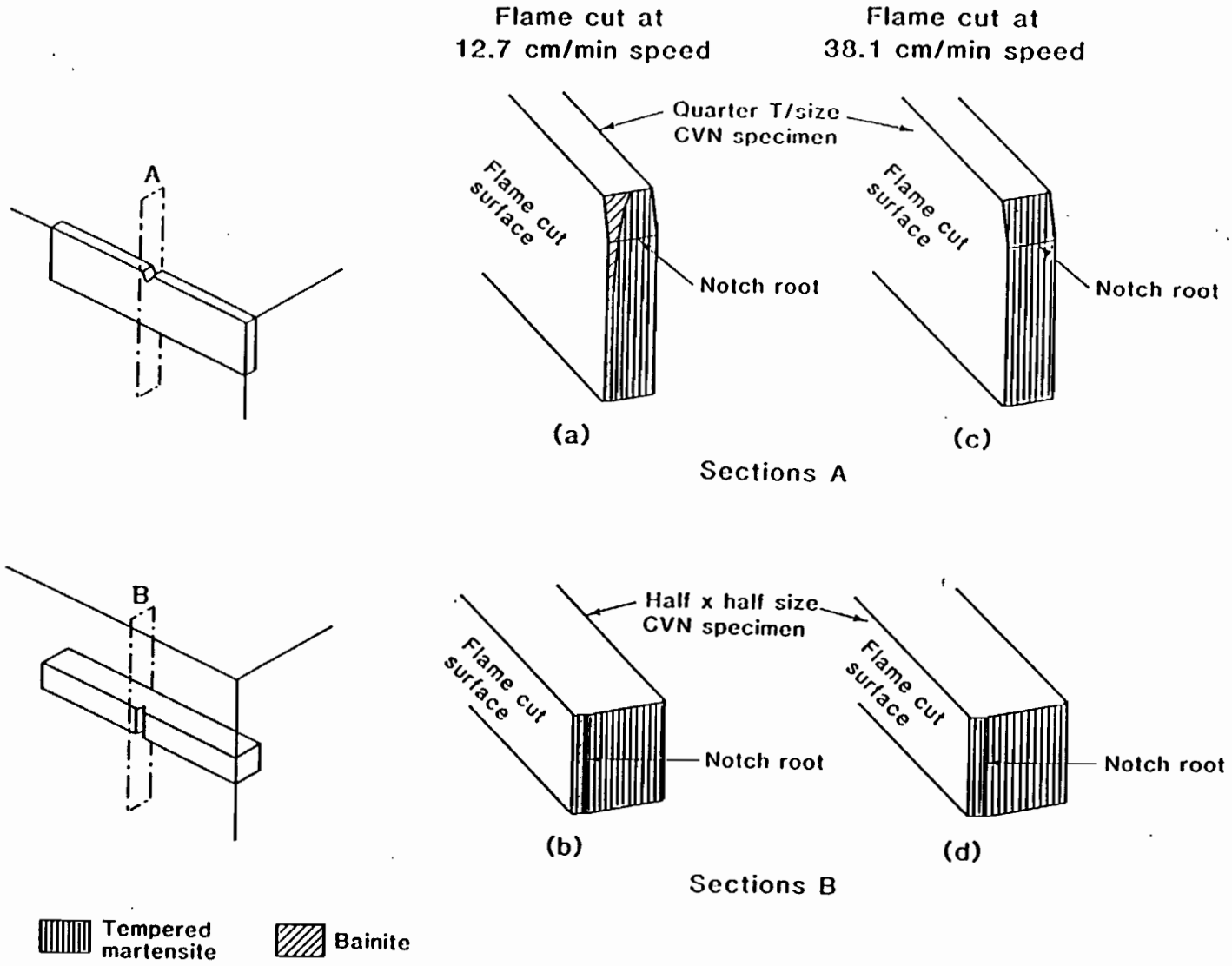

Figure-35 : Schematic representation of flame cut HAZ microstructures at notch root in A514 steel.

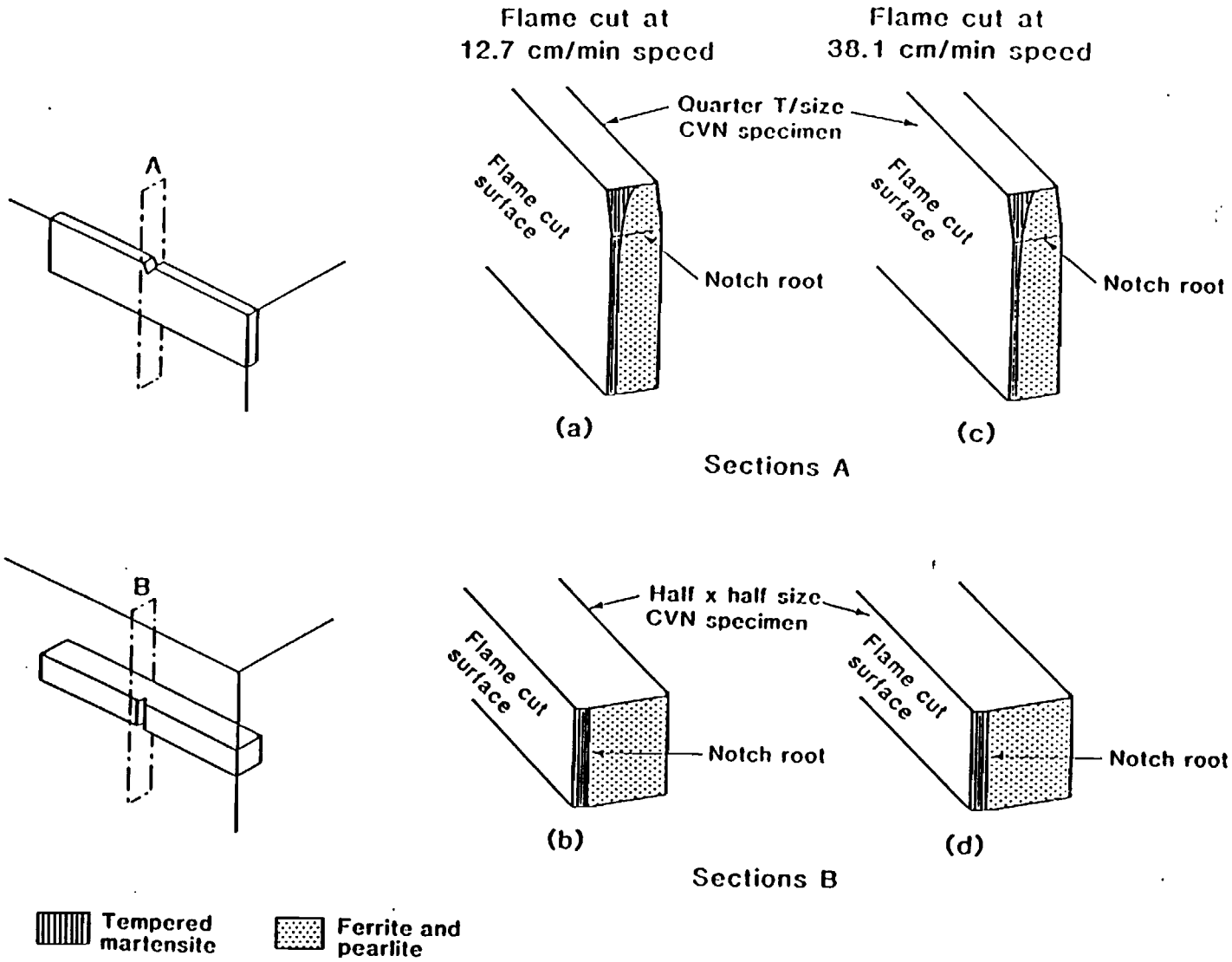

Figure-36 : Schematic representation of flame cut HAZ microstructures at notch root in A572 steel.

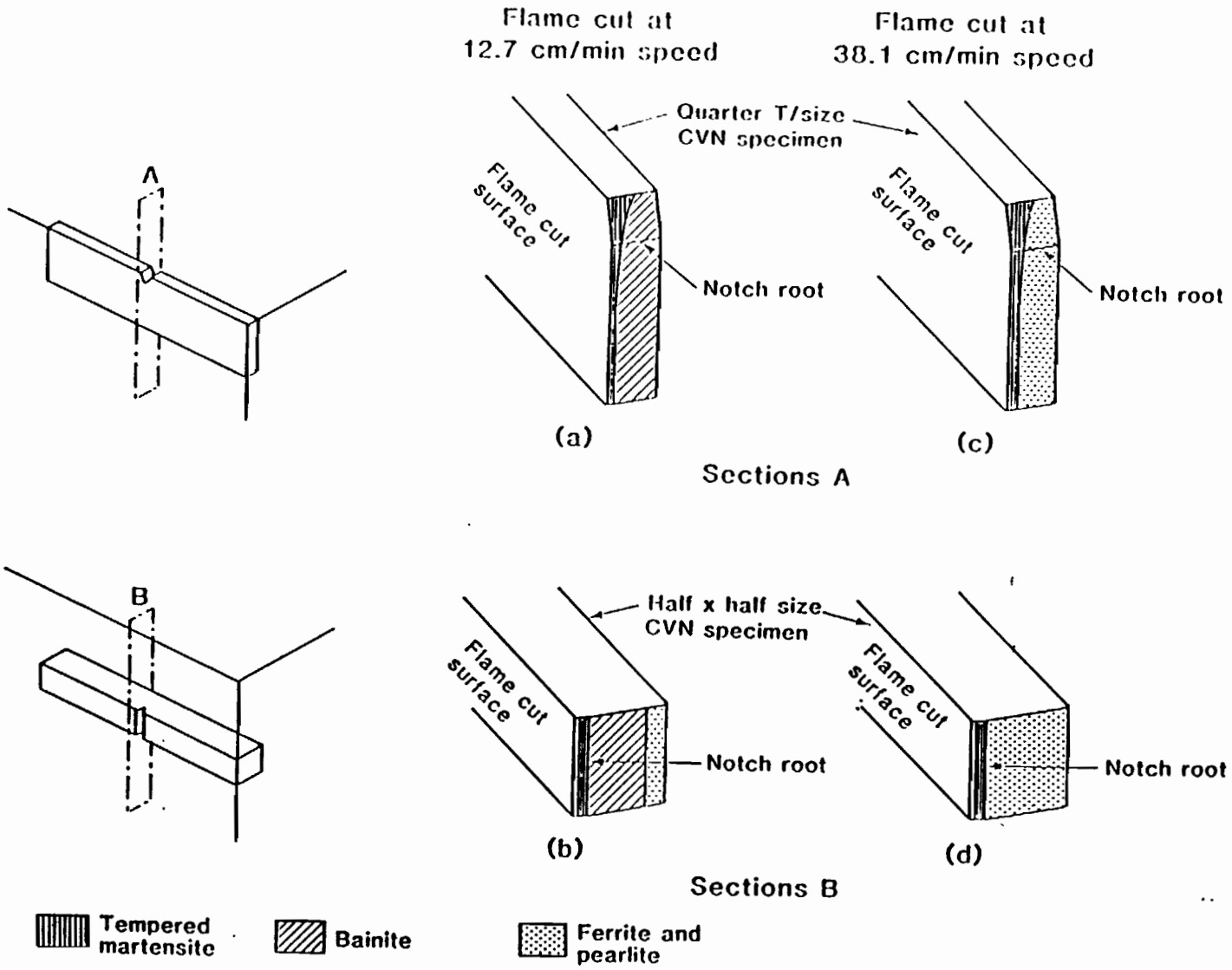

Figure-37 : Schematic representation of flame cut HAZ microstructures at notch root in A588 steel.

(a) Flame cut at slower cutting speed

(b) Flame cut at faster cutting speed

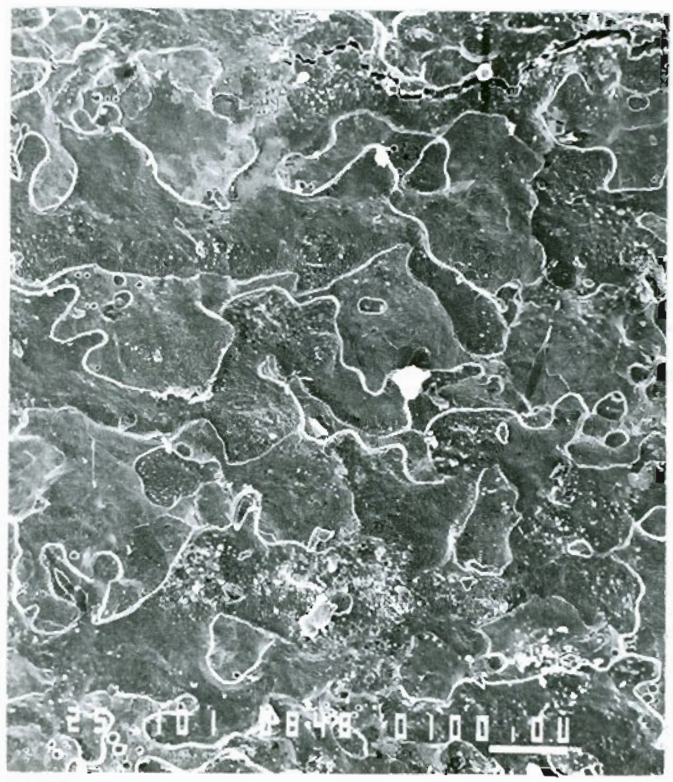

Figure-38 : Flame cut surfaces of A514 steel.

(a) Flame cut at slower cutting speed.

(b) Flame cut at faster cutting speed.

Figure-39 : Flame cut surfaces of A572 steel.

(a) Flame cut at slower cutting speed.

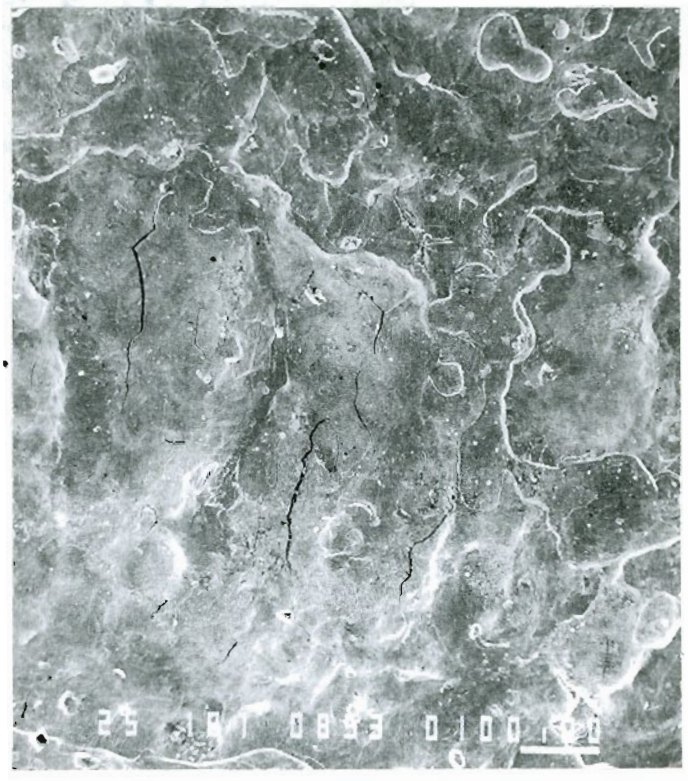

(b) Flame cut at faster cutting speed.

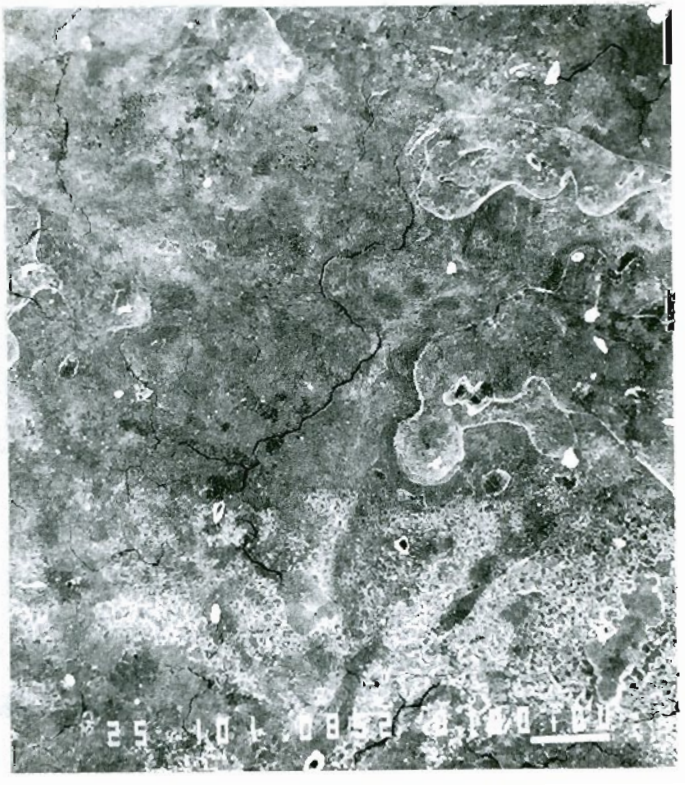

Figure-40 : Flame cut surfaces of A588 steel.

(a)

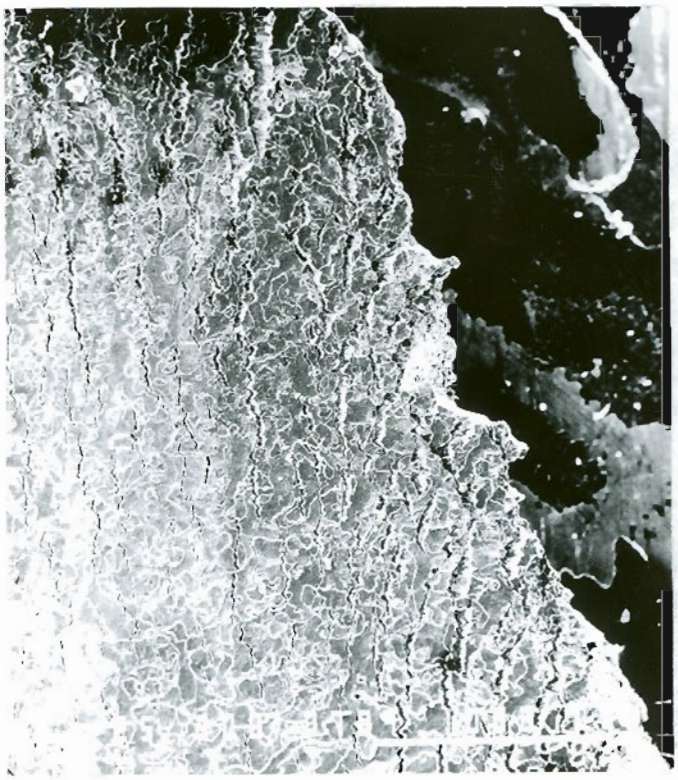

(b)

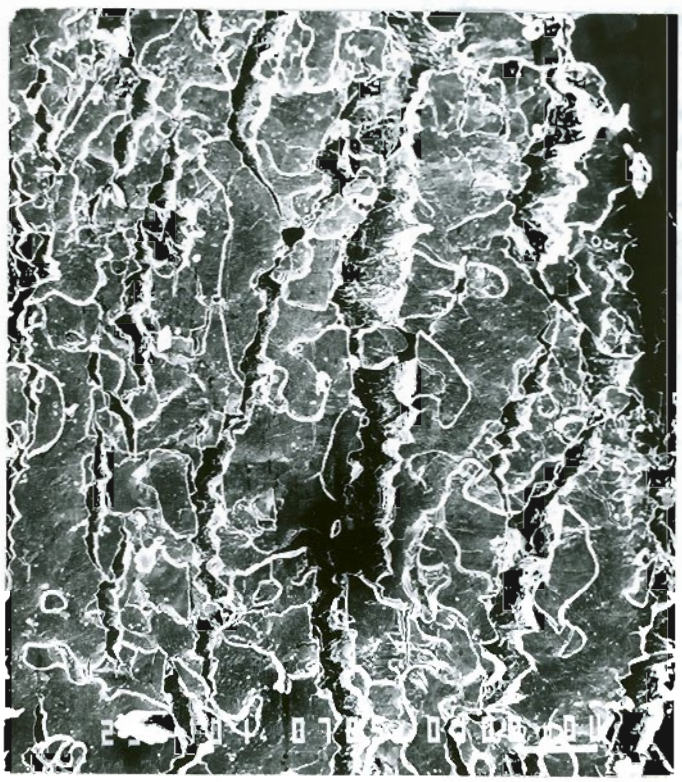

Figure-41 : Flame cut surface of fractured tensile specimen for A572 steel flame cut at faster cutting speed.

(a) At room temperature and low strain rate

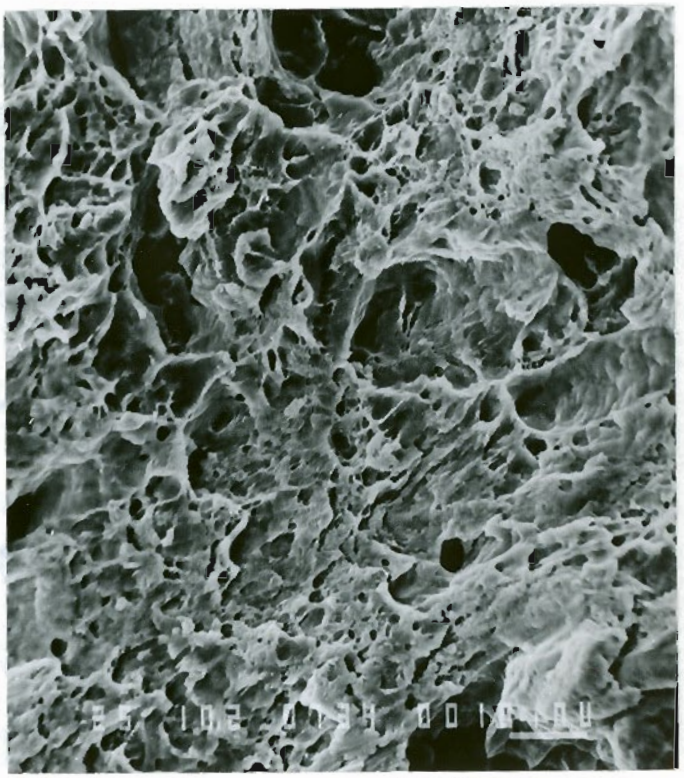

(b) At room temperature and intermediate strain rate

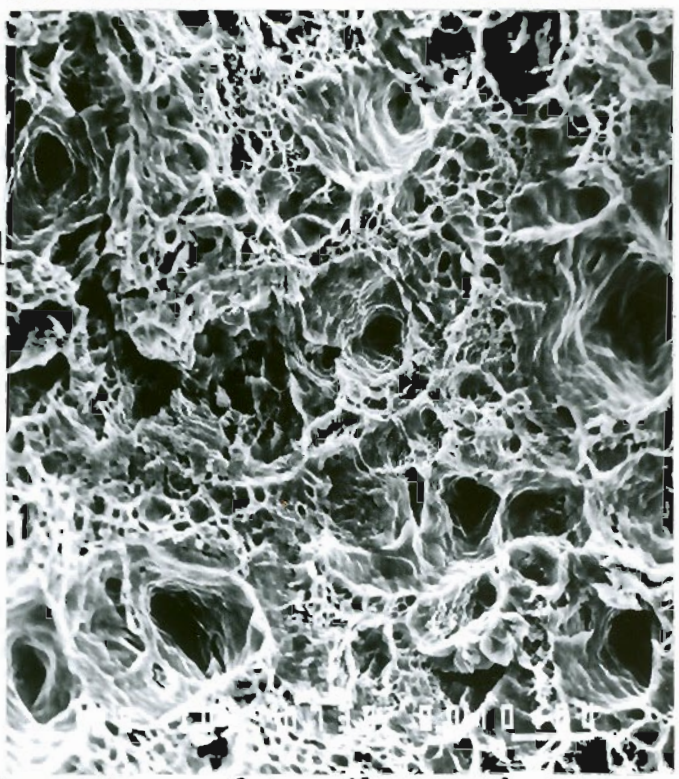

Figure-42 : Fractured surfaces of tensile specimen of A572 steel, base metal.

(a) At room temperature and low strain rate

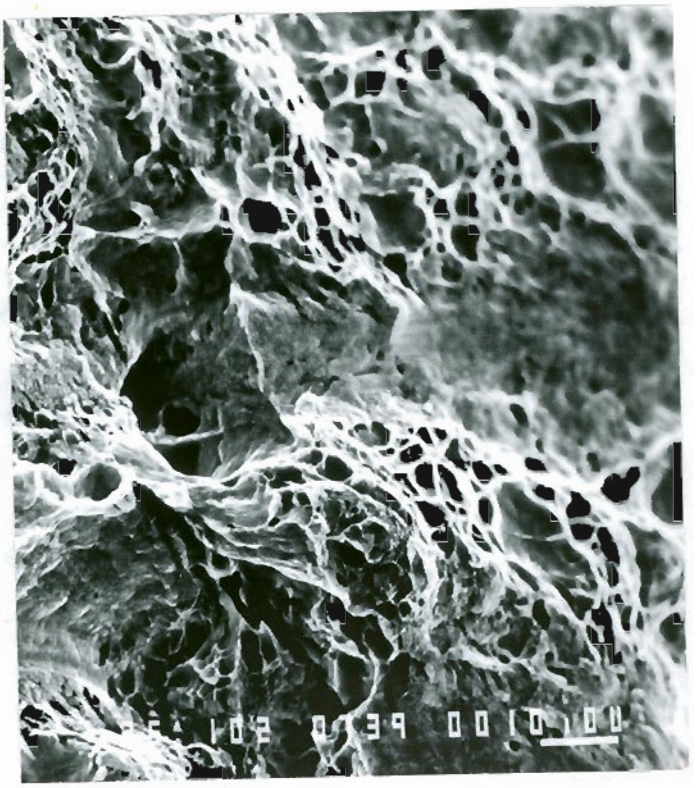

(b) At room temperature and intermediate strain rate

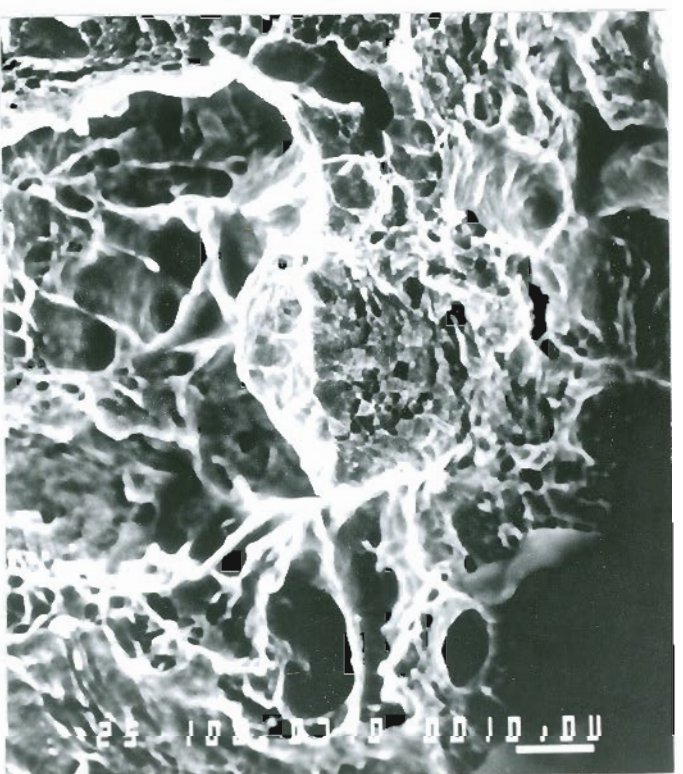

Figure-43 : Fractured surfaces of tensile specimen of A572 steel flame cut at faster cutting speed.

(a) At low temperature and low strain rate

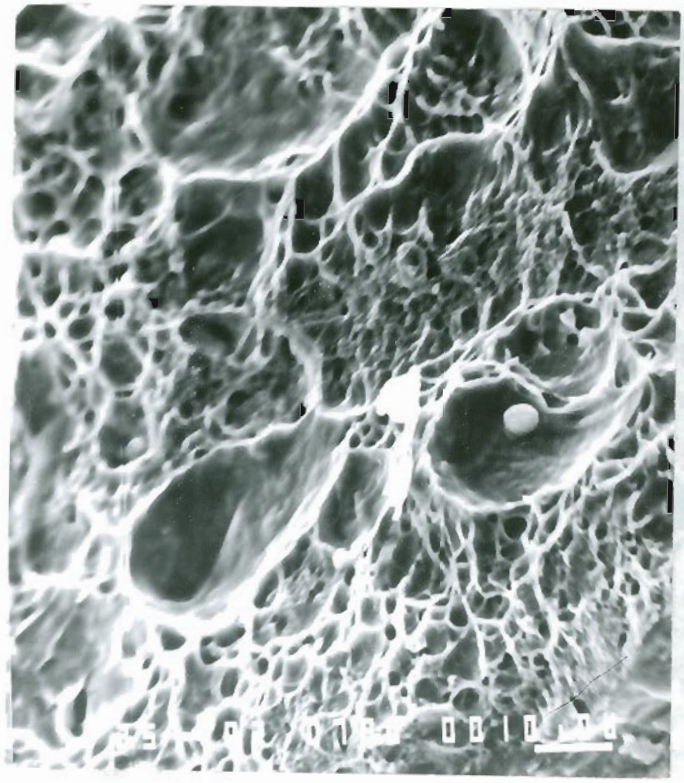

(b) At low temperature and intermediate strain rate

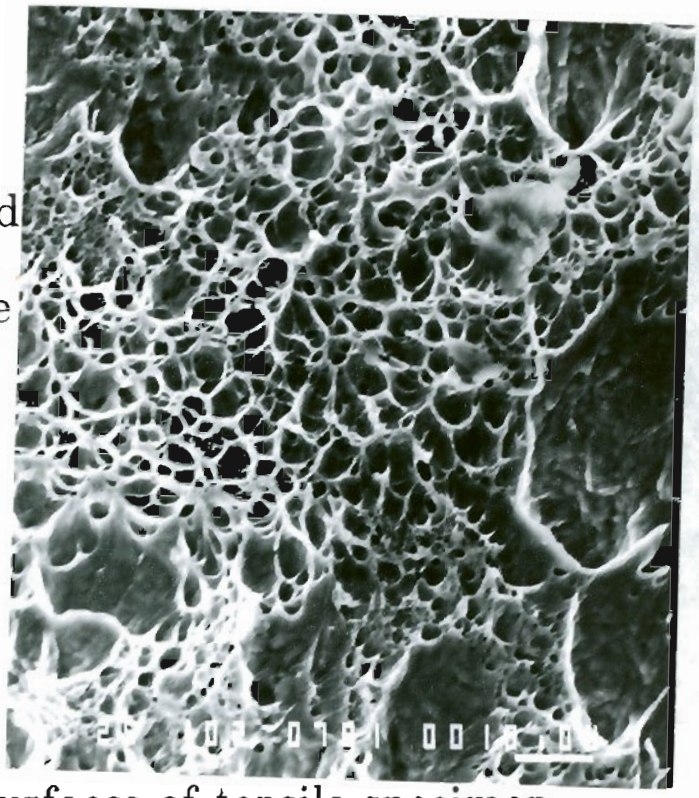

Figure-44 : Fractured surfaces of tensile specimen of A572 steel flame cut at faster cutting speed.

(a) Base metal.

At room temperature

and low strain rate

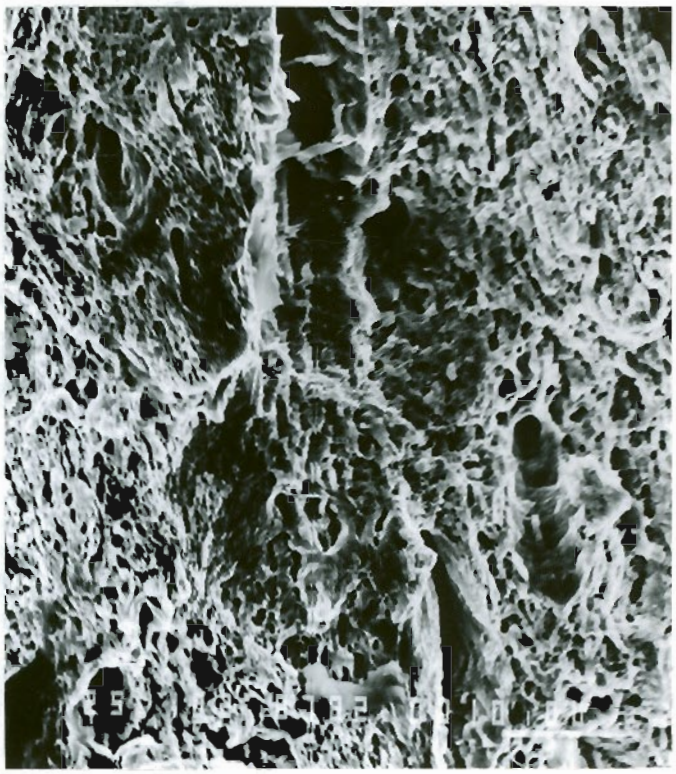

(b) Flame cut at

faster cutting speed.

At low temperature and

intermediate strain rate

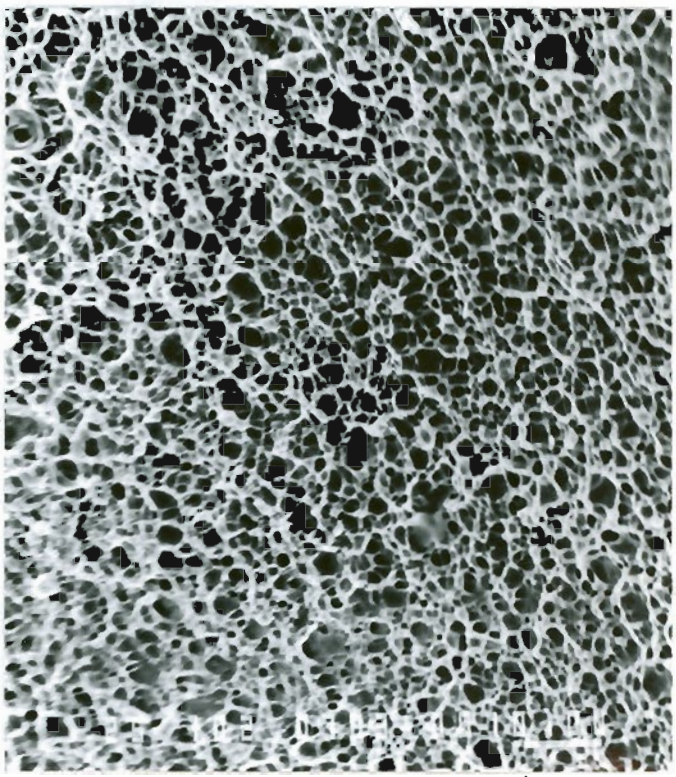

Figure-45 : Fractured surfaces of tensile specimen of A514 steel.

(a) Base metal

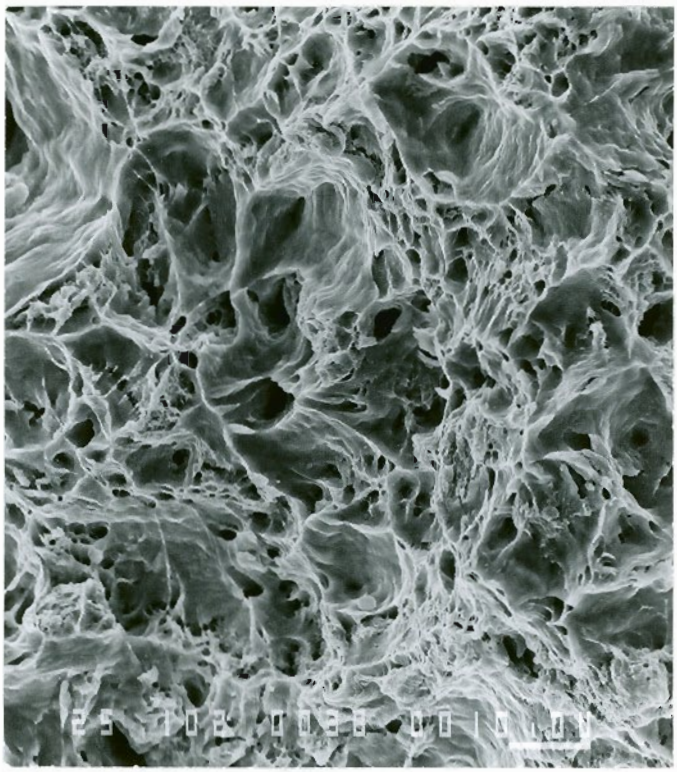

(b) Flame cut at slower cutting speed

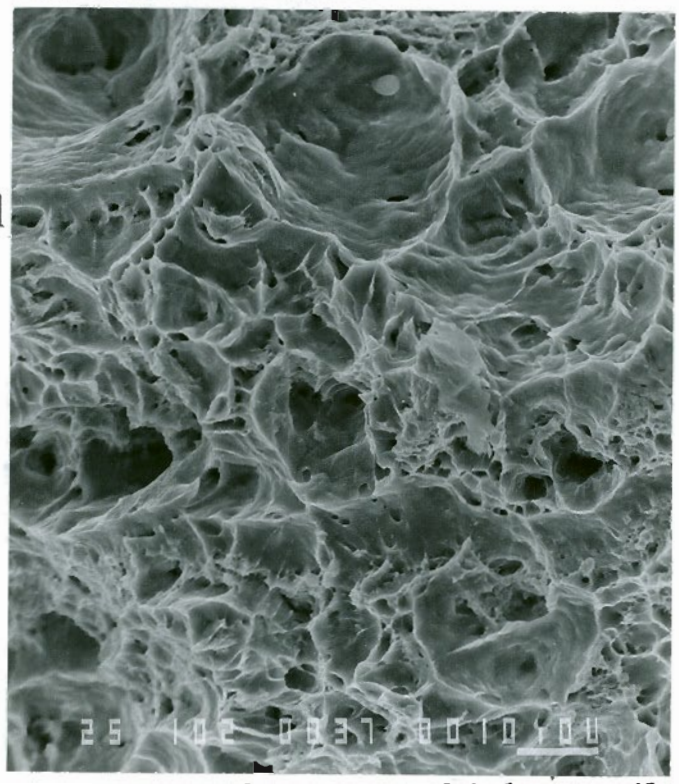

Figure-46 : Fractured surfaces of 6.4mm thick tensile specimens of A514 steel, tested at low temperature and intermediate strain rate.

(a) Base metal

(b) Flame cut at slower cutting speed

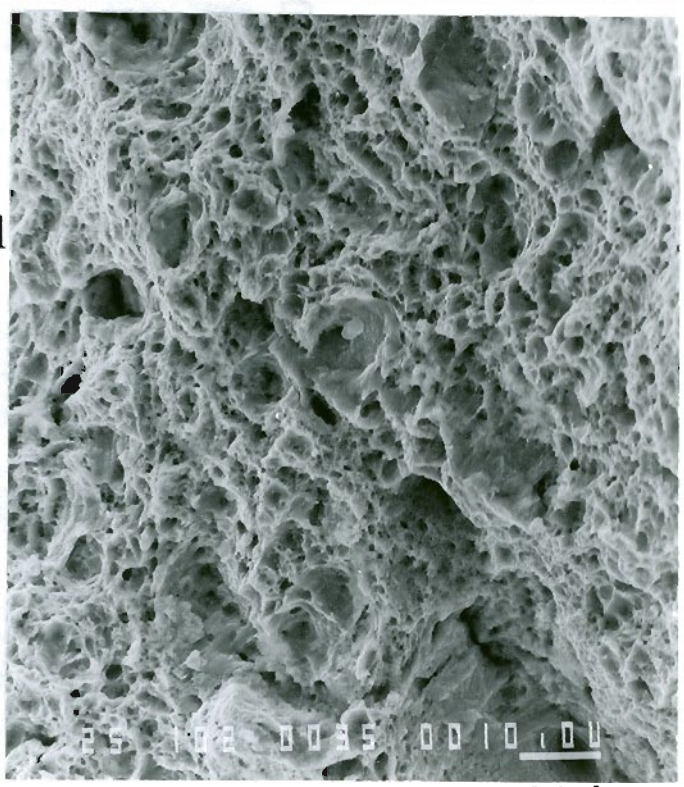

Figure-47 : Fractured surfaces of 6.4mm thick tensile specimens of A572 steel, tested at low temperature and intermediate strain rate.

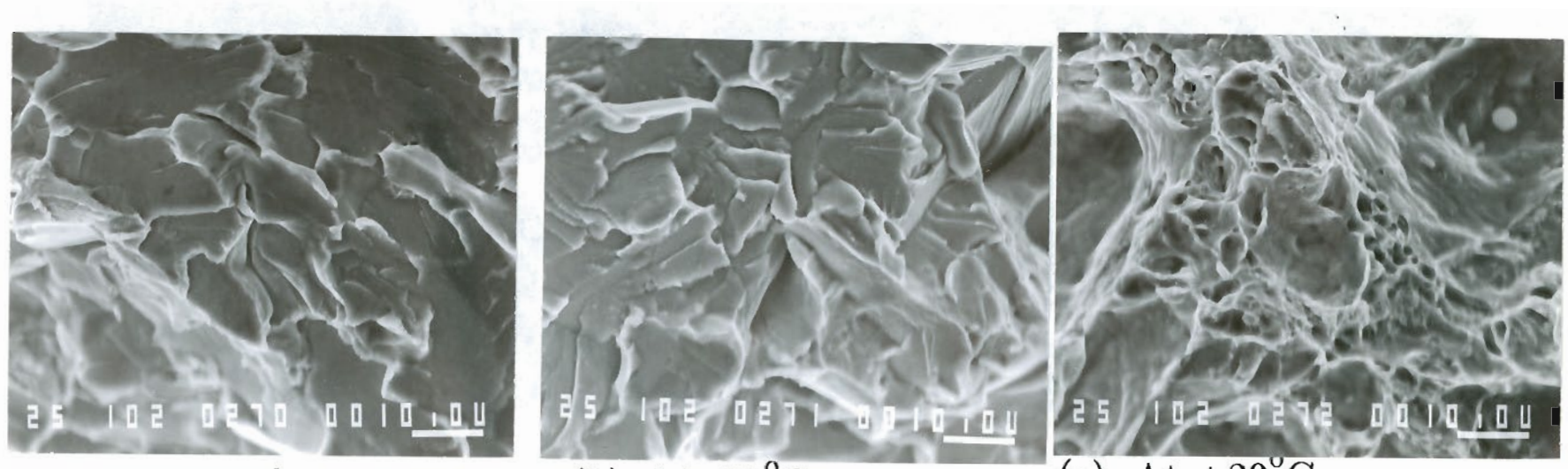

(a) At -100°C (b) At -30°C (c) At +20°C

Figure-48 : Fractured surfaces of full size CVN impact specimens for A572 steel, base metal.

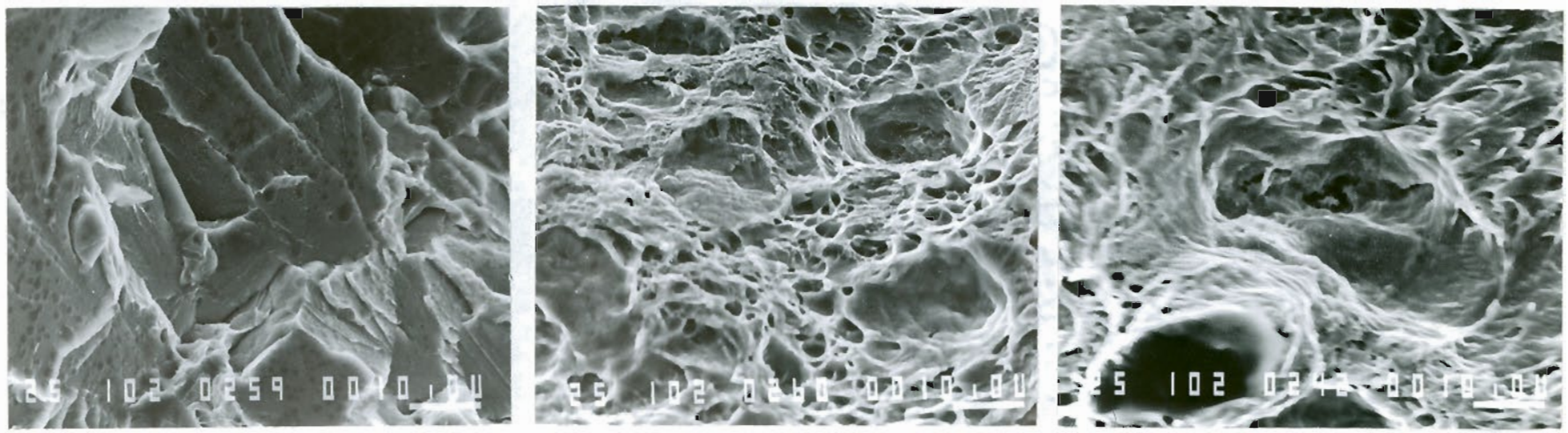

(a) At -85°C (b) At -57°C (c) At +19°C

Figure-49 : Fractured surfaces of quarter size CVN impact specimens for A572 steel, base metal.

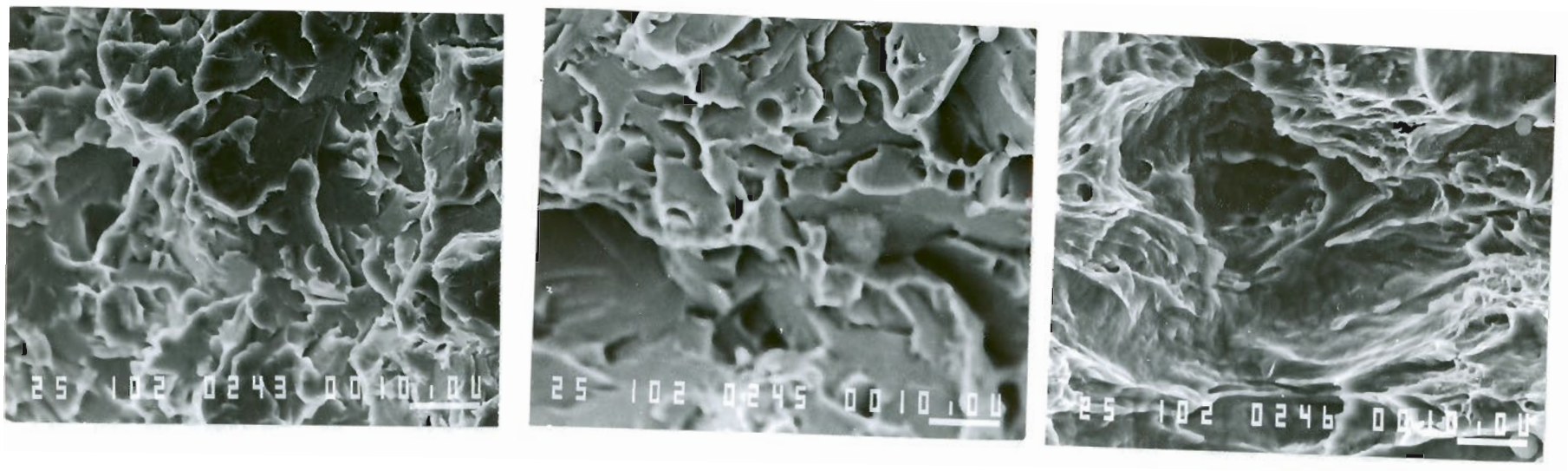

(a) At -87°C (b) At -45°C (c) At +19°C

Figure-50 : Fractured surfaces of quarter size CVN impact specimens for A572 steel, flame cut at slower cutting speed.

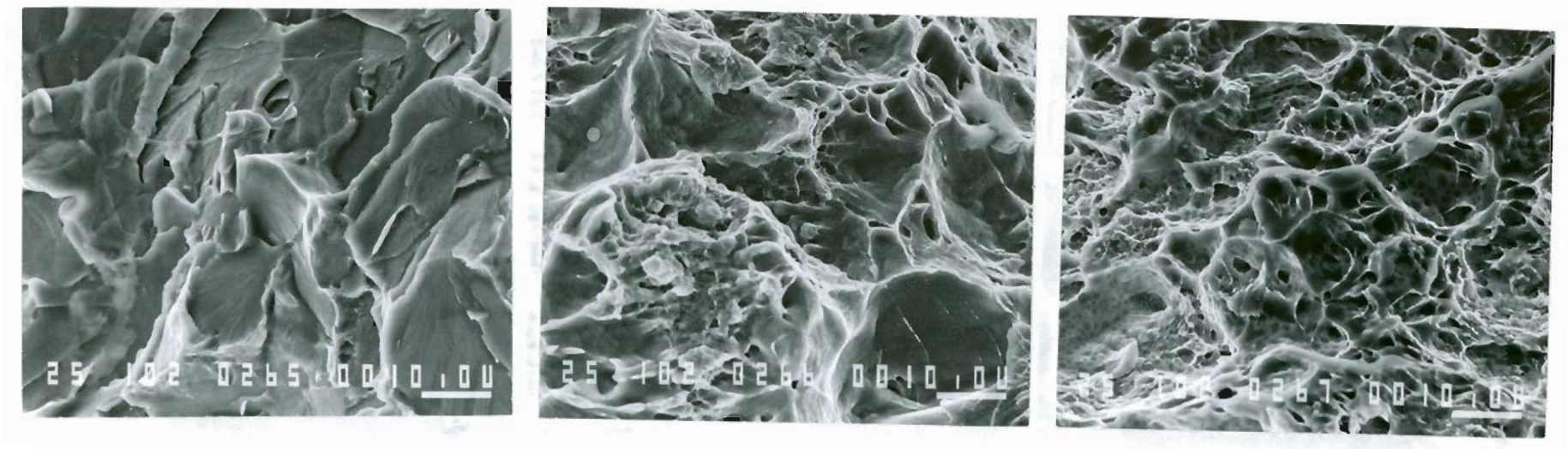

(a) At -85°C (b) At -21°C (c) At +19°C

Figure-51 : Fractured surfaces of quarter size CVN impact specimens for A572 steel, flame cut at faster cutting speed.

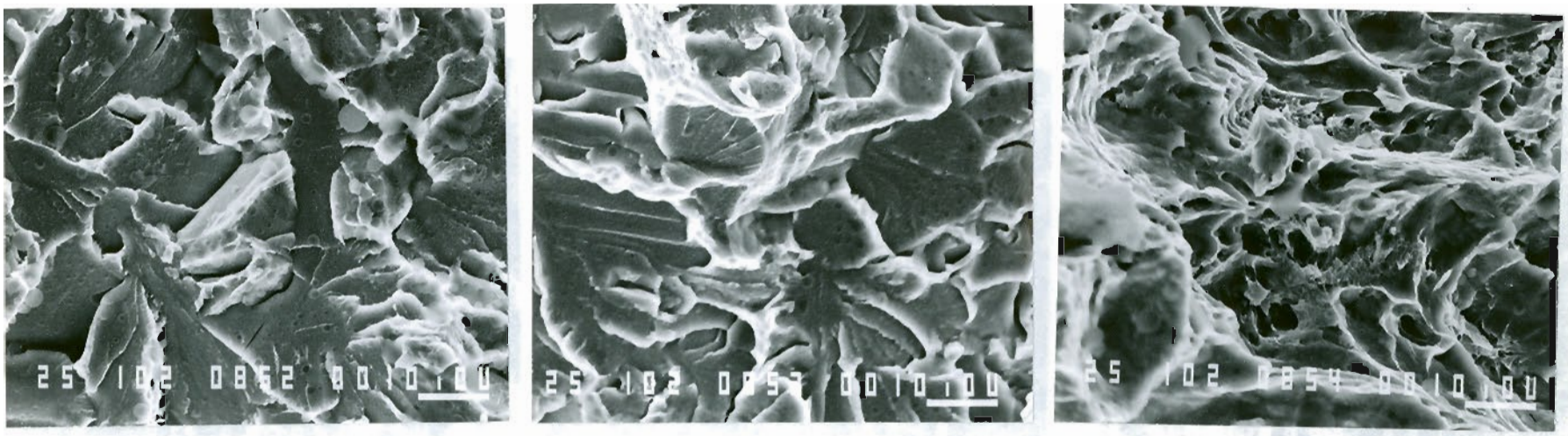

(a) At -131°C (b) At -62°C (c) At +31°C

Figure-52 : Fractured surfaces of half size CVN impact specimens for A572 steel, base metal.

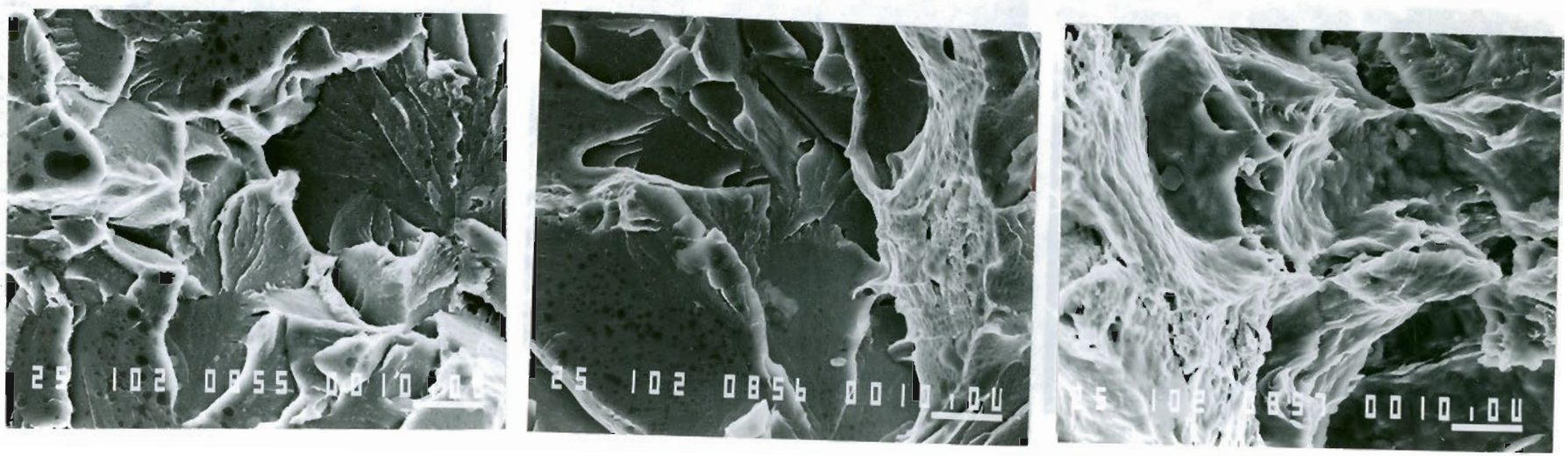

(a) At -128°C (b) At -30°C (c) At +31°C

Figure-53 : Fractured surfaces of half size CVN impact specimens for A572 steel, flame cut at slower cutting speed.

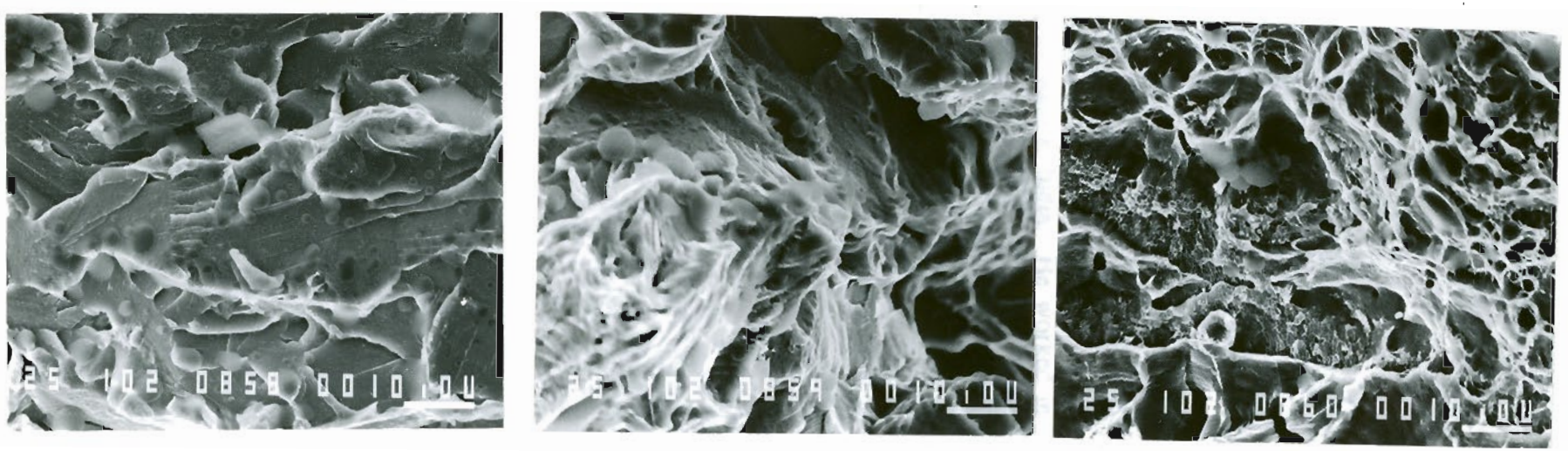

(a) At -89°C (b) At -9°C (c) At +31°C

Figure-54 : Fractured surfaces of half size CVN impact specimens for A572 steel, flame cut at faster cutting speed.

BIOGRAPHICAL NOTE

The author was born on July 30, 1959, in Madras, India. He obtained his B.Sc. (Chemistry) degree (Vivekananda College) from Madras University in 1979. He received both his B.E. (1983) and his M.E. (1987) in Metallurgy from Indian Institute of Science, Bangalore, India. He worked in the grade of Scientist "B" in Combat Vehicles Research and Development Establishment (CVRDE), Avadi, Madras, India for a period of 2-1/2 years. He jointed the Oregon Graduate Center in September 1987 and completed his requires for the Master of Science in August 1989.